Aus dem Institut für Physiologische Chemie

Kommissarische Leitung: Prof. Dr. Marco Rust

des Fachbereichs Medizin der Philipps-Universität Marburg

Loss of the miR379-410 cluster in mice leads to alterations in social and anxiety-related behaviours

INAUGURAL-DISSERTATION

zur Erlangung des Doktorgrades der gesamten Naturwissenschaften (Dr. rer. nat.)

dem Fachbereich Medizin der Philipps-Universität Marburg

vorgelegt von

Martin Lackinger

aus Herford

Marburg, 2018

Angenommen vom Fachbereich Medizin der Philipps-Universität Marburg am: 05.11.2018

Dekan: Herr Prof. Dr. H. Schäfer

Referent: Herr Prof. Dr. G. Schratt

1. Korreferent: Herr Prof. Dr. C. Culmsee

Table of contents

Abstract

microRNAs (miRNAs) belong to a group of small non-coding RNAs that down regulates gene expression at the post-transcriptional level. The paternally imprinted placental mammal-specific miR379-410 cluster hosts 38 miRNAs. In the last decade, several members of the cluster have been shown to regulate synapse development and plasticity in mammals. Further, they have been implicated in a variety of diseases, including neurodevelopmental disorders. However, the potential involvement of these miRNAs in the control of complex behaviour in mammals, such as sociability, remains largely unknown. This is an important issue since aberrant synaptic dysfunction is thought to underlie neurodevelopmental diseases, such as autism spectrum disorder (ASD), characterized by deficits in social communication and interaction as well as restricted repetitive behaviour.

This study aimed at the characterization of a constitutive knock-out (ko) mouse model that carries a deletion of the miR379-410 cluster. Extensive behavioural assays across the animals' lifespan and cellular examinations of structural and functional properties of synapses were performed. Furthermore, transcriptome sequencing of adult miR379-410 ko hippocampi allowed the validation of potential direct target candidates of the miRNA cluster by using molecular and biochemical approaches.

Mice deficient for the miR379-410 cluster displayed an anti-autistic-like phenotype, consisting of hypersocial behaviour, increased ultrasonic vocalizations (USVs) and reduced repetitive behaviour in the absence of cognitive impairments. Further, miR379-410 ko mice presented an anxiety phenotype over the lifespan. Along with the behavioural phenotype, miR379-410 ko mice showed increased excitatory synaptic transmission and spine density accompanied by an elevated expression of ionotropic glutamate receptor complex components in the hippocampus. Several of these components, identified by transcriptome profiling (Cnih2, Src, Prr7 and Dlgap3) could be validated as direct miR379-410 target genes.

Taken together, the data obtained in this thesis describe for the first time a negative regulatory role of the miR379-410 cluster in social behaviour and the control of genes associated with excitatory synaptic function. Thus, interfering with miRNAs from the miR379-410 cluster could represent in the future a promising strategy for the treatment of neurodevelopmental disorders characterized by social dysfunction, such as ASD.

Zusammenfassung

mikroRNAs (miRNAs) gehören zu einer Gruppe von kleinen, nicht-kodierenden RNAs, die als negative Regulatoren der Genexpression auf post-transkriptioneller Ebene fungieren. Das plazentatier-spezifische miR379-410-Cluster, welches durch genomische Prägung auf dem väterlichen Genom inaktiv ist, beinhaltet 38 miRNAs. In den vergangenen zehn Jahren konnte für mehrere Mitglieder dieses miRNA-Clusters eine regulierende Funktion auf die Synapsen-Entwicklung und Plastizität in Säugetieren nachgewiesen werden. Ferner konnten einige dieser miRNAs mit diversen Krankheiten, einschließlich neurologischen Entwicklungs-störungen, in Verbindung gebracht werden. Die mögliche Beteiligung dieser miRNAs an der Kontrolle von komplexen Verhaltensabläufen bei Säugetieren, wie beispielsweise Soziabilität, die Fähigkeit soziale Beziehungen aufzunehmen und zu pflegen, ist jedoch weitgehend unbekannt. Dieser Sachverhalt ist von großem Interesse, da bei neurologischen Entwicklungsstörungen, wie beispielsweise Autismus-Spektrum-Störungen (ASS) angenommen wird, dass übermäßige synaptische Fehlfunktionen diesem Krankheitsbild zugrunde liegen. ASS ist dabei durch Defizite in sozialer Kommunikation und Interaktion sowie durch zwanghaft-ritualisierte, repetitive und stereotype Verhaltensweisen geprägt.

Die vorliegende Doktorarbeit befasste sich mit der Charakterisierung eines konstitutiven Knock-out (ko)-Mausmodells, welches eine Deletion des miR379-410-Clusters aufweist. Die Experimente umfassten umfangreiche Verhaltensanalysen und zelluläre Untersuchungen von Synapsen. Darüber hinaus erlaubte die Transkriptom-Analyse von Hippocampus-Proben erwachsener miR379-410 ko Mäuse, potenzielle Zielkandidatengene des miRNA-Clusters zu identifizieren, welche mit molekularen und biochemischen Methoden validiert wurden.

Ko-Mäuse, welche die Deletion des miR379-410-Cluster trugen, zeigten einen anti-autistischen Phänotyp. Dieser Phänotyp war gekennzeichnet durch hypersoziales Verhalten mit erhöhten Ultraschallvokalisationen (USVs) und verringertem repetitiven Verhalten bei normaler kognitiver Leistung. Ferner zeigten miR379-410 ko-Mäuse einen über die Lebensspanne konsistenten, ausgeprägten Angstphänotyp. Der miR379-410 ko Verhaltens-phänotyp ging einher mit verstärkter exzitatorischer synaptischer Transmission und einer erhöhten Dichte von dendritischen Dornfortsätzen im Hippocampus. Darüber hinaus konnte eine erhöhte Expression von ionotropen Glutamat-Rezeptor-Komplexen im Hippocampus

festgestellt werden. Dabei war es möglich, einige der hochregulierten exzitatorischen synaptischen Gene (Cnih2, Src, Prr7 und Dlgap3), die eingangs durch Transkriptom-Analyse identifiziert wurden, als direkte Cluster-Zielkandidaten zu validieren.

Zusammenfassend beschreibt diese Arbeit zum ersten Mal die Rolle von spezifischen miRNAs aus dem miR379-410-Cluster, die als negative Regulatoren auf das Sozialverhalten einwirken und ferner durch Kontrolle der Genexpressionen die Funktion exzitatorischer Synapsen beeinflussen. Demnach könnte der Eingriff und die Manipulation von miRNAs aus diesem Cluster eine vielversprechende Strategie darstellen um zukünftig neurologische Entwicklungsstörungen, wie beispielsweise ASS, besser verstehen und adäquat behandeln zu können.

1. Introduction

The human nervous system is a fascinating and complex structure with around 100 billion neurons that are heavily interconnected via trillions of synapses (*Kandel et al., 2012*). It helps us to deal with and adapt to many conditions and circumstances and we rely every day on an equipment of intricately formed neural circuits for many of our adaptive strategies. How this functional interplay is influenced by our genetics, by post-transcriptional regulation of gene expression and by environmental factors, is still elusive. The social interaction with conspecifics is one crucial behavioural hallmark for physical and mental health in human beings. Alterations of normal brain developmental trajectories can impair the function of specific neuronal circuits that could lead to neurodevelopmental and psychiatric diseases characterized by social dysfunction. However, which mechanisms are engaged in the healthy brain to counteract social dysfunction is still enigmatic.

1.1 microRNA definition and biogenesis

microRNAs (miRNAs or miRs) are small regulatory non-coding RNAs, approximately 22 nucleotides (nt) long, which act as post-transcriptional regulators of gene expression (reviewed in *Bartel, 2018*). They are critically important for post-transcriptional regulation of mRNAs, since they regulate around 60% of protein-coding genes (*Grun et al., 2005*). Although the first miRNA was identified more than two decades ago, we have just begun to understand the complexity of the regulatory functions of these molecules *in vivo*. Members of the miRNA family were initially discovered as small temporal RNAs (stRNA) that regulate developmental transitions in *Ceanorhabditis elegans (C. elegans)* (*Pasquinelli et al., 2002*). Since then, thousands of miRNAs across different species, including worms, flies, plants and mammals have been identified and a nomenclature system has been adopted (*He & Hannon, 2004*; *Ambros et al., 2003*). Some miRNAs are highly conserved through evolution, while other miRNAs and miRNA families are mammalian- or even primate-specific (*Kosik, 2006*). There have been 18,226 miRNAs annotated in animals, plants and viruses, including 1,527 miRNAs encoded in the human genome (*Kozomara et al., 2011*). Although the genetic accessibility of model organisms such as *C. elegans* and *Drosophila* has been instrumental for a better understanding of miRNA function, the use of higher and more complex

eukaryotes is needed to study the role of mammalian-specific miRNAs, in particular with regard to their impact on complex behaviours driven by brains of higher developed organisms. The canonical pathway of miRNA biogenesis in animals is shown in **Figure 1** (*reviewed in Schratt, 2009; Ha & Kim, 2014; Bartel, 2018*).
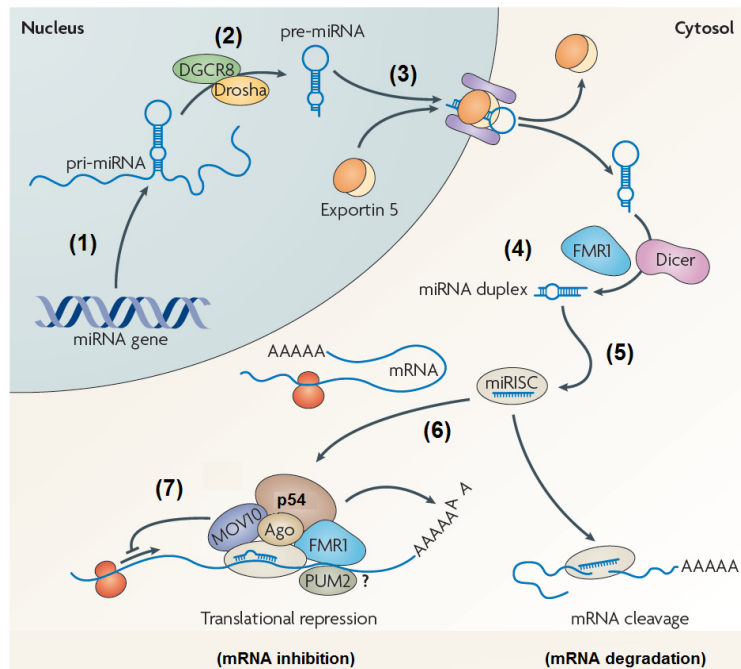
Figure 1: miRNA biogenesis in mammalian cells. (1) The miRNA gene is transcribed into a primary miRNA transcript (pri-miRNA). **(2)** The pri-miRNA is cleaved by Drosha into a hairpin precursor-miRNA (pre-miRNA). **(3)** The pre-miRNA is transported out of the nucleus by exportin-5. **(4)** The pre-miRNA is cleaved by Dicer to form a short double-stranded intermediate miRNA duplex. **(5)** A single strand of the miRNA duplex, the mature miRNA, is incorporated into the RISC. **(6)** The mRNA associates with the miRNA/RISC complex. **(7)** The mRNA is translationally repressed. Abbreviations: Ago = Agonaute, DGCR8 = DiGeorge syndrome critical region 8, FMR1 = Fragile X Mental Retardation 1, miRISC = miRNA-induced silencing complex, MOV10 = Moloney leukemia virus 10, p54 = protein 54 (also known as RCK or DDX6), Pum2 = Pumilio 2. Modified graph adapted from *Schratt, 2009*.

The production of a miRNA begins with the transcription of a primary transcript (pri-miRNA) from a miRNA gene catalyzed mostly by RNA polymerase II (Pol II). In the genome, miRNAs can exist as individual genes coding for a single miRNA, or as clusters that can contain up to 50 different miRNA sequences, and are expressed as a single transcriptional unit under the control of their own promoter (*Baskerville & Bartel, 2005*). miRNAs can be located either in intergenic regions or within protein coding sequences, often in introns, where they are co-

transcribed with the host gene. Once transcribed, the pri-miRNA is processed in the nucleus by the microprocessor, a multi-protein complex whose catalytic component is the RNAse III Drosha. Drosha cleavage releases a 70-100 nt hairpin precursor miRNA (pre-miRNA) that is exported to the cytosol in an exportin-5 dependent manner. Once the pre-miRNA reaches the cytoplasm, a second ribonuclease, the RNase III enzyme Dicer, whose activity can be modulated by accessory proteins, e.g. FMRP (*Krol et al., 2010*), further cleaves the pre-miRNA to release a ~22 nt duplex RNA. Usually one strand of the duplex, called the leading strand, is selected for loading into the RNA-induced silencing complex (RISC) based on the thermodynamic characteristics of the intermediate miRNA duplex and therefore forms the mature miRNA. The other one, called passenger strand, is usually degraded, however multiple examples of miRNAs exist for which both strands of the duplex can form a mature miRNA (termed 3p and 5p). The RISC is a ribonucleoprotein complex whose main protein components are Argonaute and GW182 (Tnrc6) family proteins. The latter, once recruited to the target mRNA via imperfect Watson-Crick base pairing between the Argonaute-loaded miRNA and mRNA, mediate translational inhibition and/or mRNA degradation.

1.2 microRNA-mediated regulation of gene expression

The miRNA programmed RISC (miRISC) recognizes and binds complementary sequences in the 3'UTR of mRNAs. Depending on the level of complementarity between the miRNA and the target sequence, miRISC binding leads either to translational repression in the case of imperfect complementarity, or cleavage if the miRNA is perfectly complementary to the target mRNA. In animals, miRNAs bind mostly to imperfectly complementary regions within the 3'UTR region of target mRNAs. Since imperfectly complementary sequence stretches to a miRNA occur rather frequently within mRNA targets, miRNAs have the potential to regulate the expression of hundreds of genes (*Bartel, 2009*). On the other hand, gene transcripts usually contain multiple miRNA binding sites in their 3'UTRs. Therefore, multiple miRNA families can potentially be involved in the control of their expression (*Bartel, 2009*). Several parameters govern the binding of a miRNA to its target. The most important requirement is a continuous base pairing between the target mRNA and nucleotides 2-8 of the miRNA, known as the seed region. Other parameters governing the functionality of miRNA binding sites are their position within the 3'UTR, and the secondary structure of the UTR region surrounding the miRNA binding sites (*Bartel, 2009*). The exact mechanisms of

translational silencing mediated by miRISC are still not fully understood, but likely involve a combination of translational inhibition at the initiation stage and the promotion of mRNA degradation by a deadenylation-dependent process (reviewed in *Fabian & Sonnenberg, 2012; Jonas & Izaurralde, 2015*).

1.3 Role of microRNAs in the nervous system

miRNAs can regulate potentially hundreds or even thousands of mammalian mRNA transcripts. Therefore, they act as master regulators of gene expression. Since many miRNAs are enriched in the central nervous system (CNS), it is not surprising that they have been shown to regulate all aspects of neuronal development and function (reviewed in *Rajman & Schratt, 2017; McNeill & Van Vactor, 2012*). Dynamic regulation of miRNA expression has been observed during embryonic and adult neurogenesis, neuronal maturation and in the mature nervous system (*Kapsimali et al., 2007; Luikart et al., 2011; Schouten et al., 2012*). Consistently, it has been shown that miRNAs play a key role in all of these processes (*Cheng et al., 2009; Liu et al., 2010*). The essential role of miRNAs in brain function has been first shown by gene targeting of Dicer, an essential component of the biogenesis pathway (*Giraldez et al., 2005; Schaefer et al., 2007; Huang et al., 2010; McLoughlin et al., 2012*). In a constitutive Dicer knockout (ko) model, early embryonic lethality due to death of differentiating cells was observed (*Bernstein et al., 2003*). Further, conditional loss of Dicer in mouse models resulted in deficits in brain development and growth (*Davis et al., 2008; Huang et al., 2010*). Dicer deficiency in the adult mouse forebrain resulted in neurodegeneration and accumulation of hyper-phosphorylated tau, a microtubule-associated protein (MAP) that is one of the major components of neurofibrillary tangles characteristic of Alzheimer diseases (AD) and other forms of dementia known as tauopathies (*Hébert et al., 2010; Brandt et al., 2005*). In order to investigate the general function of miRNAs in cognitive processes, *Konopka et al. (2010)* used an inducible mouse strain in which the Cre recombinase is under the control of the Ca^{2+} / calmodulin-dependent protein kinase II (CaMKII)-promoter to delete Dicer specifically in excitatory neurons of the adult forebrain. These genetically modified animals showed enhanced learning and memory function in multiple tasks, demonstrating that the miRNA pathway is also involved in the regulation of higher cognitive function. At the cellular level, several individual miRNAs that are highly expressed in post-mitotic neurons have been shown to play an important function

as negative or positive regulators of different aspects of neuronal development and function (summarized in **Figure 2**). miRNAs that are relevant for the maturation and function of post-mitotic neurons frequently control activity dependent gene expression at the level of local protein synthesis in the synapto-dendritic compartment. Local translation is important for both the establishment and refinement of neuronal circuits and for synaptic plasticity, a key mechanism that allows neurons to adapt to changes in the environment. The promoters of several plasticity-relevant miRNAs contain binding sites for activity-regulated transcription factors. miR-132 for example, a positive regulator of dendrite and spine development in (newborn) hippocampal neurons, is controlled by cAMP response element binding protein (CREB) (*Vo et al., 2005; Nudelman et al., 2010; Pathania et al., 2012*). A further key mechanism of synapse-specific plasticity is the translation of a subset of important synaptic mRNAs locally at activated synapses.
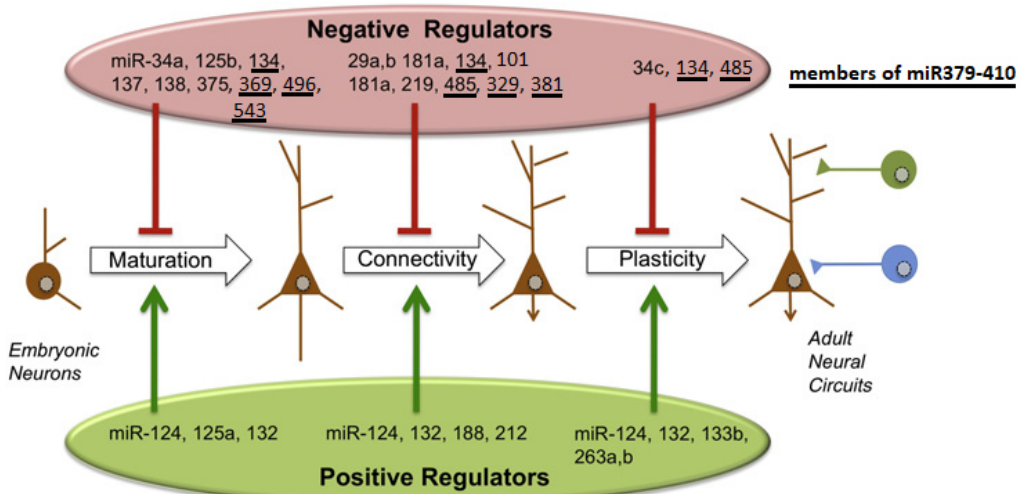
Figure 2: miRNAs involved in synaptic development and function. Several miRNAs have been identified to act as positive or negative regulators in neuronal maturation, connectivity and plasticity. Please notice that miRNAs investigated so far from the miR379-410 cluster (underlined), are highly involved in negative regulation and suppression of synaptic connections. Modified graph adapted from *McNeil & van Vactor, 2012*.

Several miRNAs and proteins involved in the miRNA pathway are localized in the synapto-dendritic compartment, where they can fine-tune local protein synthesis. Examples of dendritic miRNAs that regulate key aspects of neuronal morphology and plasticity, as illustrated in **Figure 3**, are the "miRNA troika" miR-132, -134 and -138 (reviewed in *Bicker et*

al., 2014). For instance, to negatively regulate dendritic spine size formation, miR-138 represses the expression of acyl-protein thioesterase 1 (APT1), whereas miR-134 (discussed in details in 1.5) inhibits the expression of LIM-domain containing protein kinase 1 (LimK1) (*Siegel et al., 2009; Schratt et al., 2006*). On the other hand, miR-132 positively regulates dendritic spine size by repressing the Rho GTPase-activating protein p250GAP and metalloproteinase 9 (MPP9) (*Vo et al., 2005; Jasinska et al., 2016*). Local protein synthesis regulation by miRNAs is also controlled by neuronal activity (*Vasudevan et al., 2007*). The interaction between the dendritic miR-134 and LimK1 is regulated by the neurotrophin brain-derived neurotrophic factor (BDNF) that is released in response to an elevation in neuronal activity (*Schratt et al., 2006*). Local protein synthesis of the miR-138 target APT1 is induced by neuronal activity through proteasome-dependent degradation of the RISC protein MOV10 (*Banerjee et al., 2009*). This finding suggests the existence of a regulatory framework in which miRNAs maintain plasticity-associated transcripts in a repressed state until relieved by neuronal activity.
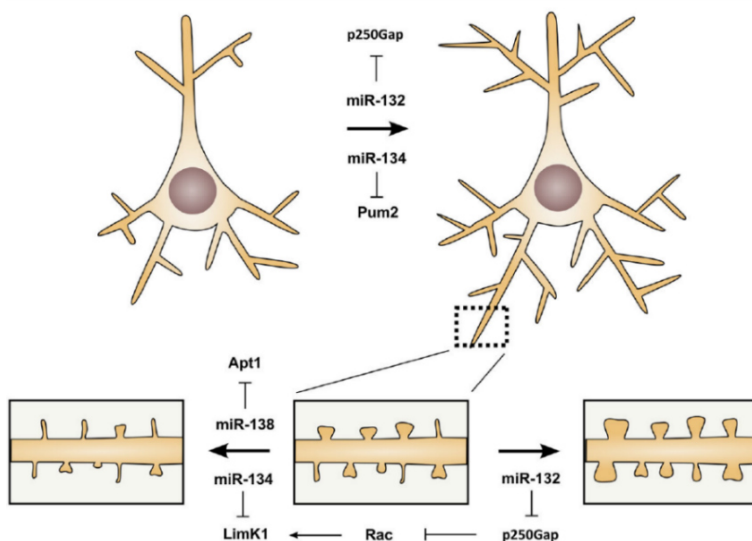
Figure 3: Dendritic complexity and spine morphology are regulated by the "miRNA troika" miR-132, -134 and -138. Increased miR-132 and miR-134 levels promote neurite growth and branching by targeting p250GAP and Pum2, respectively. Furthermore, dendritic spine morphogenesis is positively regulated by miR-132 through indirect activation of LimK1, whereas the spine size is negatively regulated by miR-134 through inhibition of LimK1 and by miR-138 through inhibition of APT1. Graph adapted from *Bicker et al., 2014*.

The picture emerging from these cell culture studies is the existence of a complex network of miRNAs that control several aspects of synaptic plasticity. The first *in vivo* evidences for a function of miRNAs in neuronal plasticity have also been provided. For instance, transgenic

overexpression of miR-132 in the mouse forebrain leads to increased dendritic spine density in the hippocampus (*Gao et al., 2010*) and impaired novel object recognition memory (*O'Neill, 2009*). Activity-dependent regulation of miR-132 levels is also necessary for ocular dominance plasticity in the visual cortex (*Tognini et al., 2011*). Further, it was demonstrated that the overexpression of miR-134 reduces mouse cortical pyramidal neuron dendritogenesis *in vivo* (*Christensen et al., 2010*). Overall, these findings provide evidence for the essential role of miRNAs in the development and function of neuronal circuits in the intact mouse brain.

1.4 The placental mammal-specific miR379-410 microRNA cluster

The paternally imprinted miR379-410 cluster hosts 38 miRNAs that are involved in several neurodevelopmental processes and act as important regulators of neuronal function (reviewed in *Winter, 2015*). Moreover, it was demonstrated that miR379-410 expression during postnatal development and adulthood is mostly restricted to the brain (*Labialle et al., 2014*). The miR379-410 cluster is located within the imprinted DLK1-DIO3 region, as illustrated in **Figure 4**, that spans approximately 850 kilobases (kb) and is situated on chromosome 14q32 in humans and on the distal part of chromosome 12qF1 in mice. It contains several coding and non-coding genes (reviewed in *da Rocha et al., 2008*). The DLK1-DIO3 region contains the paternally expressed genes DLK1, RTL1 and DIO3 and the maternally expressed genes MEG3 (Gtl2 in mice), MEG8 (RIAN in mice) and antisense RTL1 (RTL1as). DLK1 acts as an antagonist of Notch signaling and regulates cell differentiation (*Baladron et al., 2005*; *Nueda et al., 2007),* whereas RTL1 is essential for proper placental development (*Sekita et al., 2008; Brandt et al., 2005*). DIO3 encodes a type 3-iodothyronine deiodinase, an enzyme that is important in the activation and inactivation of thyroid hormones (*Hernandez et al., 1998; Galton et al., 1999*). Seitz and colleagues showed, partially through computer-assisted approaches, that the DLK1-DIO3 imprinted region contains 53 miRNAs on the forward and one miRNA on the reverse strand (*Seitz et al., 2003; 2004*). The 54 miRNAs are separated into 3 different clusters: DLK1-MEG3 (encoding miR-2392 and miR-770), MEG3-MEG8 and the miR379-410 cluster between the MEG8 and DIO3 region. miRNAs from the miR379-410 cluster are highly conserved between mouse and human and due to the broad spectrum of predicted targets, it can be assumed that miRNAs from this cluster target numerous genes in specific cell types (*Kircher et al., 2008*). The genes

and miRNAs from this locus share similar but not completely overlapping expression domains in the developing and mature brain. For example, Gtl2 is expressed during development and in the adult brain, whereas miR-410 is limited to development and early postnatal days. miR-134 and miR-485 expression is increased mainly postnatal (*Wheeler et al., 2006; Schratt et al., 2006; Cohen et al., 2011*). It was shown by *Rago et al. (2014)*, that during embryonic neocortex development miR-369-3p, -496 and -543 are expressed in neuronal progenitors and neurons, whereas miR-134 is highly upregulated in post-mitotic neurons (*Schratt et al., 2006*). Furthermore, miR-134, -369, -410 and miR-496 are all encoded within the exons or introns of the long non-coding RNA Mirg. Thus, differences in the expression of these specific miRNAs might be due to alternative Mirg splicing or differential post-transcriptional regulation (e.g. at the level of miRNA processing or stability). Interestingly, it was demonstrated that several miRNAs of the miR379-410 cluster, but not from the Gtl2 region, are upregulated in a neuronal activity-dependent manner. This effect is mediated by the transcription factor MEF2, which binds approximately 20 kb upstream of the miR379-410 cluster (*Fiore et al., 2009; Cohen et al., 2011*). An important function of the miR379-410 cluster has been demonstrated in a constitutive ko mouse model (*Labialle et al. 2014*). In this mouse line, a maternally inherited deletion of the cluster leads to a partially penetrant neonatal lethality phenotype associated with postnatal metabolic defects, including inefficient mobilization of glycogen stores. However, mice that survive to adulthood display no abnormalities when kept in standardized mouse husbandry conditions (*Marty et al., 2016*).
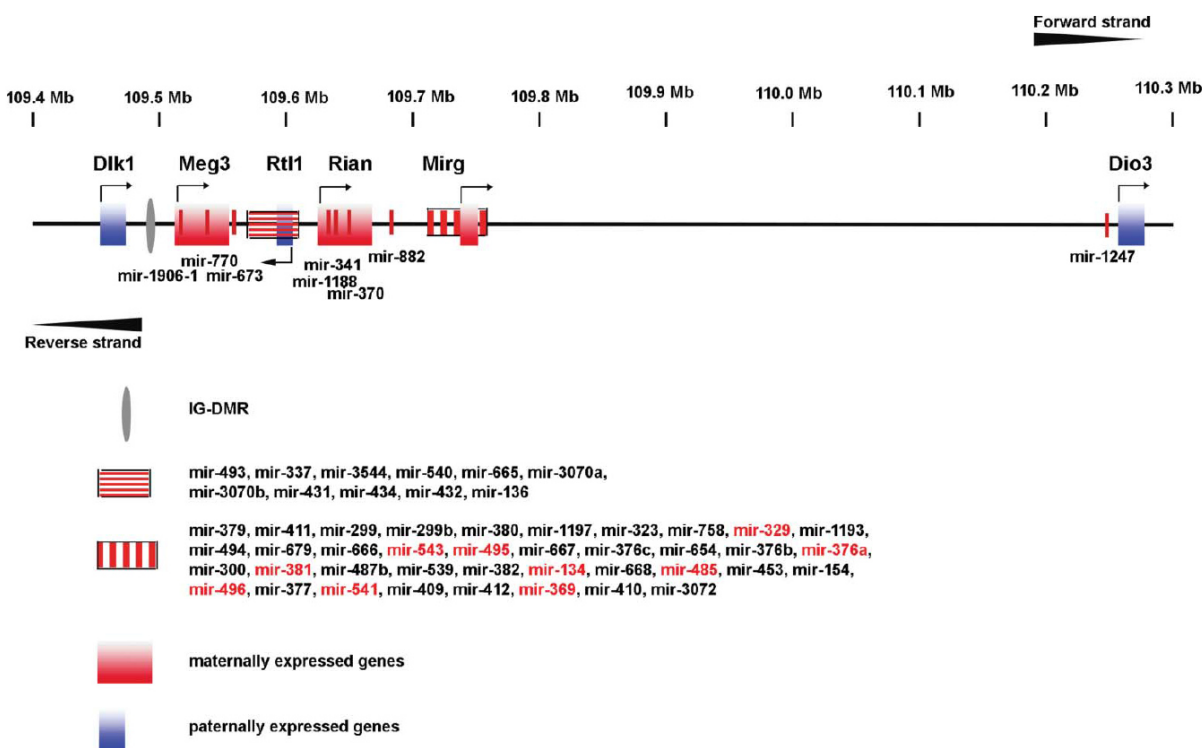
Figure 4: miR379-410 cluster at the imprinted Dlk1-Dio3 domain. Schematic representation of the ~1-Mbp imprinted Dlk1-Dio3 region on mouse distal chromosome 12 (GRCm38/mm10 Assembly). Genes, long non-coding RNAs and miRNAs are noted. microRNAs from the miR379–410 cluster that have been investigated so far in functional studies are highlighted in red. Please note that pseudogenes and small nucleolar RNAs (snoRNAs) are not shown for simplicity (for more details see *Seitz et al., 2004; Labialle et al., 2014*). Graph adapted from *Winter, 2015.*

1.5 microRNAs of the miR379-410 cluster and their function in the brain

Several miRNAs from the miR379-410 cluster have been analyzed in detail in the context of nervous system development and function. One of the most intensely studied microRNAs from the miR379-410 cluster is miR-134. The brain-enriched miR-134 was one of the first miRNAs for which a function at the synapse has been described *in vitro* (*Schratt et al., 2006; reviewed in Schratt 2009*). Further, it has been shown *in vivo* that miR-134 controls long-term potentiation (LTP) and memory formation via a pathway that contains the histone deacetylase Sirtuin 1 (SIRT1) and Creb1 (*Jimenez-Mateos et al., 2012; Gao et al., 2010*). SIRT1 represses miR-134 transcription by binding to two sites that are located approximately 1 kb and 4 kb upstream of miR-134 in the genome. In the absence of SIRT1, miR-134 levels are elevated, leading to enhanced repression of Creb1, reduced BDNF expression and impaired hippocampal LTP (*Gao et al., 2010*). Further, expression of several miRNAs from the cluster

- miR-134, -329, -381, -485, -495 and miR-541 – was found to be induced by neuronal activity, suggesting that they could be relevant for the control of neuronal maturation and function (*Fiore et al., 2009; Cohen et al., 2011*). Accordingly, it was shown that inhibition of miR-134, -329 and -381, but not miR-495 or miR-541, blocks activity-induced dendritogenesis in rat hippocampal neurons. Pumilio2 (Pum2), a dendritically expressed RNA-binding protein that acts mainly as a translational repressor (*Fiore et al., 2009; Vessey et al., 2006*), was identified as the key target mediating these effects. Intriguingly, *Fiore et al. (2014)* demonstrated in primary rat hippocampal neurons that the miR-134-dependent regulation of Pum2 is further necessary for homeostatic synaptic depression, a specific form of synaptic plasticity triggered by the chronic activation of neural networks. Furthermore, *Cohen et al. (2011)* demonstrated that miR-485 is required for homeostatic synaptic plasticity by targeting the synaptic vesicle protein SV2A. In addition, miR-369, -496 and miR-543 regulate neurogenesis and neuronal migration by fine-tuning levels of N-cadherin (*Rago et al., 2014*). Most of the neuron-expressed miRNAs, including members of the miR379-410 cluster, are enriched in the cytoplasm of neurons. However, recent evidence raised that mature miRNA localization is not restricted to the cytoplasm, but that some miRNAs can re-enter the nucleus where they may be involved in transcriptional gene silencing (*Khudayberdiev et al., 2013*). In another study, *Bicker et al. (2013)* showed that DHX36, a DEAH-box helicase, plays an important role in dendritic localization of pre-miR-134, thereby affecting synaptic protein synthesis and plasticity. Together, these findings indicate a rather complex regulation of individual miRNAs within the miR379-410 cluster (as summarized in **Table 1**), which might also explain their pleiotropic functions in diverse neurodevelopmental processes. Overall, the detailed analysis of miR-134 in cultured neurons and *in vivo* provides an interesting example of how a single miRNA can exert multiple functions in post-mitotic neurons by regulating different targets depending on the spatiotemporal context. Although first *in vivo* evidences of miR379-410 function have been reported which suggest a potential role in homeostatic synaptic plasticity and cognitive processes (*Cohen et al., 2011; Jimenez-Mateos et al., 2012; Gao et al., 2010*), the role of the whole cluster with its 38 miRNAs in higher brain functions has not been comprehensively investigated.

Table 1: miRNAs of the miR379-410 cluster are important regulators of neuronal function. Table adapted from *Winter, 2015*.

Mir379–410 cluster miRNA	Brain targets	Brain-specific function	Involvement in brain disorders	Reference
miR-134	Pum2, Chrdl-1, Dcx, Limk1, CREB	Promotes NPC proliferation, inhibits neuron migration, sensitizes neurons to BMP-induced neurite outgrowth, activity-induced, promotes activity-induced dendritogenesis, inhibits spine growth and density	Silencing miR-134 is neuroprotective in a mouse epilepsy model; downregulated in PBMCs from schizophrenia patients; upregulated in dorsolateral PFC Brodmann area 46 in schizophrenia	25,28,29,46,50-52
miR-154	—	—	Downregulated in PBMCs from schizophrenia patients, Upregulated in cerebellum in Mecp2 KO mice, downregulated in glioma	52,54,57
miR-299	—	—	Upregulated in cerebellum in Mecp2 KO mice, downregulated in glioma	54,57
miR-300	—	—	Upregulated in cerebellum in Mecp2 KO mice	54
miR-323–3p	—	—	Downregulated in PBMCs from schizophrenia patients, Upregulated in cerebellum in Mecp2 KO mice, downregulated in glioma	52,54,57
miR-329	—	Activity-induced, promotes activity-induced dendritogenesis	Downregulated in PBMCs from schizophrenia patients	28,52
miR-369–3p	N-cadherin	Promotes neuronal differentiation, inhibits neuronal migration	Upregulated in cerebellum in Mecp2 KO mice, downregulated in glioma	21,54,57
miR-376a	Hes5	Promotes neuronal differentiation	Upregulated in lymphoblastoid cell lines from ASD patients, downregulated in glioma	30,53,57
miR-377	—	—	Upregulated in cerebellum in Mecp2 KO mice	54
miR-380	—	—	Upregulated in cerebellum in Mecp2 KO mice	54
miR-381	—	Activity-induced, promotes activity-induced dendritogenesis	Upregulated in cerebellum in Mecp2 KO mice, downregulated in glioma	28,54,57
miR-382	—	—	Upregulated in cerebellum in Mecp2 KO mice	54
miR-409–3p	—	—	Downregulated in PBMCs from schizophrenia	52
miR-410	—	—	Downregulated in PBMCs from schizophrenia patients, upregulated in cerebellum in Mecp2 KO mice	52,54
miR-485	SV2A	Activity-induced, inhibits spine density and maturation, inhibits spontaneous synaptic activity	Downregulated in PBMCs from schizophrenia patients	25,26,52
miR-487b	—	—	Downregulated in PBMCs from schizophrenia patients, upregulated in glioblastoma	52,56
miR-495	—	Activity-induced	Downregulated in lymphoblastoid cell lines from ASD patients, upregulated in cerebellum in Mecp2 KO mice	28,53,54
miR-496	N-cadherin	Promotes neuronal differentiation, inhibits neuronal migration		21
miR-541	—	Activity-induced		28
miR-543	N-cadherin	Promotes neuronal differentiation, inhibits neuronal migration	Upregulated in cerebellum in Mecp2 KO mice, downregulated in glioblastoma	21,54,56
miR-544	—	—	Downregulated in PBMCs from schizophrenia patients, upregulated in cerebellum in Mecp2 KO mice	52,54
miR-654–5p	—	—	Downregulated in PBMCs from schizophrenia patients	52

1.6 microRNAs in CNS-related diseases

miRNAs in the brain play an important role in neuronal morphogenesis, development and synaptic plasticity. Therefore, it is not surprising that impaired miRNA function has been implicated in a wide range of neurodevelopmental and psychiatric diseases (reviewed in *McNeil & Van Vactor, 2012; Issler & Chen, 2015*). Numerous examples of how miRNAs are associated with specific disorders were demonstrated in the past years. Fragile X syndrome (FXS) is an X chromosome-linked disorder characterized by intellectual disability (ID) and

represents the most frequent monogenetic cause of autism. The FMR1 gene encodes the fragile X mental retardation protein (FMRP) whose loss-of-function is responsible for FXS. FMRP interacts with Argonaute proteins and is associated with several plasticity-relevant miRNAs, like miR-9, -124, -125a-b, -128, -132 and miR-219 (*Edbauer et al., 2010; Xu et al., 2008*). Two of the FMRP-associated miRNAs, miR-125b and miR-132, have been shown to regulate dendritic spine morphology and glutamatergic neurotransmission in an opposite manner. A large-scale genome-wide association study of schizophrenia (SCZ) patients revealed that a single nucleotide polymorphism (SNP) located in the MIR137 gene was among the most significant SNPs associated with the disease (Schizophrenia Psychiatric GWAS Consortium, 2011). Interestingly, miR-137 gain-of-function *in vivo* resulted in impaired presynaptic function and deficits in hippocampus-dependent learning and memory accompanied by LTP impairments (*Siegert et al., 2015*). Several lines of evidence suggest that miRNAs of the miR379-410 cluster might also be involved in CNS-related diseases, namely ASD, SCZ and bipolar disorder (BD). First, *Santarelli et al. (2011)* found numerous miRNAs from the cluster, including miR-134, -154, -323-3p, -329, -409-3p, -410, -487b, -544 and miR-654-5p that are significantly down-regulated in peripheral blood mononuclear cells from SCZ patients. In contrast, two miRNAs from the cluster, miR-134 and miR-382, were upregulated in the dorsal prefrontal cortex (Brodmann area 46) in postmortem samples of SCZ individuals (*Gardiner et al., 2012*). In a genome-wide integrative analysis, expression of several miR379-410 members was found to be dysregulated in post-mortem brain samples from autism individuals (*Wu et al., 2016*). In two studies employing the Mecp2 mouse model of Rett syndrome (RTT), members of the miR379-410 cluster, including miR-134, were strongly overrepresented among the upregulated miRNAs in the cerebellum (*Wu et al., 2010*; *Chen et al., 2014*). In addition, indications for impaired miR379-410 expression have been found in a mouse model of the 22q11.2 microdeletion syndrome, the strongest genetic cause of SCZ in humans (*Karayiorgou et al., 1995; Stark et al., 2008; Xu et al., 2013*). *Stark et al. (2008)* observed alterations in the biogenesis of brain-expressed miRNAs in this model, among them several members of the miR379-410 cluster. These global impairments in miRNA biogenesis were attributed to the lack of Dgcr8, a microprocessor complex protein that is encoded in the genomic region deleted in this model. More recently, it was demonstrated in dendrites of rat hippocampal neurons, that a transcript variant of Ube3a (Ube3a-1), which is mutated in Angelman syndrome (AS) and found to be upregulated in ASD patients, acts as a competing endogenous RNA for miR379-

410 (*Valluy et al., 2015*). Further, *Rong et al. (2011)* observed that miR-134 plasma levels can be used as diagnostic tool for BD patients. Taken together, accumulating evidence points to an important contribution of miR379-410 dysregulation in the etiology of neurodevelopmental diseases, in particular ASD and SCZ.

1.7 Excitatory and inhibitory synaptic transmission

The human brain is a very complex organ that acts as an information-processing unit in the CNS. Synapses are specialized connections between neurons that allow neuronal cells to communicate with each other, an event that is described as synaptic transmission (*Kandel et al., 2012*). These inter-neuronal communications are an essential process in the nervous system to initiate and refine neuronal networks and circuits. Neuronal connectivity allows to process all necessary functions of the brain, from simple reflexes to higher brain functions, such as social behaviour. As summarized in **Figure 5**, two functionally different types of chemical synapses exist in the mammalian brain: Excitatory and inhibitory synapses (reviewed in *Gao & Penzes, 2015*). Both classes can be found on pyramidal and interneuronal cells. While the excitatory, glutamatergic synapses are localized mostly on dendritic spines, the inhibitory, GABAergic synapses are present along the dendritic shaft, somata and axon initial segments (*Penzes et al., 2011; Fritschy & Brünig, 2003*). Glutamate is the major neurotransmitter at excitatory synapses. Before it is released into the synaptic cleft, it is packed into vesicles at the presynaptic side with the help of vesicular glutamate transporters (vGLUTs). After vesicle release it acts on postsynaptic receptors where it causes depolarization of the postsynaptic cell. Anatomically, excitatory synapses contain an electron-dense postsynaptic density (PSD) that is located opposite from the presynaptic active zone. It harbors the postsynaptic density protein-95 kDa (PSD-95), a multimeric scaffold protein that anchors two major types of ionotropic glutamate receptors: The 2-amino-3-(3-hydroxy-5-methyl-isoxazol-4-yl) propanoic acid receptor (AMPA-R) and the N-methyl-D-aspartate receptor (NMDA-R) (*Okabe, 2007; Bekkers & Stevens, 1989*). It is worth to mention that AMPA-receptors have a much lower affinity for glutamate than NMDA-receptors. Therefore, the fast component of excitatory postsynaptic currents (EPSCs) in neurons is mediated by AMPA receptors, whereas the slower decay of the EPSC is provided by NMDA receptors. Besides PSD-95, other prominent proteins belong to the PSD, such as the scaffolding proteins Shank/ProSAP (e.g. Shank1-3) and Discs large associated proteins 1-

4 (DLGAP1-4) (*Boeckers et al., 2002; Sala, et al., 2015; Rassmussen et al., 2017*). The complex interplay between PSD proteins and the AMPA-/NMDA-receptors is important for the regulation of excitatory postsynaptic transmissions at glutamatergic synapses.

On the other side, gamma-Aminobutyric acid (GABA) and glycine are the neurotransmitters at inhibitory synapses. At the presynaptic side, they are packed into vesicles with the help of vesicular GABA transporters (vGATs). When released into the synaptic cleft, they act on postsynaptic $GABA_A$- and glycine receptors which are the major inhibitory receptors in the CNS. One hallmark of inhibitory synapses is the absence of a PSD. Nevertheless, scaffolding proteins, such as gephyrin, exist at the inhibitory synapse. Gephyrin interacts with cytoskeletal elements and stabilizes glycine receptors and individual subtypes of GABA receptors (*Meyer et al., 1995; Lynch, 2004*). Both types, excitatory and inhibitory synapses are held together by trans-synaptic interactions between pre-synaptic and postsynaptic cell adhesion molecules, such as neurexin and neuroligin (*Gatto & Broadie, 2010*).

Information transfer in the brain relies on a functional network balance between excitatory and inhibitory synaptic transmission. Emerging evidence gathered over the last years implicates disturbed structure and/or function of synapses to neurodevelopmental and psychiatric diseases, such as ASD and SCZ (*Cohen & Greenberg, 2008; Ebert & Greenberg, 2013*). These defects can lead to impaired excitatory and inhibitory ratios (E/I imbalance) that result in hyper- or hypoactivation of specific brain regions. It was even speculated that the commonly found disturbances in the E/I balance could at least partly explain the large degree of overlap in pathophysiological symptoms between different neuropsychiatric conditions, such as defects in social communication (*Baroncelli et al., 2011; Gogolla et al., 2014*). For instance, postmortem studies in ASD and SCZ individuals demonstrated structural and functional changes in both glutamatergic excitatory and GABAergic inhibitory circuits (*Hutsler & Zhang, 2010; Chattopadhyaya & Cristo, 2012; Glausier & Lewis, 2013*). Moreover, optogenetic manipulation of specific excitatory and inhibitory circuits demonstrated a direct link to altered social and cognitive behaviour in mice (*Yizhar et al. 2011; Tye & Deisseroth, 2012*). Overall, findings from animal models suggest that disturbed E/I balance during postnatal development can contribute to neurodevelopmental and psychiatric disorders.
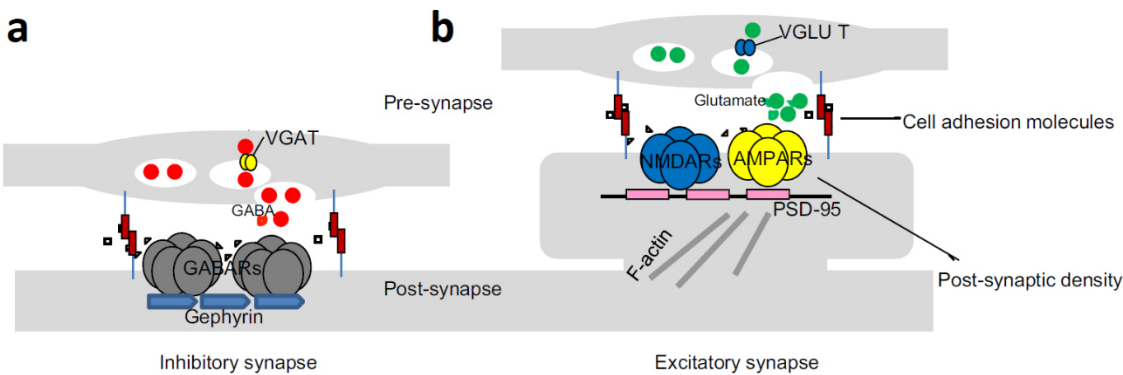
Figure 5: Schematic overview of excitatory and inhibitory synapses on pyramidal cells. a, Inhibitory synapses. **b,** Excitatory synapses. Please refer to 1.7 for more details. Graph adapted from *Gao & Penzes, 2015*.

1.8 The social brain

Social behaviours among conspecifics are crucial for health, survival and development of mammals (reviewed in *Chen & Hong, 2018*). It is one of the most complex interplay that animals and humans can perform. Social behaviour depends on the ability to properly communicate with other individuals, interpret social cues and finally respond with appropriate behaviours. Our understanding of the "social brain" with its multiple brain regions and neural circuits that are related to social behaviours accumulated in the previous years. It is believed that inadequate stimulation and social-related input processing of the social brain can lead to social disabilities. Several key brain regions were identified to participate in different aspects of social behaviour, such as the medial prefrontal cortex (mPFC), the amygdala and the hippocampus (*Frith, 2007; Barak & Feng, 2016; Ko, 2017; Montagrin et al., 2017*). The prefrontal cortex is the most broad and complex member of the neuronal network that has been implicated to social behaviour through its massive reciprocal connections to other brain regions (*Ko, 2017*). While the lateral prefrontal cortex (lPFC) is more involved in semantic and episodic memory, the mPFC is more related to associative information processing and social cognition (*Li et al., 2013*). Another essential brain region is the amygdala that is part of the limbic system. The amygdala is specialized for input and processing of anxiety, emotion and social recognition (*Yang & Wang, 2017; Barak & Feng, 2016*). Interestingly, both key brain regions modulate anxiety and social behaviour through projections from the amygdala to the mPFC (*Felix-Ortiz et al., 2016*). Although, the hippocampus has been traditionally associated with long-term, declarative or

episodic memory, new evidences arose over the last years that implicate the region also in the control of social behaviour and emotional responses (*Montagrin et al., 2017; Bannerman et al., 2014; Rubin et al., 2014*). Recently, *Hitti & Siegelbaum (2014)* elegantly demonstrated in a transgenic mouse model with inactivated CA2 pyramidal neurons that this specific hippocampal area is essential for social memory. Moreover, optogenetic investigations indicated that amygdala inputs to the ventral hippocampus (vCA1) are proficient to modulate social behaviours in mice (*Felix-Ortiz & Tye, 2014*). In addition to the key brain regions of the social brain, one of the most studied molecular mechanisms related to social behaviour concerns the neuropeptide oxytocin (*Fineberg & Ross, 2017*). It is synthesized in the hypothalamus and released by the posterior pituitary where it then extensively affects the CNS (*Heinrichs et al., 2009*). For instance, it was demonstrated in oxytocin-null mice by *Ferguson et al. (2000)* that this neuropeptide is essential for social memory. Taken together, studies conducted in animal models indicate that different neural circuit mechanisms underlie the complex regulation of social behaviour. One of the main challenges is undoubtedly the behavioural phenotyping of animal models related to neurodevelopmental and psychiatric diseases. Further studies are needed together with the development of advanced animal models in rodents and primates to decipher social behaviour and circuits in more detail (*Birling et al., 2017; Niu et al., 2014; Bauman & Schumann, 2018*).

1.9 Behavioural assays to model neurodevelopmental disorders in rodents

Animal models on the one hand provide a powerful research tool to understand the cause of human diseases and to identify novel therapeutic treatments. On the other hand, they present a unique challenge to the correct modelling and interpretation of specific diseases. As illustrated in **Figure 6**, studying disease-relevant phenotypes in mice requires optimal animal ages.

Neurodevelopmental diseases, including ASD, ID and SCZ, are characterized by a wide range of syndromes with diverse symptoms including cognitive impairments, social abnormalities, anxiety, depression and seizures among others (*Jeste & Tuchman, 2015; Castren et al., 2012*). Comorbidity, such as anxiety and epilepsy, is often observed in patients suffering from ASD. Genetic defects have been found that are associated with high rates of ASD and SCZ, including the 22q11.2 deletion syndrome, Shank3 mutations and duplication in the

Williams syndrome locus 7q11.23 (*Tebbenkamp et al., 2014*; Schneider et al., 2014*; Guiltmatre et al., 2014*). ASD is beyond doubt one of the most prominent neurodevelopmental disorders. Autism is estimated to affect about 1% of people worldwide and is currently diagnosed by the Diagnostic and Statistical Manual of Mental Disorders (DSM-5) into two categories of behavioural core symptoms (*Lord et al., 2015*). The first category includes impaired social interaction and communication, whereas repetitive behaviour belongs to the second one. Patients suffering from ASD display specific impairments in social approach, eye contact, joint attention, delayed language development and trouble in understanding intensions, nuances of words or body language of other people. In case of neurodevelopmental disorders, the following assays were established in mice to determine core symptoms of ASD. The evaluation of ultrasonic vocalizations (USVs) during juvenile play behaviour in the reciprocal social interaction test provides an excellent tool to determine vocal communication and social skills in mice (reviewed in *Silverman, 2010; Wöhr & Scattoni, 2013, Wöhr et al., 2015*). For instance, *Scattoni et al. (2013)* observed in juvenile BTBR T+ tf/J mice, an established mouse model of autism, reduced social interaction behaviours and emitted USV calls. The three-chamber social approach and memory assay, that was first established by *Nadler et al. (2004)*, is a less sensitive sociability test as only one subject can freely explore and interact with another animal that sits under a wire cage. Nevertheless, it became a standard tool to determine not only social deficits, but also (social) memory in mice (reviewed in *Silverman, 2010*). For instance, *Peca et al. (2011)* observed in a three-chamber assay reduced social preference and disturbed social memory in Shank3B ko mice, a highly relevant mouse model of ASD. To evaluate repetitive behaviour in mice, self-grooming and the marble burying test became reliable assays in rodents (reviewed in *Kim et al., 2016*). In the previously mentioned Shank3B ko mouse model, *Peca et al. (2011)* further discovered excessive grooming behaviour in these animals that resulted in severe skin lesions. However, about 75% of people suffering from ASD have general intellectual disabilities. To evaluate cognitive functions in mouse models, standard learning and memory tasks, such as novel object recognition, Morris water maze and T-maze tests can be performed. Mice carrying a haploinsufficiency in the AT-rich interactive domain 1B (ARID1B) gene, that causes ASD and ID in humans, displayed - besides social impairments and increased grooming behaviour - disabilities in spatial learning (Morris water maze), working memory (T-maze) and novel object memory (*Jung et al., 2017*).

Taken together, comprehensive behavioural assays have to be conducted to cover all symptomatic aspects of neurodevelopmental disorders, as successfully demonstrated in Shank1 and Shank3 ko mouse models among others (*Silverman et al., 2011; Wang et al., 2011; Peca et al., 2011*), to link the observed phenotype to the appropriate syndrome. Interestingly, the ASD risk genes Shank1 and Shank3 belong to neurotransmitter complexes present at excitatory synapses, indicating an involvement in homeostatic compensation deficits that can lead to neurodevelopmental diseases (reviewed in *Jiang & Ehlers, 2013; Ebert & Greenberg, 2013*). Although behavioural phenotyping assays in rodents can help to determine neurodevelopmental disorders, it is important to keep in mind that many affective and emotional responses are restricted to and uniquely present in humans. Therefore, behavioural investigations have to be carefully conducted to avoid over-interpretation of behavioural phenotypes. Nevertheless, phenotyping behavioural assays can be a powerful tool in basic research to pave the way towards clinical application, ideally in combination with other model systems and approaches, such as *in vitro* assays (e.g. in primary neuronal culture, human induced pluripotent stem cells), proteomics (e.g. liquid chromatography mass spectrometry), high-throughput genomic screens (e.g. microarrays, RNA sequencing) and bioinformatic predictions.
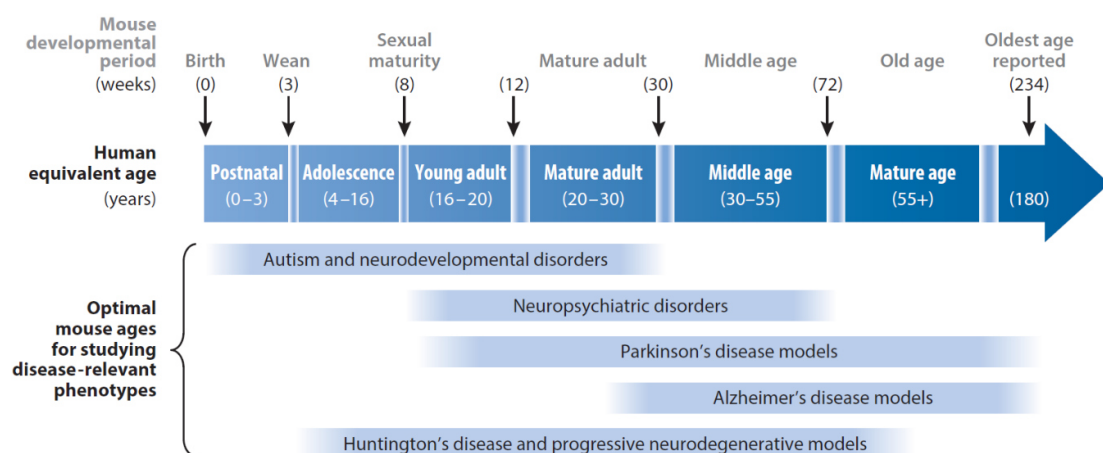
Figure 6: Optimal mouse ages for studying CNS-related diseases. Behavioural phenotyping assays should be matched to the specific human symptoms relevant to that stage of life. Graph adapted from *Sukoff Rizzo & Crawley, 2017.*

1.10 Aim of the thesis

There is growing evidence that non-coding RNAs, in particular miRNAs, play a key role as regulators of fundamental processes in the nervous system. However, these insights are mostly gleaned from studies performed in *ex vivo* systems, such as primary neuronal cultures and tissue explants, and real *in vivo* studies involving genetically modified animal models are still scarce. This is particularly true for the study of complex behaviours displayed preferentially by higher developed animals, such as social behaviour and emotion.

The paternally imprinted placental mammal-specific miR379-410 miRNA cluster, which encompasses 38 miRNAs, appears to play an important role in synapse development and plasticity and has further been associated with several neurological diseases (reviewed in *Winter, 2015; Seitz et al., 2004; Wu et al., 2016*). Previously, our laboratory identified miRNAs of the miR379-410 cluster and their targets that are involved in dendrite and spine morphogenesis in rat hippocampal neurons. Further, activity-dependent miRNAs from the cluster were described that are relevant for specific forms of synaptic plasticity (*Schratt et al., 2006, Fiore et al., 2009, Fiore et al., 2014; Valluy et al., 2015*). Overall, these findings indicate that members of the miR379-410 cluster are important synaptic regulators in mammalian neurons. Therefore, we hypothesized that the miR379-410 cluster in the mammalian brain might play an important role in the control of complex behaviours and cognition associated with proper development and plasticity of neural circuits. To address this hypothesis, the aim of my thesis was to investigate the (patho)physiological relevance of the miR379-410 cluster in the rodent brain during animal's lifespan using a loss-of-function mouse model. Therefore, a constitutive miR379-410 ko mouse model was characterized on the behavioural, cellular and molecular level. First, ko animals were investigated in extensive behavioural assays. Next, the morphology of dendritic spines in hippocampal pyramidal neurons was analyzed as a proxy for the development of excitatory synaptic connections. Finally, transcriptomic analysis of ko mouse hippocampi was performed in order to identify potential direct target candidates of the miR379-410 cluster that could be involved in the control of cellular and behavioural phenotypes.

In summary, this study aimed at contributing to a better understanding of the physiological role of the largest placental mammal-specific miRNA cluster during brain development, thereby providing first links to its potential involvement in neurodevelopmental and psychiatric diseases, such as ASD and SCZ.

2. Materials and Methods

2.1 Chemicals

If not otherwise mentioned, standard chemicals were purchased from Sigma (Steinheim, Germany), Fluka (Steinheim, Germany), Carl Roth (Karlsruhe, Germany), Invitrogen (Karlsruhe, Germany), Roche (Basel, Switzerland), Merck (Darmstadt, Germany) and AppliChem (Darmstadt, Germany). The ddH$_2$O used for solutions was prepared with Milli-Q-Water System (Millipore, Schwalbach, Germany).

2.1.1 Chemicals and reagents

Acetic acid, Carl Roth

Albumin, ApplChem

(2R)-amino-5-phosphonovaleric acid (AP5), Tocris

Aqua-Poly/Mount, Polysciences

Chloral hydrate, Sigma-Aldrich

1,4-Dithiothreitol (DTT), Sigma-Aldrich

Dabco, Sigma-Alderich

D-amphetamine sulfate, Sigma-Aldrich

DNA Gel Loading Dye, Thermo Scientific

Dulbecco's Phosphate-Buffered Saline (DPBS), Life Technologies

Ethylenediaminetetraacetic acid (EDTA), Sigma-Aldrich

Ethidium bromide (EtBr), Carl Roth

5-fluorodeoxyuridine (FUDR), Sigma-Aldrich

Gelatine, Carl Roth

Glucose, Sigma-Aldrich

Glycerol, Sigma-Aldrich

Hydrochloric acid (HCL), Carl Roth

4-(2-hydroxyethyl)-1-piperazineethanesulfonic acid (HEPES) Sigma-Aldrich

Hoechst, Invitrogen

Ketchum Green Tattoo Paste, Ketchum Manufacturing Inc.

Laminin, BD Biosciences

LB Broth, Sigma-Aldrich

Lipofectamine 2000, Invitrogen

Lipofectamine RNAiMax, Invitrogen

Magnesium acetate (MgAc), Fisher Scientific

Magnesium chloride (MgCl2), Carl Roth

Methanol, VWR Chemicals

Milk powder, Carl Roth

Paraformaldehyde, Carl Roth

Phenol, Carl Roth

Poly-L-Lysine, Sigma-Aldrich

Poly-L-Ornithine, Sigma-Aldrich

Polyvinyl alcohol, Sigma-Aldrich

Precision Plus Protein Dual Color Standard, Bio-Rad

Sodium azide, Carl Roth

Sodium chloride (NaCl), Carl Roth

Sodium deoxycholate (NaDOC), Sigma-Aldrich

Sodium dodecyl sulfate (SDS), Carl Roth

Sucrose, Carl Roth

Tris(hydroxymethyl)aminomethane (Tris), Carl Roth

Triton X-100, Carl Roth

Tween 20, Carl Roth

2.1.2 Enzymes and inhibitors

Turbo DNase, Ambion

Complete Protease inhibitors, Roche

PfuPlus! DNA Polymerase, Roboklon

2.1.3 Kits

Amersham ECL Prime Western Blotting Detection Reagent, GE Healthcare

Dual-Luciferase Reporter Assay System, Promega

iScript cDNA synthesis Kit, Bio-Rad

TaqMan MicroRNA Reverse Transcription Kit, Applied Biosystems

iTaq SYBR Green Supermix with ROX, Bio-Rad

Kapa Mouse Genotyping Kit, Merck

mirVanaTM Isolation Kit, Ambion

Pierce BCA Protein Assay Kit, Thermo Scientific

QuickChange Site-Directed mutagenesis kit, Stratagene

2.1.4 Buffers and solutions

50x TAE buffer:	2 M Tris-acetate
	50 mM EDTA
KCM solution:	100 mM KCL
	30 mM CaCl2
	50 mM MgCl2
10x RIPA:	0.5 M Tris pH 8.0
	1.5 M NaCl
	10% Triton X-100
	5% NaDOC
	0.5% SDS
	20 mM EDTA
RIPA (+):	1 pellet proteinase inhibitor (complete EDTA-free, Roche) ad
	50 ml 1x RIPA solution
4x Laemmli sample buffer:	250 mM Tris-HCl (pH 6.8)
	8% SDS
	40% glycerol
	8% β-mercaptoethanol
	0.04% bromophenol blue
	TBS-T: 50 mM Tris
	150 mM NaCl
	0.1% Tween 20
	pH 7.5
Running buffer:	25 mM Tris
	192 mM glycine
	0.1% SDS
Blotting buffer:	25 mM Tris

	192 mM glycine
	20% methanol
8% lower gel:	3.5 ml ddH20
	1.875 ml 1.5 M Tris
	2ml 30% Acrylamide
	37,5 µl APS
	15 µl TEMED
4% upper gel:	1.5 ml ddH20
	625 µl 0.5 M Tris
	325 µl Acrylamide
	12.5 µl 10% APS
	5 µl TEMED
PBS+NaN3	0.02 % (w/v) NaN3 in 1x PBS
4 % PFA	4 % (w/v) PFA in 1x PBS
Embedding medium	45 g albumin
	0.75 g gelatine
	in 150 ml 0,1 M phosphatbuffer
	1.5 ml 2% sodium azide

2.1.5 Cells and culture media

Growth medium (NB+):	Neurobasal medium (NB) Invitrogen
	2% B27 supplement Invitrogen
	1 mM GlutaMax Invitrogen
	100 U/ml Penicillin/Streptomycin Invitrogen
Transfection medium (TM):	Neurobasal medium (NB) Invitrogen
	2% B27 supplement Invitrogen
	1 mM GlutaMax Invitrogen
L15+H (medium to collect mouse tissue):	Leibovitz`s L15 medium (Life Technologies, Carlsbad, CA, USA) with 7 mM HEPES (L15+H)

2.1.6 Laboratory equipment

Cell culture plates (6-well, 24-well), Corning

Microcentrifuge Biofuge fresco, Heraeus

Microcentrifuge Biofuge pico, Heraeus

Mid bench centrifuge Multispeed PK121R, ALC

ELX808 Ultra Microplate Reader, Bio-Tek Instruments

Plastic stamper Micropistill, Eppendorf

Coverslips, Carl Roth

Digital gel documentation system E-Box, Vilber

Elevated Plus Maze, home made

Eppendorf reaction tubes (1.5 ml/2 ml), Eppendorf

Film developing machine Curix 60, AGFA

GloMax R96 Microplate Luminometer, Promega

Hyperfilm ECL, GE Healthcare

Light-Dark Box, TSE Systems

Makrolon Polycarbonate Breeding/Home Cages, Ehret Life Science Solutions

Microtiter plate (96-well), Nunc

Microplates 96-well, Greiner Bio-One

Mini-PROTEAN Tetra Vertical Electrophoresis Cell, Bio-Rad

MJ Mini Personal Thermal Cycler, Bio-Rad

Mouse-E motion universal data logger, Infra-E-Motion GmbH

Nano Drop 2000c, Thermo Scientific

Neubauer cell counting chamber, Marienfeld-Superior

Olympus Multiphoton microscopy BX36, Olympus

Olympus IR-Laser-1 INSIGHT DS-OL, Olympus

Open field box, TSE Systems

PVDF membrane, Millipore

Step One Plus Instrument, Applied Biosystems

Thermal cycler S1000TM, Bio-Rad

Three-chamber apparatus, home made

Vibratome VT1000S, Leica

2.1.7 Software

The following software were used to collect, manage and analyze the data:

Avisoft-SAS Lab Pro software, Avisoft Bioacoustics

GraphPad Prism 6, GraphPad Software Inc.

SPSS 21, IBM

ImageJ 1.46, NIH

FluoView FV30S-SW, Olympus

FG3xcap, HaSoTec GmbH

Mini Analysis Program, Synaptosoft Inc.

Mouse-E Motion software 2.3.6, Infra-E-Motion GmbH

Observer XT10, Noldus Information Technologies

VideoMot2, TSE Systems

TargetScan 7.1 (2016), David Bartel Lab

R, R development core team

Cytoscape 3.4.0, Cytoscype development core team

StepOne Software v2.1, Applied Biosystems

MS Office, Microsoft

KC junior v.<1.10, Bio-Tek Instruments

2.2 Animals and housing

All animal experiments were performed in accordance with the animal protection law of Germany and were approved by the local authorities responsible for the Philipps University Marburg (Regierungspräsidium, Gießen, Germany). For reciprocal social interaction test, Pnd22 juvenile mice were housed in isolation for 24h before testing. Otherwise, all rodents were housed under standard cage conditions with food and water ad libitum and maintained on a 12 h / 12 h light/dark cycle. Sprague-Dawley rats (Harlan-Winkelmann, Borchen, Germany) were used for rat cell culture preparation. The miR379–410 constitutive ko mouse was generated at Taconic Artemis (Cologne, Germany) and described previously (*Valluy et al., 2015*). We compared wildtype (wt) littermate controls to heterozygote miR379-410 animals (for simplicity termed "miR379-410 ko") that received the cluster deletion from the maternal allele. Due to the paternal-imprinted character of the miR379-410 gene cluster, miR-379-410 miRNAs are not expressed in the latter animals as previously

demonstrated (*Valluy et al., 2015*). Thy1-GFP reporter mice were provided by Marco Rust (Philipps University Marburg). For three-chamber social memory test, stimulus C57BL/6N mice were taken, provided by Charles River (Sulzfeld, Germany).

2.3 Cell culture, transfection and stimulation

2.3.1 Rat primary neuronal cell culture

Primary cultures of embryonic day 18 (E18) old Sprague Dawley rats (Charles River Laboratories, Sulzfeld, Germany) hippocampal (HC) and cortical neurons (CTX) were done as described previously in the protocol (*Schratt et al., 2006*) with minor modifications and routinely prepared by Eva Becker, Renate Gondrum, Ute Beck and Heinrich Kaiser. After dissociation, rat cortical neurons were directly plated on Poly-L-Ornithine (Sigma, Steinheim, Germany) coated 24-well plates. Rat hippocampal neurons were plated on nitric acid-treated coverslips that were coated with Poly-L-Lysine and Laminin in a 6-well or 24-well format.

2.3.2 Mouse primary neuronal cell culture

Primary neurons were cultured in Neurobasal medium (NB+) at 37 °C and 5% CO2. Primary cultures of miR379-410 mice hippocampal neurons from Pnd1 old pups were performed, using the same procedure as for the rat culture, except from following changes. Each hippocampus was dissected and later collected in Leibovitz`s L15 medium (Life Technologies, Carlsbad, CA, USA) with 7 mM HEPES (L15+H) in a 1.5 ml reaction tube. Afterwards, L15+H medium was carefully removed and 500µl of TrypLE Express was added for 7 min at 37°C by gently inversing the tube every minute for three times. Then, TrypLE Express was carefully removed from the cells and washed twice with pre-warmed NB+. Dissociation of the cells were done in 500µl NB+ by pipetting cells carefully with a combination of a 1000µl and 200µl pipette tip. Afterwards, cells were counted with a Neubauer cell counting chamber according to the manufacturer's instructions. Cells, with a density of 110.000/per well (24-well format), were plated on Poly-L-Lysine coated coverslips and after 5 h of plating, medium were removed completely and fresh NB+ medium was added to the cells.

2.3.3 Transfection and stimulation of neuronal culture

Neuronal transfections were performed with Lipofectamine 2000 (Thermo Fisher Scientific, Darmstadt, Germany) as described earlier (*Rajman et al., 2017*). Per well (in a 24-well format), a total amount of 1 µg of DNA, balanced with varying amounts of pcDNA3 basic vector, was mixed with a 1:50 dilution of Lipofectamine 2000 in 100 µl Neurobasal medium. Transfection mixes were incubated at room temperature (RT) for 20 min and further diluted 1:5 in NB medium and gently applied to the cells. Neurons were incubated for 2 h at 37 °C and 5% CO_2. Afterwards, cells were washed with NB and incubated with the NMDA-receptor antagonist (2R)-amino-5-phosphonovaleric acid (AP5, 20 µM) in NB+ for 45 min at 37 °C and 5% CO_2 to prevent procedure-induced excitation. After one washing step with NB, cells were provided with one third of fresh NB+ medium mixed with two third of conditioned medium that was collected before the transfection procedure. For stimulation, 18 DIV neurons were treated with Picrotoxin (PTX; 100 µM final concentration; Merck, Darmstadt, Germany) or solvent (ethanol absolute) as vehicle control for the indicated times. Cells were transfected with respective anti-miRs (pLNAs, Exiqon, Vedbaek, Denmark) or miRNA mimics (pre-miR miRNA precursor Ambion, Thermo Fisher Scientific, Darmstadt, Germany).

2.4 miRNA mimics and inhibitors

2.4.1 miRNA mimics: Ambion pre-miR miRNA precursor (Thermo Fisher Scientific, Darmstadt, Germany)

Table 2: List of used miRNA mimics.

Pre-miRNA	Product
pre-miR Negative Control#1	PM 4464058
rno-miR-299a-3p	PM20119
mm-miR-329-3p	PM10406
hsa-miR-377-3p	PM10524
hsa-miR-411-3p	PM13107
hsa-miR-485-5p	PM10837
has-miR-495-3p	PM11526

2.4.2 Anti-miRNAs (pLNAs): miRCURY LNA Power Inhibitor (Exiqon, Vedbaek, Denmark)

Table 3: List of used anti-miRNAs.

Anti-miRNA	Product
Negative control A	199006-100
rno-miR-329-3p	4101481-100
rno-miR-485-5p	4100744-100
has-495-3p	4101229-100

2.4.3 Anti-miRNA oligonucleotides for Western blot analysis

Anti-miR-329-3p, -485-5p, -299 and control LNA anti-miR-518b (miRNA absent in mouse) were produced and purchased by Jørgen Kjems, Dept. of Mol. Biol. and Genetics and Interdisciplinary Nanoscience Center, Aarhus University, Denmark.

2.5 DNA constructs (performed by M. Soutschek)

3' UTRs of Prr7 (NM_001030296.4), Src (NM_009271.3), Cnih2 (NM_009920.4), Dlgap3 (NM_198618.5), JunD (NM_010592.5) and Rgs14 (NM_016758.3) were amplified either from mouse genomic DNA or mouse cDNA and cloned into the pmirGLO dual-luciferase expression vector (Promega, Madison, WI, USA) using the following primers:

Table 4: List of used primer sequences.

Primer	Sequence 5' → 3'
Cnih2_UTR_Fwd	AAACTCGAGAGTATGGTTTATACGTTGGTGAGCTTC
Cnih2_UTR_Rev	TTTGTCGACGCTGGACTCCTCCAGGCAAC
Dlgap3_UTR_Fwd	AAACTCGAGCCAGACCAGGCTGTGACC
Dlgap3_UTR_Rev	TTTGTCGACTTCCGGTGCAGTTCTGCGG
JunD_UTR_Fwd	AAACTCGAGTGTACCTCCGAGTAGGGGCTC
JunD_UTR_Rev	TTTGTCGACGGAAACACACACTCAACACGCAAC
Prr7_UTR_Fwd	AAACTCGAGAGGACTACAGCCGTATAGAGG
Prr7_UTR_Rev	TTTGTCGACGTACCAAAGCAGATCACACACC
Rgs14_UTR_Fwd	AAACTCGAGTCCTCTGGCATCTGTGTAACAATC
Rgs14_UTR_Rev	TTTGTCGACCACCAGTACACCCAGGTCTTAC

Src_UTR_Fwd	AAACTCGAGCTCTCTGGAGTTAGCCTGCTTC
Src_UTR_Rev	TTTGTCGACATGGACACAAGGGAAGACACACAG

Mutants of conserved miR binding sites were produced by site directed mutagenesis using PfuPlus! DNA Polymerase (Roboklon) or with the QuickChange Site-Directed mutagenesis kit (Stratagene, San Diego, CA, USA) according to manufacturer`s instructions. The following primers were used for mutagenesis:

Table 5: List of used primer sequences.

Primer	Sequence 5' → 3'
Cnih2_mut_Fwd	GCACTGGTGCCTCCCGGGTCTCCACCCCCCAAACTGCTG
Cnih2_mut_Rev	CAGCAGTTTGGGGGGTGGAGACCCGGGAGGCACCAGTGC
Dlgap3_mut_Fwd	ACCTGTGGCTGTTCTAGAATCCCTTTGAGTATCCCAG
Dlgap3_mut_Rev	TACTCAAAGGGATTCTAGAACAGCCACAGGTGTGGTGAGG
Prr7_mut1_Fwd	TACCCTGTTGAATTCATTTTGAGGATAATAAAGG
Prr7_mut1_Rev	TCCTCAAAATGAATTCAACAGGGTAAGAAATCC
Prr7_mut2_Fwd	ATAATAAAGGTCTAGAATCTGCTTTGGTACGtCG
Prr7_mut2_Rev	ACCAAAGCAGATTCTAGACCTTTATTATCCTCAAAATG
Src_mut_Fwd	GGTGGTTTTCCATCTAGGACCCACTGCGCTCACCTGG
Src_mut_Rev	CCAGGTGAGCGCAGTGGGTCCTAGATGGAAAACCACC

2.6 Luciferase reporter plasmids

Table 6: Plasmids used for luciferase reporter assay.

Plasmid / 3'-UTR	Reference / Company	Miscellaneous features
pcDNA3	Invitrogen	
pmirGlo Cnih2-wt	unpublished	
pmirGlo Cnih2-mut	unpublished	miR-485 binding site mutation
pmirGlo Dlgap3-wt	unpublished	
pmirGlo Dlgap3-mut	unpublished	miR-299 binding site mutation

pmirGlo JunD-wt	unpublished	
pmirGlo Prr7-wt	unpublished	
pmirGlo Prr7-mut	unpublished	miR-329, -377, -411, -495 binding site mutations
pmirGlo Rgs14-wt	unpublished	
pmirGlo Src-wt	unpublished	
pmirGlo Src-mut	unpublished	miR-485 binding site mutation

2.7 Luciferase reporter assay

Primary neurons were transfected in triplicates in 24-well plates using for each well 100 ng (for CTX cells) or 50 ng (for HC cells) of pmirGLO Dual-Luciferase expression vector reporter (Promega, Madison, WI, USA) with respective 10 pmol miRNA mimics (pre-miR miRNA precursor, Ambion, Thermo Fisher Scientific, Darmstadt, Germany) or 20 pmol anti-miRs (pLNAs, Exiqon, Vedbaek, Denmark). Luciferase assays were performed using the Dual-Luciferase reporter assay system after a modified homemade luciferase protocol described earlier (Barker & Boyce, 2014), without Triton X-100 pure liquid reagent in the triton lysis buffer, on a GloMax R96 Microplate Luminometer (Promega, Madison, WI, USA). Neurons were washed once with cold DPBS and lysed using 100 µl passive lysis buffer (Promega) per well. The 24-well plate was frozen for minimum of 2 h to increase lysis efficiency. After thawing, cells were shaken for 20 min. Luciferase activity was measured on the GloMax R96 Microplate Luminometer (Promega, Madison, WI, USA) according to manufacturer's instructions, using 75 µl per well of each reagent. The relative luciferase activity (RLA) was determined by calculating the ratio of Firefly to Renilla signal.

2.8 Animal perfusion and tissue preparation

For spine analysis, adult mice were anesthetized with a lethal i.p injection (10ml/kg bodyweight) of chloral hydrate. Mice were perfused with 4% paraformaldehyde (PFA) according to *Zimmermann (2012)*. Brains were post-fixed in the same fixative for 12 h and washed twice with PBS. Afterwards, 50 µm-thick coronal brain sections were prepared using a VT1000S vibratome (Leica, Wetzlar, Germany), therefore brains were put in blocks of embedded medium that consists out of a gelatin solution. Brain slices were mounted on microscope slides using Aqua-Poly/Mount (Polysciences Inc., Valley Road, PA, USA) or

stored in 1x PBS with 0.01% sodium azide at 4°C. For RNA extraction (qPCR & RNA sequencing), brains were rapidly removed after cervical dislocation of the animals and hippocampi were dissected on ice. Afterwards, RNA was isolated with the mirVana miRNA isolation kit (Thermo Fisher Scientific, Darmstadt, Germany) according to the manufacturer's instructions. For protein extraction, hippocampal tissue from juvenile mouse brain was removed quickly after cervical dislocation and homogenized on ice with a small plastic stamper in RIPA+ buffer and continued with extraction steps as described in 2.10 in more details.

2.9 Image analysis

For spine analysis, the miR379-410 line was cross-breed with a Thy1-GFP line. The used GFP-M line, described earlier in more details (*Feng et al., 2000*) expresses green fluorescent protein (GFP) under the control of a modified, neuronal specific, Thy1 promoter region, containing the sequences required for neuronal expression but missing the sequences required for expression in non-neural cells. Up to 10% of all neurons express GFP and are therefore a useful tool for fluorescent labeling of neural tissues. For Thy1-GFP/miR379-410 mice brain sections, images were taken with a multiphoton microscopy BX36 (Olympus, Hamburg, Germany) at the core facility of the ZTI (Zentrum für Tumor- und Infektionsbiologie, University Marburg, Germany) equipped with a 25x objective, the numerical aperture was set to 1.05. An excitation wavelength of 880-940 nm (laser power: 1.3%; HV: 500-600V) was chosen for imaging GFP tissue fluorescence. Images (1024 × 1024 pixels) with a 4x zoom were recorded in time series of z-stacks (with 0.5 µm step size) using the software FluoView FV30S-SW (Olympus, Hamburg, Germany). Morphological changes in hippocampal CA1 basal and apical dendrites were examined over two 50 µm-thick coronal sections per animal. Thy1-GFP immunofluorescence images were captured and spines were examined over 20 µm dendritic segments (on average 36 segments per animal were analyzed) as described in a protocol earlier in more details (*Hansen et al., 2010*). Spine density and volumes were subsequently analyzed with ImageJ software (NIH, Bethesda, MD, USA) and a plugin as previously described (*Fiore et al., 2014*).

2.10 Transfection and preparation of protein extracts

For transfection experiments with oligonucleotide anti-miRs (LNAs), that were used to determine protein expression, a total number of 2.7 million rat hippocampal cells were plated on one 6-well plate and treated with fluorodeoxyuridine (FUDR, F-0503; Sigma, Steinheim, Germany) + uridine (F-303; Sigma, Steinheim, Germany) in a final concentration of 10 µM from 3 DIV to stop proliferation of non-neuronal cells as described previously (*Rajman et al., 2017*). Each well was transfected on 17 DIV with Lipofectamine RNAiMAX (Thermo Fisher Scientific, Darmstadt, Germany) and 200 nM or 400 nM of anti-miRs as indicated. For one well, a mixture of 200 µl TM medium + 4.2µl RNAiMax was incubated for 10 min at RT and mixed together afterwards with 200 µl TM medium with 200 nM or 400 nM of anti-miRs as indicated. After incubation time of 20 min, 1.5ml conditional medium was collected, washed once with TM medium and replaced with 1ml of fresh TM medium. Then 400 µl of the transfection solution was gently applied onto the plate and incubated for 6 h at 37°C and 5% CO_2. Afterwards, cells were washed twice with NB medium and incubated with 20 µl AP5 (1:1000) for 30 min. Cells were washed with NB and replaced with a mixture of the previously collected, conditional medium + fresh NB+. To extract the proteins, cells were lysed on DIV 20 by washing the culture once with cold DPBS, adding a modified RIPA (+) buffer containing Complete Protease Inhibitor Cocktail EDTA-free (Merck, Darmstadt, Germany) and shaking them for 20 min at 4°C on a horizontal shaker (Rotamax, Heidolph, Germany). To remove cell debris the lysates were centrifuged at maximum speed for 10 min at 4°C. The protein concentration of the collected supernatant was determined by Pierce BCA Protein Assay Kit (Thermo Fisher Scientific, Darmstadt, Germany) according to manufacturer`s instructions.

2.11 Western blot

Antibodies were used as listed in tables 7 and 8. For each protein sample, 20 µg were mixed with 4x loading buffer (Laemmli WB sample buffer) and heated for 5 min at 95 °C. Afterwards, samples were separated on a 8 % polyacrylamide gel (Mini-PROTEAN system; Bio-Rad, Dreieich, Germany) next to the Precision Plus Protein Dual Color Standard (Bio-Rad, Dreieich, Germany) in SDS-PAGE running buffer and transferred to a methanol-activated Amersham Hybond PVDF (poly-vinylidene difluoride) membrane (GE Healthcare, Freiburg im Breisgau) by tank blotting at 90 V for 90 min in a cold room (4-6 °C) in blotting buffer. The membrane was blocked for 2 h in TBS-T (tris buffered saline supplemented with Tween)

containing 5 % milk powder. Antibody dilutions, as indicated in the table 7, were prepared in TBS-T/milk and membrane were incubated overnight at 4°C under slight shaking. After three washes with TBS-T/milk, the membrane was incubated with HRP (horseradish peroxidase)-conjugated secondary antibodies in TBS-T/milk for 1.5 h under slight shaking. Then membranes were washed three times with TBS-T before developing with Amersham ECL plus reagent (GE Healthcare, Freiburg im Breisgau, Germany) for 2 min in the dark. Signals were detected using Amersham Hyperfilm ECL films (GE Healthcare, Freiburg im Breisgau, Germany).

2.11.1 Primary Antibodies

Table 7: List of used primary antibodies.

Antibody	Species	Dilution	Source
anti-ß-Actin	monoclonal mouse	1:25,000 (overnight 4°C)	Sigma-Aldrich, A5441
anti-Cnih2	polyclonal rabbit	1:1000 (overnight 4°C)	Synaptic Systems, 253203, Lot 253203/3
anti-Dlgap3 (Sapap3)	polyclonal rabbit	1:1200 (overnight 4°C)	Thermo Fisher Scientific, PA5-20465, Lot SD2377616
anti-Prr7 (TRAP3/10)	monoclonal mouse	1:1000 (overnight 4°C)	Thermo Fisher Scientific, MA1-10448, Lot 74833187
anti-v-Src (327)	mouse	1:1000 (overnight 4°C)	Calbiochem (Merck), OP07L, Lot D00082488
anti-α-Tubulin	rabbit	1:10,000 (overnight 4°C)	Cell Signaling, 05/2015, Lot 9

2.11.2 Secondary Antibodies

For recognition of the primary antibodies HRP-conjugated goat anti-rabbit antibody or HRP-conjugated rabbit anti-mouse antibody was used.

Table 8: List of used secondary antibodies.

Antibody	Species	Dilution	Source
HRP-anti-Rabbit	Goat	1:20,000 (1.5h RT)	Calbiochem (Merck), 401315, Lot 2625715
HRP-anti-Mouse	Rabbit	1:20,000 (1.5h RT)	Calbiochem (Merck), 402335, Lot D00160409

2.12 RNA extraction and quantitative real-time PCR

Total RNA from fresh mice tissue was mechanical lysed on ice with a small plastic stamper and purified using the mirVana miRNA Isolation Kit (Thermo Fisher Scientific, Darmstadt, Germany) and treated with TURBO DNase (Thermo Fisher Scientific, Darmstadt, Germany) to remove genomic DNA, according to manufacturer's instructions. Afterwards, RNA quantity and quality were determined using the NanoDrop 2000c spectrophotometer (Thermo Fisher Scientific, Darmstadt, Germany). Quantitative real-time PCR was performed with a StepOnePlus Real Time PCR System (Applied Biosystems, Foster City, CA, USA) using SYBR Green System (iTaq SybrGreen Supermix with ROX; BIO-RAD, Hercules, CA, USA) for pre-miRNA and mRNA detection according to manufacturer's instructions. The housekeeper genes U6 snRNA, Rp2 and Ywhaz were used as qPCR normalization control by taking their geometric mean for mRNA targets. U6 snRNA was used only to normalize pre-miRNas targets. For detection of mature miRNAs, RNA sample were reverse transcribed using the TaqMan MicroRNA Reverse Transcription Kit and the respective miRNA-specific primers (TaqMan MicroRNA Assays; Applied Biosystems) according to manufacturer's instructions. The average of triplicate CT values from each sample was used to calculate the relative RNA levels ($2^{-\Delta CT}$). Primer sequences for pre-miRNA and mRNA targets are provided below and were purchased by Invitrogen (Thermo Fisher Scientific, Darmstadt, Germany) and were diluted to a stock concentration of 100 µM with nuclease-free ddH2O.

41

Table 9: Primer sequences used for qPCR.

Primer	Sequence 5' → 3'
Camk2n2 fw	ATGTCCGAGATCCTACCCTACG
Camk2n2 rev	AGCGAAGAAGGAGTTGGTGTC
Cnih2 rev	GTACCTCCAGAGGTGGTAGAA
Cnih2 fw	CCTCCCTCATCTTCTTTGTCATC
Creb1 fw	AGCCGGGTACTACCATTCTAC
Creb1 rev	GCAGCTTGAACAACAACTTGG
Dlgap3 fw	AGCAGTACCTTCCCCAGGAT
Dlgap3 rev	AAACTGGTCCAGGAGTGTGG
Fmr1 fw	AGATCAAGCTGGAGGTGCCA
Fmr1 rev	CAGAGAAGGCACCAACTGCC
Gabra1 fw	GTCCTCTGCACCGAGAATTGC
Gabra1 rev	TCAAATTCTTTAGGACAGAGGCAGTA
Gabra4 fw	GCTCACTTAGCTTCCAGTCCAAA
Gabra4 rev	GATGAAAGACCTCTGGCTGCA
JunD fw	GGCGGGATTGAAACCAGGG
JunD rev	AGCCCGTTGGACTGGATGA
Limk1 fw	CCTCCGAGTGGTTTGTCGA
Limk1 rev	CAACACCTCCCCATGGATG
Lzts2 fw	GCAGCGTGAGCAGTCTTATCT
Lzts2 rev	AGGTAAAGCTATTGCCTGGGA
Mpp2 fw	GCCACGAACTCCGAGTCTG
Mpp2 rev	GCCTCGAAGAAAGATCAGGTC
Neurl1a fw	CTTCCACCCCCACACTAAGG
Neurl1a rev	GCCTGACTTGCTCGTAGATGA
pre-miR-124a fw	CGTGTTCACAGCGGACCTT
pre-miR-124a rev	TCACCGCGTGCCTTAATTG
pre-miR-132 fw	ACCGTGGCTTTCGATTGTTAC
pre-miR-132 rev	CGACCATGGCTGTAGACTGTTAC
pre-miR-137 fw	GGTGACGGGTATTCTTGGGT
pre-miR-137 rev	CGACTACGCGTATTCTTAAGCAAT

pre-miR-138.2 fw	AGCTGGTGTTGTGAATCAGGC
pre-miR-138.2 rev	GTGAAATAGCCGGGTAAGAGGAT
pre-miR-329 fw	CGCTTCTGGTACCGGAAGAG
pre-miR-329 rev	GGTTAGCTGGGTGTGTTTCATTC
pre-miR-369 fw	GTACTTGAAGGGAGATCGACCG
pre-miR-369 rev	AGATCAACCATGTATTATTCGAAGTCAG
pre-miR-485 fw	GAGAGGCTGGCCGTGATG
pre-miR-485 rev	GACACTAGAAGAGAGGAGAG
Prr12 fw	GCGGGATGGAGTTACGAGAG
Prr12 rev	CGATGCAAGATGTCGGTTTCT
Prr7 fw	GCTTTCGTTGCCACTGTCTG
Prr7 rev	TTCGAACTCGTCTTCCTGCC
Pum2 fw	GGTTTCAGAAGTATGAACCAGCTTTC
Pum2 rev	GCACAATACCCTGACTTCAATTGA
qClock fw	CTTCCTGGTAACGCGAGAAAG
qClock rev	TCGAATCTCACTAGCATCTGACT
Rgs14 fw	GGCTTACTTCACTGAGTTCCTG
Rgs14 rev	ACTCGTGGTAGATGTTGTGGG
RP2 fw	CCACAGAAGCCAATAGAAGCA
RP2 rev	CGGGAGAAGCCTTTACCAAC
Shank1 fw	AGCCTGCAGCAGTGCCCAGCA
Shank1 rev	ATGCGAGGCCGCCAGGCCCA
Shank3 fw	TGGTTGGCAAGAGATCCAT
Shank3 rev	TTGGCCCCATAGAACAAAAG
Shb fw	CTGATGACTACTCCGATCCCTT
Shb rev	GGGGTGTCGTACAACTGGATG
Shisa4 fw	CCTTCAGTCCCAAGACCATAGC
Shisa4 rev	CGCCTTCGGTATAGGTAACAAC
Src fw	TACGAGGCCCAAAAGATGATGG
Src rev	GTGTCATAGAGAGGTAGGGGTT
U6 snRNA fw	CTCGCTTCGGCAGCACA
U6 snRNA rev	AACGCTTCACGAATTTGCGT

Ube3a1 fw	ATCCCAGTCTGAGGACATTGA
Ube3a1 rev	GCACAAAACTCATTCGTGCAG
Ywhaz fw	TGGAAGTCCTGCCCTAAATG
Ywhaz rev	GAGGAGGAGGAGGAGGAAGA

2.13 Genotyping of the miR379-410 and Thy1-GFP mice

Before weaning, mice were marked and genotyped at Pnd21 with the Kapa Mouse Genotyping kit (Merck, Darmstadt, Germany) by using earmark tissues. miR379-410 animals were genotyped and validated as described previously in details (*Valluy et al, 2015*). The Thy1GFP reporter mouse line (*Feng et al., 2000*) that was cross-bred with the miR379-410 line for spine morphology analysis, was purchased by Marco Rust (Institute for Physiology Chemistry, University Marburg, Germany) and genotyped followed their instruction protocols. Primer sequences for PCR are provided below:

Table 10: Primer sequences used for PCR.

Primer	Sequence 5' → 3'
169–379lox-fw	GCCACTGCTTACTCTCATCTGC
170–379lox-rev	CCGTATTATCCCATCAAGTAGC
171–410lox-fw	CCAGATGTGCAATGGATGG
173–410lox-rev	AAAGAGAGGTGACCATGCACTG
Thy1GFP-555	TCTGAGTGGCAAAGGACCTTAGG
Thy1GFP-556	CGCTGAACTTGTGGCCGTTTACG

2.13.1 PCR program for genotyping miR379lox animals:

1) Initial denaturation   3min   95°C
2) Denaturation   15min 95°C
3) Annealing   20min 60°C
   1-3) *35 cycles*
4) Extension   20min 72°C

   Final extension   10min 72°C

Primer pairs: 169/173 (ko; band at ca. 500 bp), 171/173 (wt, band at 277 bp), 169/170 (wt, band at 360 bp)

44

2.13.2 PCR program for genotyping Thy1GFP animals:

1) Initial denaturation   2min   95°C
2) Denaturation   30sec   95°C
    Annealing   30sec   64°C
    Extension   60sec   72°C
    2 cycles
3) Denaturation   30sec   95°C
    Annealing   30sec   61°C
    Extension   60sec   72°C
    2 cycles
4) Denaturation   30sec   95°C
    Annealing   30sec   58°C
    Extension   60sec   72°C
    13 cycles
5) Denaturation   30sec   95°C
    Annealing   30sec   55°C
    Extension   60sec   72°C
    13 cycles

    Final extension   5min   72°C

Primer pair: 555/556 (Thy1pos, band at 300 bp)

2.13.3 Agarose gel electrophoresis

For genotyping earmark samples, the separation of DNA fragments according to their size was performed by agarose gel electrophoresis. Therefore, DNA samples that were isolated and processed with the Kapa Mouse Genotyping Kit, according to the manufacturer's instructions, were loaded onto a 1.5% agarose gel in 1x TAE buffer containing ethidium bromide (1:200). The gel was run at 90 V for ca. 45 minutes. The bands were visualized by UV-light in a digital gel documentation system (Vilber, Eberhardzell, Germany).

2.14 Electrophysiology in primary mouse culture (performed by R. Daswani)

Spontaneous miniature excitatory postsynaptic currents (mEPSCs) were recorded, as described previously (*Saba et al., 2012*) in the whole-cell voltage-clamp mode using an EPC-10 patch-clamp amplifier and PULSE software (HEKA Elektronik, Lambrecht, Germany) from *in vitro* mouse hippocampal culture at DIV 8-10 visualized with a charge-coupled-device (CCD) camera (VX55, TILL Photonics GmbH, Gräfelfing, Germany) mounted on an upright

microscope (BX51WI, Olympus, Hamburg, Germany). Coverslips with transfected cells were transferred at room temperature with a bath solution containing 156 mM NaCl, 2 mM KCl, 2 mM CaCl 2, 1 mM MgCl2, 16.5 mM glucose, and 10 mM HEPES (pH 7.3 with NaOH) to which PTX (50 μM) and tetrodotoxin (0.5 μM) were added during recording. The pipette solution contained 110 mM CsMeSO3, 25 mM CsCl, 30 mM HEPES, 2 mM MgCl2, 0.362 mM CaCl2, 1 mM EGTA, 4 mM MgATP, and 0.1 mM Na2GTP (pH7.2 with CsOH). Patch pipettes were pulled from borosilicate glass (Science Products, Hofheim am Taunus, Germany) and had resistances of 3 to 7 MΩ when filled with the pipette solution. Neurons were held at a potential of −70 mV, and mEPSCs were analyzed for 100 s current recordings made after 10 min of equilibration in the whole-cell configuration. Data were acquired at a sampling rate of 20 kHz and filtered at 3 kHz. Series resistance was controlled every 5 min, and only experiments with uncompensated series resistances of <25 MΩ were accepted. Mean event amplitude and frequency were determined off-line with the Mini Analysis program (Synaptosoft Inc., Fort Lee, NJ, USA) using an amplitude threshold of −5 pA. The inter-event interval was calculated through the software Mini Analysis putting the bin to 1 ms. We considered the cumulative distribution of the events in the range from 1 ms to 3 s interval. Please note that the average of inter-event interval that were showed has time binning intervals of 100 ms. For the inter-event calculation two cell conditions (one wt and one ko) were taken out due to technical data problems.

2.15 RNAseq and bioinformatic analysis (performed by C. Dieterich, University Heidelberg, Germany and M. Soutschek)

Total RNA was isolated from three miR379-410 wt and three ko adult male hippocampi. Stranded polyA+ enriched RNA sequencing libraries were prepared at the GENCORE (EMBL, Genomics Core Facility, Heidelberg, Germany) and sequenced on an Illumina HiSeq2000 machine using a 50nt paired-end protocol. We removed sequencing adapter and quality-trimmed all short reads from the 3'end using FLEXBAR 2.5 (Dodt et al., 2012). All reads longer than 18 bp were retained and rRNA reads were subtracted in silico. We used the STAR aligner 2.4. (Dobin et al., 2013) to map against the mouse genome (EnsEMBL 79 genome + annotations). We performed differential gene expression analysis using the Cuffdiff 2.2.1 and used TargetScan 7 to annotate miRNA binding sites in our gene set.

2.15.1 GO-Term Enrichment Analysis and Bipartite Network representation

Bioinformatic analysis were compiled using R-Studio (1.1.383) with R version 3.4.3. Bioconductor packages topGo (2.30.0) (*Alexa et al., 2006*) and org.Mm.eg.db (3.5.0) were used for the GO-Term enrichment analysis as described in the topGo script. The *elim* algorithm (*Alexa et al., 2006*) with Fisher's exact test was employed to compare the enrichment of cellular component GO-Terms in the differentially expressed genes (DEG, 3068 genes) against the specific sequencing background (13975 genes). Minimum nodeSize was set to 5, as suggested in the documentation. GO-Terms and associated genes were subsequently plotted as bipartite Terms-Genes network, using the FGNet (3.12.0) package (*Aibar et al., 2015*). The source code of the package was rewritten to use the elim algorithm of the topGo package together with Fisher's exact test to build a terms-genes incidence matrix as described in the FGNet documentation. The layout of the resulting bipartite network was modified with Cytoscape (3.4.0). Synapse associated GO-Terms and associated genes are enlarged in the final figure. GO-Terms with more than 300 annotated genes are not included in the plots.

2.15.2 String Database Protein Interaction Network

To perform hierarchical clustering (unweighted pair group method with arithmetic mean) of identified GO-Terms and associated Genes, the FGNet derived terms-genes incidence matrix was converted into a binary distance matrix. The resulting Dendrogram was plotted together with the distance matrix using R packages ComplexHeatmap (1.17.1) (*Gu et al., 2016*), RColorBrewer (1.1-2) and circlize (0.4.3). Next, DEG associated with GO-Terms referring to synaptic function ("Chloride channel complex", "GABA-A receptor complex"," GABA receptor complex", "Synaptic membrane", "Postsynaptic membrane", "Ionotropic glutamate receptor complex" and "AMPA glutamate receptor complex") were used as input in the String Database (Version 10.5) to construct a protein interaction network. String-DB Settings were the following:

Meaning of network edges: evidence

Active interaction sources: text mining, experiments and databases

Minimum required interaction score: medium confidence

Max numbers of interactors to show: 1st shell (80 interactors), 2nd shell (20 interactors).

The network layout was adapted with Cytoscape.

2.15.3 miRNA overrepresentation analysis

A list of all the transcripts containing predicted miR379-410 miRNAs was generated. First, mouse miRNAs and their conserved binding sites (8mer sites, 7mer-m8 sites and 7mer-1a sites) were extracted from the file "Summary Counts, all predictions" (Targetscan 7.1; *Agarwal et al., 2015*) using the R package data table (1.10.4-3). Subsequently miRNA names were used to filter for transcripts containing miR379-410 Cluster miRNA binding sites. Mmu-miR-1962, which shares the same seed as mmu-miR-485-5p, was not included in the analysis. Next, each transcript from obtained list was compared to its log2-fold change in ko animals determined by RNA-seq (see RNAseq and bioinformatics analysis). This allowed summing up miRNA binding sites in significantly up- and downregulated transcripts with Microsoft Excel 2016. miRNAs with less than 5 total binding sites in differentially expressed transcripts were excluded. To enhance specificity in the analysis, miRNAs with an expression value (RPM) of less than 100 in the mouse brain (values obtained from *Chiang et al., 2010*) were filtered out. The plot was compiled with the R package plotly (4.7.1).

2.16 General behavioural procedures

Approximately two weeks after pairing for breeding, heterozygote miR379-410 females were individually housed and inspected daily for pregnancy and delivery. The day of birth was considered as Pnd0. To distinguish between the animals, pups were tattooed on the paw with animal tattoo paste (Ketchum Manufacturing Inc., Brockville, Canada) as described previously (*Scattoni et al., 2008*). The procedure was performed between Pnd2-3, depending on the first day of behavioural testing. After weaning on Pnd21, mice were socially housed in groups of 2–4 with same-sex partners except for the social interaction test which was performed on Pnd23. For detecting a wide range of behavioural phenotypes, i.e. locomotor activities and anxiety-related tests, subject mice of two independent cohorts were examined. To gain insight into more neurodevelopmental-relevant behavioural phenotypes, common social behaviour assays were performed as described earlier (*Wöhr et al., 2013 and Sungur et al., 2016*). The behaviour battery included isolation-induced pup USV, social motivation, i.e. social approach and reciprocal social interaction, social cognition and repetitive behaviour. In addition, a non-social memory task, i.e. novel object recognition, was examined. Behavioural assays were performed, in mice of both sexes and were tested as pups to juveniles and again as adults between 12 and 32 weeks of age. All animals were used for the same test and order. To examine developmental milestones, a

third, independent cohort was used to minimize handling stress in the cohorts that were used for behavioural assays. Additionally, for the home cage activity experiment animals from a separate, fourth cohort were used. All behavioural tests, except for the elevated plus maze, were performed under dim red light during the light phase of the 12h/12h light/dark cycle. Before and after each test, behavioural equipment was carefully cleaned using a 0.1% acetic acid solution followed by drying. Experimenters were blind to genotypes during data acquisition and analysis. Behaviour experiments shown here were done in the following test order as indicated in the table 11.

Table 11: Overview of behavioural tests performed in miR379-410 wt and ko animals.

Behavioral approach	Type of test (category)	Age	CohortID
Developmental milestones	Early postnatal insults	Pnd2-14	1
Isolation-induced pup USV	Communication / autism	Pnd3,6,9,12	2-3
Open field	Locomotion / anxiety	Pnd18	2-3
Nest homing / maternal interaction	Sociability / autism	Pnd19	2-3
Reciprocal Social Interaction	Sociability / autism	Pnd23	2-3
Three-chamber assay: Social memory	Sociability / autism / cognition	Pnd25-42	2-3
Three-chamber assay: Novel object recognition	Cognition	Pnd25-42	2-3
Three-chamber assay: Social memory	Sociability / autism / cognition	Pnd84-224	2-3
Three-chamber assay: Novel object recognition	Cognition	Pnd84-224	2-3
Open field	Locomotion / anxiety	Pnd84-224	2-3
Marble Burying	Repetitive behavior / autism	Pnd84-224	2-3
Elevated plus maze	Anxiety	Pnd84-224	2-3
Light-Dark-box	Anxiety	Pnd84-224	2-3
Tail-Suspension test	Depression	Pnd84-224	2-3
Amphetamine induced locomotor activity	Mania / schizophrenia	Pnd84-224	2-3

Home cage activity	Long-term activity / locomotion	Pnd21-28	4
Home cage activity	Long-term activity / locomotion	Pnd84-224	4

2.16.1 Developmental milestones and somatosensory reflexes

Pups were tested according to a modified Fox battery for developmental milestones and somatosensory reflexes as described previously (*Wöhr et al., 2013*). The tests were examined between 09:00–14:00h during the light phase of the 12 h/12 h light/dark cycle. Each pup was tested at approximately the same time of day. Every other day from Pnd2–14, body weight, body length and tail length were recorded. Body weight was measured using a palmscale (PS6-250; My Weigh Europe, Hückelhoven, Germany). The following physical landmarks were also recorded: Pinnae detachment, eye opening, incisor eruption. Somatosensory reflexes, surface righting, grasping reflexes and auditory startle (acoustic stimulus: hand clapping) were scored. Latencies were measured in seconds for surface righting and cliff avoidance (maximum: 60 s). Other somatic and behavioural variables were rated as indicated by measuring the time or semi-quantitatively, as followed: 0 = no response/not present, 1 = slight response/slightly present, 2 = strong response/strongly present, 3 = complete response/completely present.

2.16.2 Ultrasonic vocalizations in isolated pups (USV calls analyzed by L. Stemmler)

Emission of USV calls indicate social behaviour, since it is well established that pup USVs are important communicative signals to stimulate maternal search, retrieval and nursing behaviour (*Okabe et al., 2013; D'Amato et al., 2005*). To initiate isolation-induced USV, the protocol was used as described earlier (*Sungur et al., 2016*). Briefly, pups were tested on Pnd3, 6, 9 and 12 by isolating from their mother and littermates for 10 min under room temperature (20–23°C). Pups were randomly selected and individually removed from the nest and gently placed into a glass isolation container, filled with fresh bedding material. As it is known that pup vocalization frequency varies by age, room temperature, circadian rhythm and even by the position of the pup (*Branchi et al., 1998; Barnes et al., 2017*), animals were always recorded at the same daytime and placed in an equal position in a sound-attenuating chamber (styrofoam box) with constant room temperature, to avoid

negative parameters on the recordings. USV emission was monitored by an Ultra Sound Gate Condenser Microphone CM16, sensitive to frequencies of 15–180 kHz (flat frequency response between 25 and 140 kHz; ±6 dB; Avisoft Bioacoustics, Berlin, Germany), that was placed in the roof of the sound attenuating box, 22 cm above the floor. Emitted USV calls from the pups were recorded and analyzed afterwards by a trained person.

2.16.3 Early homing test (Pnd9)

The homing test was performed as previously described (*Scattoni et al., 2008*). On Pnd9, individual pups were transferred to a small Plexiglas cage (36 cm×22.5 cm, walls 10 cm high). The cage was then separated in three equally areas. One side area was filled with home cage bedding, whereas the other areas were filled with fresh, clean bedding. The subject pups were placed in the middle area of the Plexiglas cage and time was taken for ten minutes. Homing activity was scored as latency to reach the nest bedding area and time spent within this area.

2.16.4 Nest homing test / maternal interaction test

The nest homing and maternal interaction tests were performed as described previously (*Zhan et al., 2014*) and is divided into two sessions: Nest homing test, followed up by the maternal interaction test. For the nest homing experiment, Pnd19 juvenile mice were placed into one corner (start) of a novel open arena filled with fresh, clean bedding and with familiar bedding material from the home cage into the opposite corner (nest). The other two corners were also filled with fresh, clean bedding material. Time spent in each corner: start, nest, corner 1 and corner 2 was recorded during a three-minute session automatically by VideoMot2 (TSE Systems, Bad Homburg, Germany). Subsequently, the mice were removed while wired-cages were placed into corner 1 and corner 2 and the mother was placed into one of the wired-cages. Time spent at the corner with the wired-cage constraining the mother or at the corner with the empty wired-cage was recorded during a five-minute session automatically by TSE VideoMot2 (TSE Systems, Bad Homburg, Germany).

2.16.5 Open field locomotion

General locomotor activity of juvenile (Pnd18) and adult mice were examined in a novel open field. In juvenile, the open field box consisted of white PVC with a square base dimension of 40 cm x 40 cm and a center area of 24 x 24 cm. For adults, the open field arena, purchased from TSE Systems (Bad Homburg, Germany), consisted of light-gray PVC plates, the size of 50 cm x 30 cm constituting the walls and forming a square shaped base with the dimension of 50 cm x 50 cm. The center area, 15 cm off the borders, had a size of 30 cm x 30 cm. A video camera, that was connected to a DVD/HD- recorder and a computer, was placed about 2.5 m above the arena. Individual mice were placed randomly in one of the corners of a standard open field box (TSE System, Bad Homburg, Germany) and the locomotor activity was recorded for 10 min. Center time and center entries were automatically collected using the TSE VideoMot2 analyzer software (TSE Systems, Bad Homburg, Germany).

2.16.6 Elevated plus maze

The elevated plus maze, as described previously (*Wöhr et al., 2013*) was used to examine anxiety-related behaviour in the miR379-410 animals. The EPM apparatus consisted of a plus-shaped platform at a height of 52.5 cm with two open arms (7 cm x 40 cm) and two closed arms (7 cm x 40 cm) bordered by PVC-plates with a height of 29 cm connected by a central zone (7 cm x 70 cm). Adult mice were tested in the EPM during room light that was approximately set to 30 lux. Mice were individually placed in the center, facing one of the closed arms. The subject was allowed to freely explore the maze for 5 min. Time spent in the open arms and numbers of entries into the open arms were recorded automatically by the TSE VideoMot2 analyzer software (TSE Systems, Bad Homburg, Germany).

2.16.7 Light-Dark Box Test

The Light-Dark box consist of a brightly illuminated, open box made of white PVC (27 cm x 30 cm x 26 cm) and a dark, closed box made of black PVC (27 cm x 145 cm x 26 cm), respectively and was purchased from TSE Systems (Bad Homburg, Germany). Both boxes were connected by a small passage (7.5 x 0.7.5 cm) that allowed mice to move freely between the light arena and the dark chamber. In the light arena, illuminance was set to 350 lux, whereas <5 lux was set in the dark chamber. Locomotor activity, collected as distance traveled in the light, open arena and time spent in the dark chamber were recorded

for a 10 min session and automatically analyzed by TSE VideoMot2 software (TSE Systems, Bad Homburg, Germany).

2.16.8 Marble burying test

The marble burying protocol was performed as described earlier (*Sungur et al., 2014; Angoa-Pérez et al., 2013*). A standard makrolon cage was equidistantly arranged with 20 glass marbles (diameter size: 15 mm) in a 4 × 5 arrangement on top of a 4.5 cm layer of fresh bedding material. Mice were tested for a duration of 30 min and the numbers of marbles buried (half- and completely buried) were recorded.

2.16.9 Reciprocal social interaction and USV analysis (USV calls analyzed by L. Stemmler)

The reciprocal social interaction assay was performed in juvenile mice on Pnd23 as described earlier (*Wöhr et al., 2015*). Before testing, animals were housed for 24 h in isolation, in order to enhance social motivation of interacting mice, as well as boost emission of USV. To observe social interactions in a novel testing standard cage with fresh bedding, two mice of the same age, sex and genotype that were unfamiliar to each other were put together for 5 min, after one mouse of the pair being habituated to the test environment for 1 min. Social behaviours of each pair, i.e. nose-to-nose sniffing, anogenital sniffing and following were videotaped and time of social events were recorded by an investigator blind to the genotypes. In addition, USV emission of juvenile pairs during the social interaction was recorded by an Ultra Sound Gate Condenser Microphone CM16 that where placed 20 cm above the testing cage. Before testing the social interaction of mice-pairs, one of the two subjects were placed alone for one minute in the neutral cage, for USV baseline recordings, before the other was placed to it. USV were analyzed with Avisoft-SAS Lab Pro software (Avisoft Bioacoustics, Glienicke, Germany). A fast Fourier transform was conducted (512 FFT length, frame size: 100%, Hamming Window and 75%-time window overlap), producing spectrograms at 488 Hz frequency resolution and 0.512 ms temporal resolution. USV were marked and counted by a trained observer blind to genotypes.

2.16.10 Three-chamber box

The three-chamber box apparatus, made of black PVC and consisted of two side chambers (23 x 34.5 x 35 cm) that are connected through a smaller chamber (14.5 x 70 x 35 cm) located

centrally between the two side chambers, was used in 4-6 weeks old juvenile and adult animals for social approach, social recognition and novel object recognition, as previously described (*Sungur et al., 2017*). In brief, behavioural testing was conducted on three consecutive days. On day 1 (habituation phase), subject mice were individually kept for 30 min in a Makrolon type III IVC cage (isolation period) and was then allowed to explore the empty three-chamber box for 30 min for habituation. On day 2 and day 3, subject mice were again kept first individually for 30 min (isolation period) and after that, the social behaviour assay (social approach/recognition) or non-social memory assay (novel object recognition) were performed in a balanced order.

2.16.10.1 Three-chamber box - social approach and social recognition

After isolation period for 30 min, subjects were tested for sociability (social approach) and social memory (social recognition). The assay consists of three phases: the social approach trial (10 min), the inter-trial interval (30 min break), and the social recognition trial (10 min). In the social approach trial, each individual mouse was allowed to freely explore for 10 min the three-chamber box, containing an empty wired-cage (object) on one side and a stimulus mouse constrained in an identical wired-cage (subject) on the other side. After the social approach trial, the test subject was individually kept for 30 min in the previously used Makrolon type III IVC cage for the inter-trial interval break. After a 30 min delay, the subject was returned to the three-chamber box for a 10 min social recognition trial. During the social recognition trial, subject mice were given the choice between the stimulus mouse (familiar) from the previous social approach trial on the same side where it has been presented before and a novel stimulus mouse (novel) replacing the empty wired-cage. Stimulus mice were age- and sex-matched C57BL/6N mice (Charles River Laboratories, Sulzfeld, Germany) and were group-housed under similar conditions as subject mice and habituated to the wired-cages for 30 min prior to testing. Location and stimulus mice used in this assay were counter-balanced between testing of the subject mice.

2.16.10.2 Three-chamber box - novel object recognition

After an isolation period of 30 min, subjects were tested for novel object recognition. The assay consists of three trial phases: the object acquisition trial (10 min), the inter-trial interval (30 min break), and the novel object recognition trial (10 min). In the object acquisition trial, each subject mouse was allowed to freely explore for 10 min the three-

chamber box containing two identical sample objects, which were centrally placed in each of the two side chambers. After the object acquisition trial, the subject was individually kept for 30 min in the previously used Makrolon type III IVC cage for the inter-trial interval break before being placed again in the middle of the three-chamber box. For the novel object recognition trial, one of the old (familiar) objects was replaced with a novel object of similar size but different in color, shape and material (novel object) to test novel object recognition. In the object memory trial, each subject was allowed to freely explore for 10 min the three-chamber box containing two different sample objects, which were centrally placed in each of the two side chambers. Location and type of objects presented were counter-balanced between subject mice.

2.16.11 Tail-Suspension test

The Tail-suspension test was performed after a modified protocol described earlier *(Can et al., 2012*). Each mouse was suspended 35 cm above a table, using adhesive tape. Each mouse was taped to the shelf with a 17cm long adhesive tape, creating a distance of approximately 35 cm to a soft crash pad (made of foam rubber) on a table in case of eventually tape break. A short plastic tube (4cm) was put over the tail to avoid possible self-amputation. Each test session was recorded by a side mounted video camera for 6 min, captured by the *FG3xcap* (HaSoTec GmbH, Rostock, Germany) software. The immobile phases were quantified manually with a stopwatch. Mice were considered to be mobile when they pulled themselves up, held their hind legs, moved their legs or rotated. Swinging behaviour due to prior movements but without moving a part of the body was considered as immobile. After each measurement mice were checked for possible injuries and subsequently put back to their litter cage.

2.16.12 Amphetamine-induced locomotor activity (measured by L. Stemmler)

The pharmacology treatment was carried out as followed: D-amphetamine sulfate (Sigma, MO, USA) was dissolved in 0.9% saline and administered intraperitoneally (i.p.) at a concentration of 2.5 mg/kg. Amphetamine-induced hyperactivity in adult mice was assessed in an open field box (TSE Systems, bad Homburg, Germany) as described above. Testing procedure occurred on three consecutive days for 45 min each. On day1 (baseline), mice were habituated to the test apparatus. On day2 (veh), mice received saline (vehicle) injections. On day3 (amph), mice were administered amphetamine immediately before

testing. Locomotor activity indicated as distance traveled (cm) was videotaped and automatically detected by VideoMot2 (TSE Systems, Bad homburg, Germany).

2.16.13 Home cage activity

Home cage activity of single-housed juvenile (3-4 weeks) and adult mice, were performed in standard mouse cages (Type II) for 24 h (12 h day/night cycle) using Mouse-E motion universal data logger (Infra-E-Motion GmbH, Hamburg, Germany) as described previously (*Zimmermann et al., 2015*). Mice were transferred to new cages with fresh beddings. After a habituation period of 12 h, locomotion (activity counts) was recorded. Afterwards, data were transferred to a PC via Mouse-E Motion software 2.3.6 (Infra-E-Motion GmbH, Hamburg, Germany). Activity counts were calculated as cumulative activity per 4-min recording intervals.

2.16.13 Behaviour analysis

For the three-chamber box social approach, social recognition, and novel object recognition test, time spent within each chamber and time spent with subject/object investigation were examined from videos using Noldus Observer XT software (Noldus Information Technology, Wageningen, The Netherlands) on a personal computer by a trained observer blind to genotypes. Object investigation was defined as time spent sniffing the social stimulus/object when the nose was oriented towards it, i.e. with the nose object distance being 3 cm or less. Social and object recognition (novelty) were defined as spending significantly more time sniffing the novel than the familiar object or mouse, respectively. For the three-chamber box social recognition and novel object recognition assays, behaviour recorded within the first 5 min of each trial was included in the statistical analysis, as described previously (*Sungur et al., 2017*).

2.17 Statistical analysis

Sample sizes are indicated in the figures or legends and were chosen to meet sample sizes typically used in similar experiments. Normal distribution was tested by using Kolmogorov-Smirnov test. Statistical significance was determined using either two-tailed, unpaired Student`s t-test for two population comparisons or paired Student`s t-test for comparing identical population. For isolation-induced pup USV and developmental milestones, a

repeated measurements ANOVA with the within subject factor "postnatal day" and between subject factor "genotype" was used. Data were analyzed using GraphPad Prism and SPSS. Unless otherwise stated, data are presented as mean ± s.e.m. P values for each comparison are described in the figure legends, $P < 0.05$ was considered statistically significant. Animals were assigned randomly to the various experiments and the investigator did not have knowledge about the animal's genotype. Control animals were selected from the same litter as the test group.

3. Results

The brain enriched placental-mammal specific miR379-410 miRNA cluster has been implicated in several aspects of neurodevelopment as well as in neuropsychiatric diseases such as ASD and SCZ. Mice deficient for the miR379-410 cluster were generated by homologous recombination in embryonic stem cells followed by crossing with a Cre deleter line (Tg(CMV-cre)1Cgn/ Cre-D) (*Schwenk et al., 1995*) as overviewed in **Figure 7a**. A large set of behavioural, cellular and molecular phenotyping investigations were performed. Assays were conducted in both constitutive miR379-410 ko male and female mice from pup to adult stage, according to the breeding strategy described in **Figure 7b**. Before behavioural and molecular phenotyping of the animals, macroscopic brain anatomy was evaluated by nuclear counter staining and no major abnormalities were observed (*Valluy et al., 2015*).

a
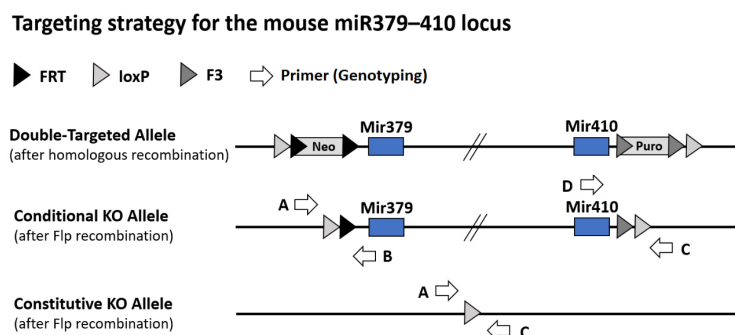
b
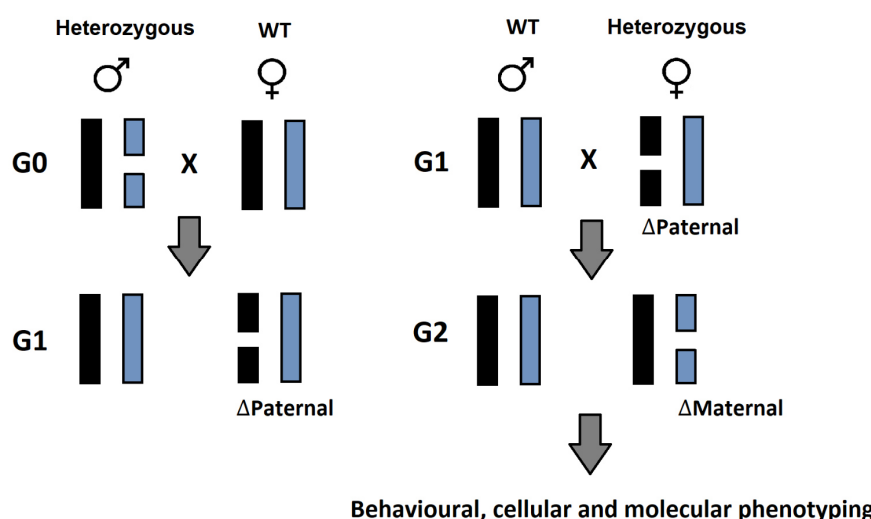
Figure 7: The miR379-410 ko mouse model. Continued on p59.

Figure 7: a, Schematic illustration of the targeting strategy for the mouse miR379-410 locus as described previously in more details (*Valluy et al., 2015*). Target sequences of recombinases and the location of primers (A-D) used for genotyping are indicated. **b**, A schematic representation of the breeding strategy for behavioural, cellular and molecular phenotyping of miR379-410 wt / ko mice (G2) is shown. Please note that the miR379-410 cluster is paternally imprinted and therefore only expressed from the maternal allele (*Seitz et al., 2004*). To study the physiological relevance of the cluster, wildtype (wt) male were bred with miR379-410 heterozygous mutant female mice (G1), that carried the mutation on the paternal allele (ΔPaternal) to obtain mice deficient for the miR379-410 cluster. Heterozygous mice resulting from this breeding (G2) carried the deletion on the maternal allele (ΔMaternal). Therefore, the miR379-410 cluster is not expressed in these animals (in the following named as "ko" mice) as previously demonstrated (*Valluy et al., 2015; Marty et al., 2016*). Abbreviation: G=Generation.

3.1 Pups lacking the miR379-410 cluster have no general developmental delays in somatic growth and neurological reflexes

In order to assess early postnatal development of miR379-410 ko animals, several developmental milestones and neurological reflexes were analyzed in wildtype (wt) and ko mouse pups from postnatal day (pnd) 2-14. As shown in **Figure 8** the majority of parameters tested were not different between wt and ko mice. Body weight (**Fig. 8a**), body length **(Fig. 8b)**, eye opening **(Fig. 8d)**, incisor eruption **(Fig. 8e)**, pinnae detachment **(Fig. 8f)**, grasping reflex **(Fig. 8g)**, righting reflex **(Fig. 8h)**, acoustic startle **(Fig. 8i)**, bar holding **(Fig. 8l)**, visual placing **(Fig. 8j)**, level screen **(Fig. 8n)**, forelimb placing **(Fig. 8o)**, cliff avoidance **(Fig. 8p)**, fur development front **(Fig. 8q)** and fur development back **(Fig. 8r)** were not significantly different between genotypes. Minor delays in tail length at pnd 8 **(Fig. 8c)**, reduced time in negative geotaxis at pnd 6, 8 and 10 **(Fig. 8k)**, increased time in vertical screen at pnd 10 and 14 **(Fig. 8m)** and increased level screen score at pnd 10 **(Fig. 8n)** were observed. Overall, results indicate no major developmental delay in neonatal miR379-410 ko mice.

Importantly, a pup homing test was performed in these animals at pnd 9 as shown in **Figure 9**. This test is used to measure interest in social odor, as judged by exploring the home area, and the cognitive ability of the pups to differentiate between home cage odor and neutral odor. Further, the homing test investigates motor abilities that are required to navigate towards the test cage. There was no significant effect for the latency to reach the nest area in miR379-410 ko male (**Fig. 9a**), female (**Fig. 9c**) and in pooled data from male and female

pups (**Fig. 9e**). Also, miR379-410 ko male (**Fig. 9b**), female (**Fig. 9d**), and pooled male and female pups (**Fig. 9f**) did not spend significantly more time in the nest area, suggesting intact olfaction and motor/navigation capability in the ko animals.
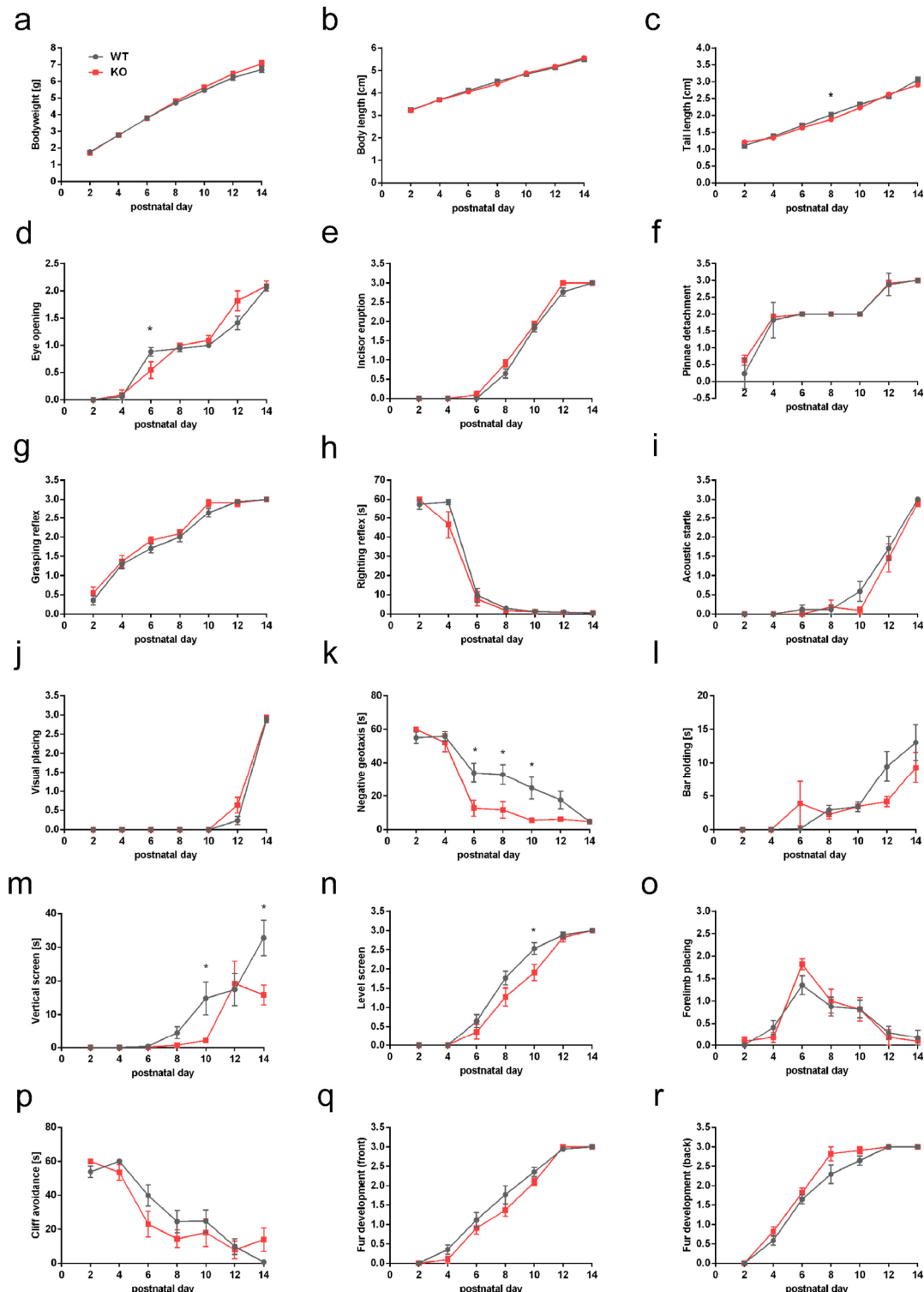
Figure 8: Developmental milestones analysis: Somatic growth and neurological reflexes in miR379-410 wt and ko mouse pups.

Figure 8: Milestones tested during early development (Pnd2-14). **a**, Body weight. **b**, body length. **c**, tail length, development x genotype: F_6=2.699, p=0.016, rm-ANOVA; Pnd8 *p=0.0158, unpaired Student`s t-test. **d**, eye opening, development x genotype: $F_6$=3.279, p=0.005, rm-ANOVA; Pnd6 *p=0.0461, unpaired Student`s t-test. **e**, incisor eruption. **f**, pinnae detachment. **g**, grasping reflex. **h**, righting reflex, development x genotype: F_6=2.119, ns p=0.054, rm-ANOVA. **i**, acoustic startle. **j,** visual placing. **k,** negative geotaxis, development x genotype: F_6=2.831, p=0.012, rm-ANOVA; Pnd6 *p=0.0148, Pnd8 *p=0.0201, Pnd10 *p=0.0259; unpaired Student`s t-test. **l,** bar holding. **m,** vertical screen, development x genotype: $F_6$=2.736, p=0.015, rm-ANOVA; Pnd10 *p=0.0487, Pnd14 *p=0.0225, unpaired Student`s t-test. **n,** level screen, development x genotype: F_6=2.491, p=0.025, rm-ANOVA; Pnd10 *p=0.0214, unpaired Student`s t-test. **o,** forelimb placing. **p,** cliff avoidance, development x genotype: F_6=1.960, p=0.075, rm-ANOVA. **q,** fur development on the front. **r,** fur development on the back. **a-r**, Grey line: miR379-410 wildtype littermate control n=17 (male n=8, female n=9); red line: miR379-410 ko mice n=11 (male n=5, female n=6). Data are presented as mean ± s.e.m.

a

b

c

d

e

f
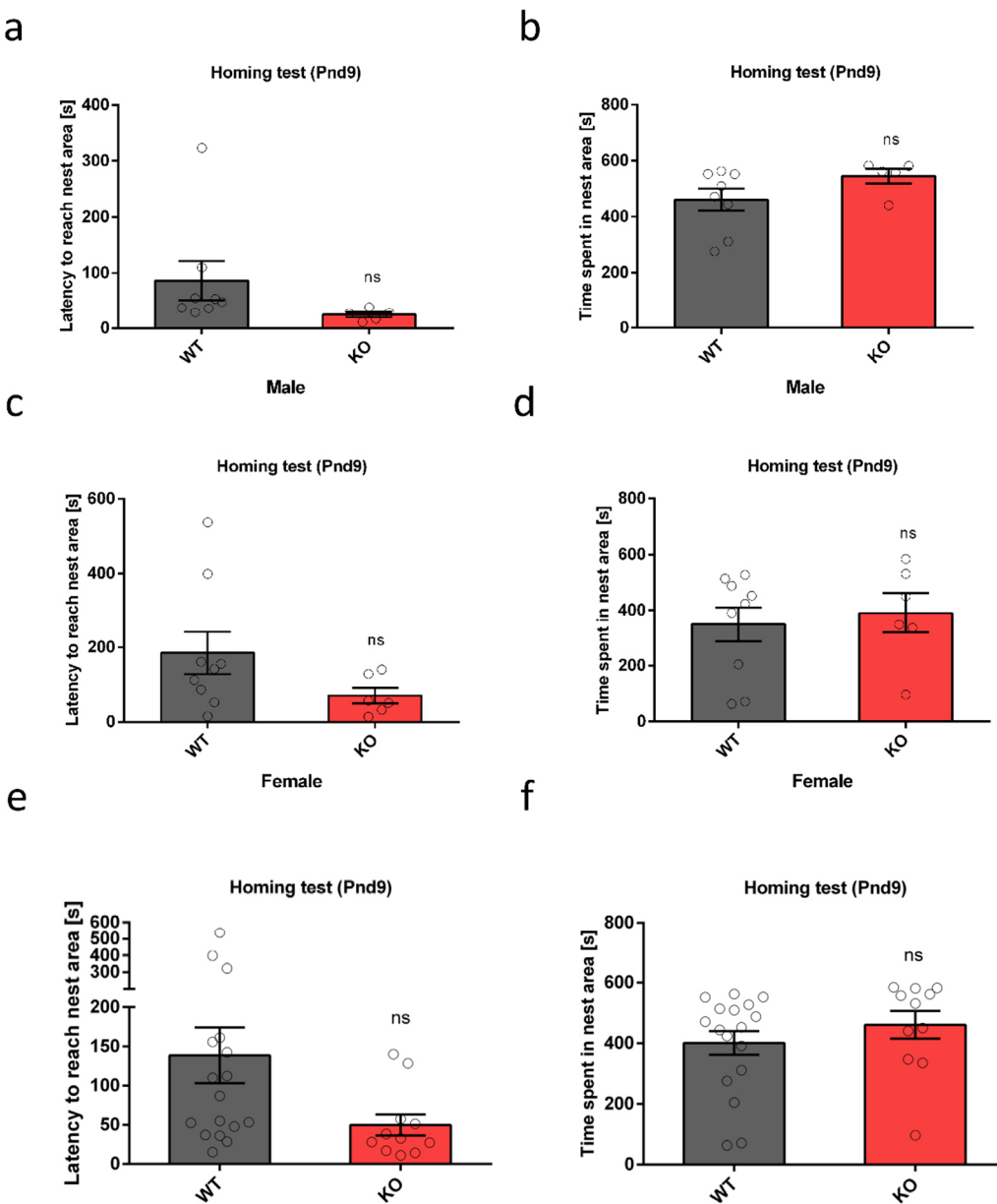
Figure 9: Pup homing test in miR379-410 wt and ko animals performed at Pnd9. a, c, e, Latency to reach the area containing nest material from their home cages. **a,** male pups, ns p=0.1969, unpaired Student`s t-test. **c,** female pups, ns p=0.1411, unpaired Student`s t-test. **e,** pooled male and female data, ns p=0.0632, unpaired Student`s t-test. **b, d, f,** Time spent in the nest area. **b,** male pups, ns p=0.1470, unpaired Student`s t-test. **d,** female pups, ns p=0.6644, unpaired Student`s t-test. **f,** pooled male and female data, ns p=0.3345, unpaired Student`s t-test. **a-f**, miR379-410 wt n=17 (male n=8, female n=9); ko n=11 (male n=5, female n=6). Data are presented as mean ± s.e.m.

3.2 miR379-410 ko pups isolated from the mother emit more ultrasonic vocalizations

The emission of ultrasonic vocalizations (USVs) from pups isolated from the mother were investigated at pnd3, 6, 9 and 12 **(Fig. 10)**. These specific USV calls are important signals that can stimulate search and retrieval behaviours in the maternal animal. There were no sex specific significant differences, neither in the developmental time course of total number of USV calls in male pups (**Fig. 10a, c**), nor in the total number of USV emitted on average from pnd3, 6, 9 and 12 (**Fig. 10 b, d**). However, a significant increase of emitted USV at pnd 9 in the pooled data of male and female pups was detected (**Fig. 10e**), as well as increased emitted USV calls in the pooled data of both sexes (**Fig. 10f**), indicating a generally enhanced communicative behaviour in neonatal miR379-410 ko animals.
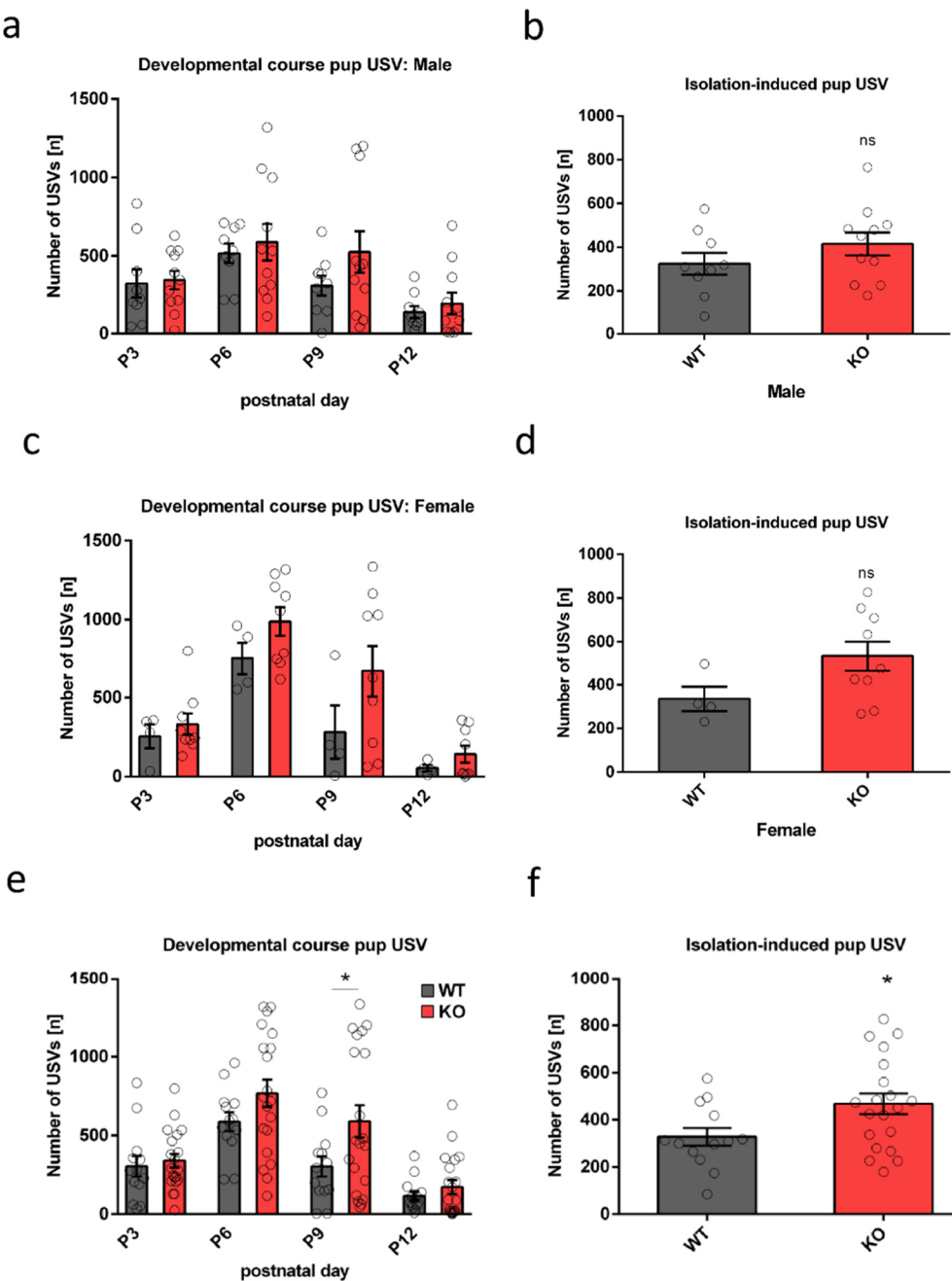
Figure 10: Ultrasonic vocalizations (USVs) in isolated miR379-410 wt and ko mouse pups measured on Pnd3, Pnd6, Pnd9 and Pnd12. a, c, e, Developmental time course for total number of USV. **a,** male pups. **c,** female pups. **e,** pooled male and female data, (development: $F_{3,87}=25.463$, p<0.001; genotype: $F_{1,29}=4.979$, p=0.03; development x genotype: $F_{3,87}=1.403$, p= 0.22, rm-ANOVA), P9 *p=0.044, unpaired Student`s t-test. **b, d, f,** Total number of ultrasonic vocalizations (USV) emitted on average postnatal days (P3, 6, 9 and 12) by miR379-410 wt and ko mouse pups when isolated from the mother. **b,** male pups, ns p=0.2351, unpaired Student`s t-test. **d,** female pups, ns p=0.1034, unpaired Student`s t-test. **f,** pooled male and female data, *p=0.0301, unpaired Student`s t-test. **a-f,** miR379-410 wt n=13 (male n=9, female n=4), ko n=20 (male n=11, female n=9). Data are presented as mean ± s.e.m.

3.3 Nest homing and maternal interaction behaviour are not affected in juvenile miR379-410 ko mice

Neurodevelopmental disorders such as ASD are characterized by social impairments and withdrawal. Thus, the social aspect of juvenile animal behaviour (pnd19) was investigated in the nest homing and maternal interaction test (as indicated in **Figure 11**). Juvenile mice were separated from their mother and individually placed into one corner of a novel test box which contained clean bedding except from one corner that had bedding from the home cage. Both genotypes and sexes spent significantly more time in the corner with the home cage bedding during the test period (**Fig. 11a, c, e**). These data confirmed, in agreement with the previously described pup homing test (cp. **Fig. 9**), an intact ability to detect and respond to familiar olfactory cues in juvenile miR379-410 ko animals. Subsequently, an empty wire cage was placed into one corner and another wire cage containing the mother was placed on the diagonally opposite corner of the box. Male and female miR379-410 wt and ko juvenile showed a significant preference for investigating the wire cage containing the mother compared to the empty one (**Fig. 11b, d, f**). These observations suggest intact social interest and motivation as judged by normal maternal approach behaviour in juvenile miR379-410 ko mice.
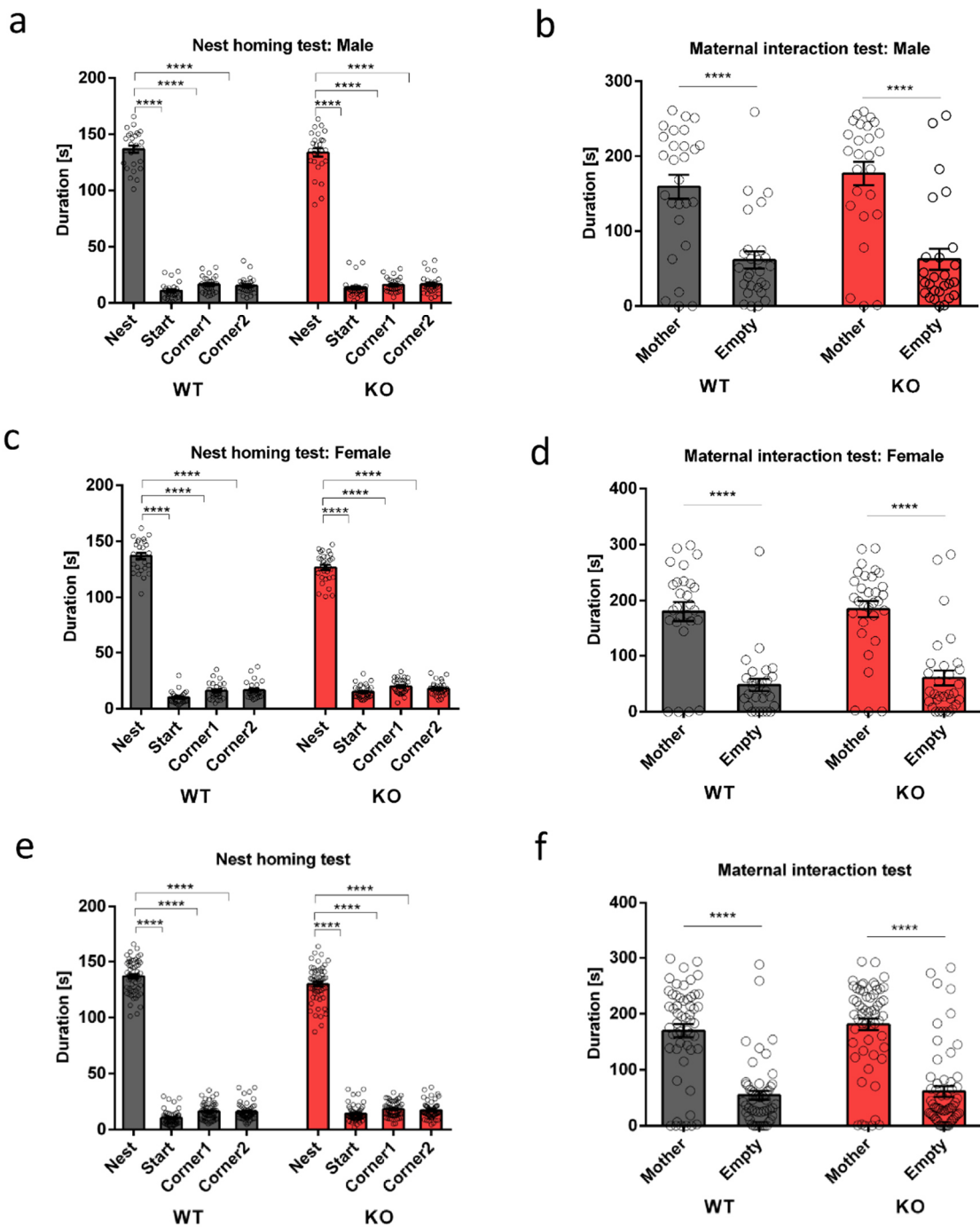
Figure 11: Nest homing and maternal interaction test in juvenile miR379-410 wt and ko animals. a, c, e, Nest homing test in Pnd19 animals. **a,** juvenile male, ****$p<0.0001$. **c,** juvenile female, ****$p=0.0001$. **e,** pooled male and female data, ****$p<0.0001$. **b, d, f,** Maternal interaction test in Pnd19 animals. **b,** juvenile male, ****$p<0.0001$. **d,** juvenile female, ****$p<0.0001$. **f,** pooled male and female data, ****$p<0.0001$. **a-f**, miR379-410 wt n=54 (male n=27, female n=27), ko n=57 (male n=26, female n=31); unpaired Student`s t-test. Data are presented as mean ± s.e.m.

3.4 Increased sociability in juvenile miR379-410 ko mice

Since many neurodevelopmental disorders are characterized by social withdrawal with conspecifics in early lifetime, the reciprocal social interaction test was performed to evaluate social interaction capabilities in juvenile mice. As shown in **Figure 12**, male ko-pairs spent significantly more time interacting with each other compared to male wt-pairs (**Fig. 12a**), whereas no significant difference in interaction time was detected between female ko- and wt-pairs (**Fig. 12d**). By pooling data of male and female wt- and ko-pairs, a significant increase in interaction time was observed in ko-pairs (**Fig. 12e**), indicating that lack of the miR379-410 positively affects sociability. This hypersocial phenotype was paralleled by a significant increase in the emission of pro-social USV calls detected during the reciprocal social interaction test. An increased number of USV calls was observed for male ko-pairs (**Fig. 12b**), female ko-pairs (**Fig. 12d**) and in the pooled data from male and female ko-pairs (**Fig. 12f**).
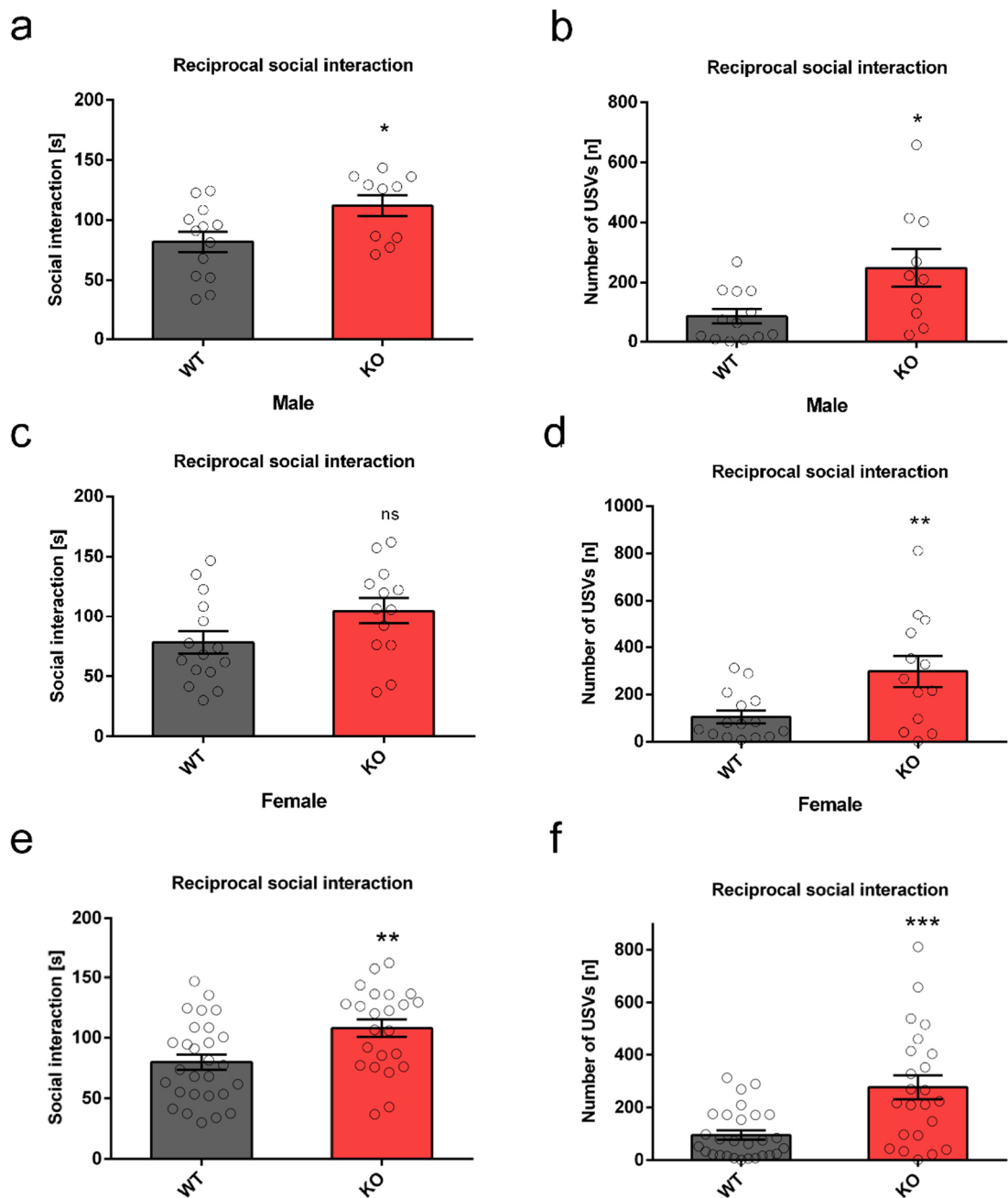
Figure 12: Reciprocal social interaction in juvenile miR379-410 wt- and ko mice pairs at Pnd23. **a, c, e,** Time spent in social interaction activity in ko-pairs compared to their control wt littermate pairs. **a,** male pairs, *p=0.0240. **c,** female pairs, ns p=0.0723. **e,** pooled male and female data, **p=0.005. **b, d, e,** Emitted USVs during social interaction activity in genotype-matched pairs in juvenile mice at Pnd23. **b,** male pairs, *p=0.0133. **d,** female pairs, **p=0.0081. **f,** pooled male and female data, ***p<0.001. **a-f**, miR379-410 wt-pairs n=28 (male n=15, female n=13), ko-pairs n=23 (male n=10, female n=13); unpaired Student`s t-test. Data are presented as mean ± s.e.m.

3.5 Increased social approach behaviour in the absence of social recognition deficits in juvenile and adult miR379-410 ko mice

To evaluate social approach in juvenile and adult animals, the three-chamber social approach task was conducted. This test measures also social behaviour in mice but in a less sensitive way compared to the reciprocal social interaction test, since only one test subject can freely move in the apparatus whereas the other subject is contained under a wire cage. Nevertheless, the three-chamber assay has the advantage that it allows to combine different parameters for the evaluation of social approach and social memory. Juvenile female (**Fig. 13c**) ko animals and the pooled data of both sexes (**Fig. 13e**) demonstrated enhanced social approach behaviour. While the social approach pattern was comparable between ko and wt males (**Figure 13b**), ko females showed increased sociability compared to wt (**Fig. 13d**) as highlighted by the social preference index, calculated as time spent with the subject divided through the time spent with the object. In the pooled data, this social-over-object preference was still prominent in the ko mice compared to wt controls (**Fig. 13f**), suggesting a pro-social effect of the miR379-410 deletion in juvenile mice, in agreement with the data from the social interaction tests (cp. **Fig. 12**). In contrast, social recognition was not impaired in juvenile ko mice (**Fig. 14**), neither in male (**Fig. 14a-b**), female (**Fig. 14c-d**) nor in pooled data of both sexes (**Fig. 14e-f**), indicating intact social memory function in juvenile miR379-410 ko mice.

To clarify if the hypersocial behaviour observed in juvenile ko mice is still present in older animals, the same mice were tested again for social approach (**Fig. 15**) and social recognition (**Fig. 16**) behaviour in 3-month-old animals. As in juvenile ko males, the social approach behaviour was unaltered in adult ko males compared to wt **(Fig. 15a-b)**, whereas the social approach behaviour was enhanced in both ko females **(Fig. 15c-d)** and in the pooled data of both sexes **(Fig. 15e-f)**. Thus, these results indicate that loss of the miR379-410 cluster promotes social behaviour across the lifespan. Social recognition in adult ko males (**Fig. 16a-b**), females (**Fig. 16c-d**) and in pooled data of both sexes (**Fig. 16e-f**) was not impaired, pointing to normal social memory function in adult ko mice. Taken together, these findings demonstrate that lack of the miR379-410 cluster increases sociability across the entire lifespan with no impairments in social memory.
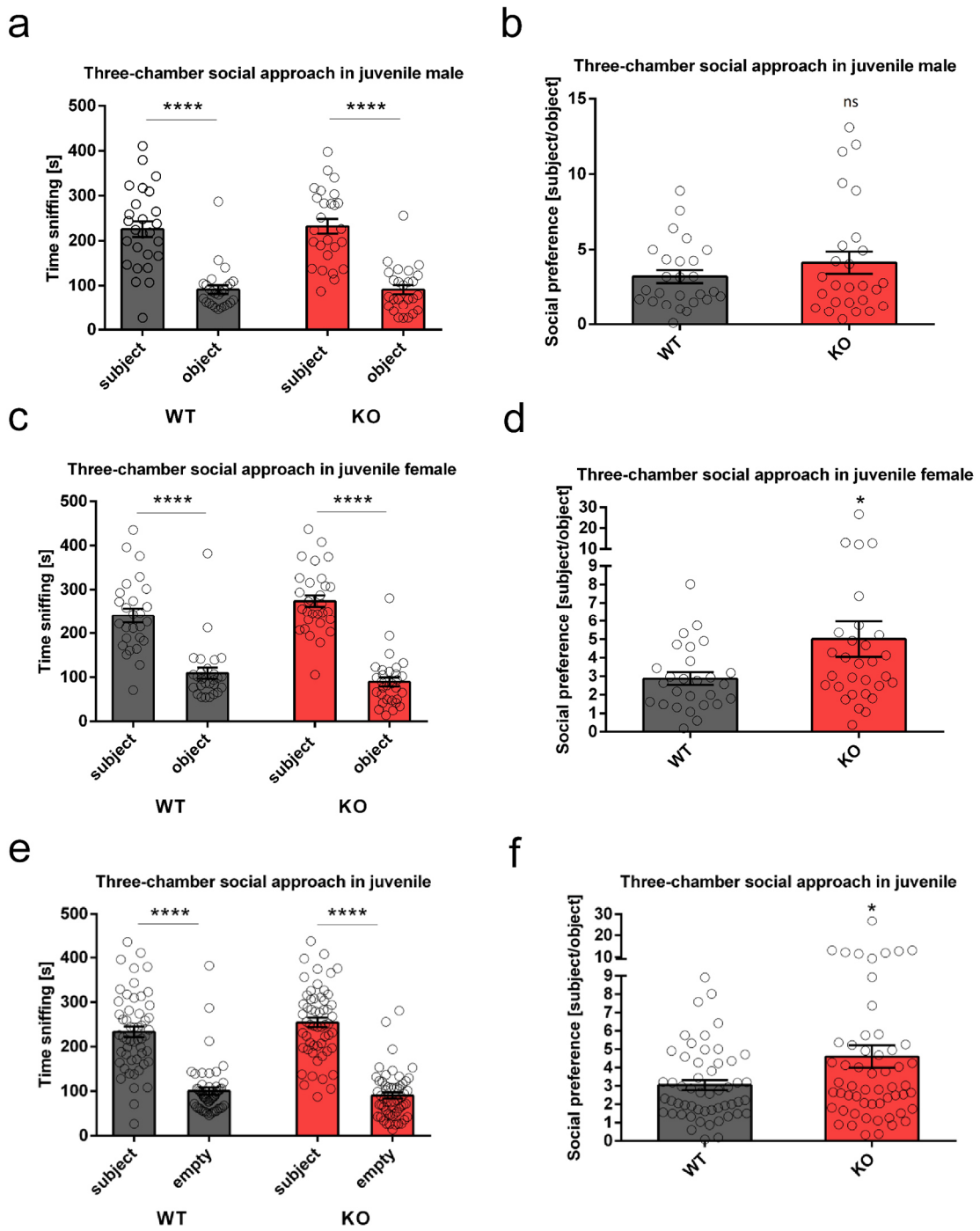
Figure 13: Three-chamber social approach test in juvenile miR379-410 wt and ko mice. **a, c, e,** Time sniffing subject and object is shown. **a,** juvenile male, ****p<0.0001, paired Student`s t-test. **c,** juvenile female, ****p<0.0001, paired Student`s t-test. **e,** pooled male and female data, ****p<0.0001, paired Student`s t-test. **b, d, f,** Social preference index - defined as the ratio of time sniffing a stranger mouse vs. an object - is shown. **b,** juvenile male, ns p=0.2876, unpaired Student`s t-test. **d,** juvenile female, *p=0.0486, unpaired Student`s t-test. **f,** pooled male and female data, *p=0.0244, unpaired Student`s t-test. **a-f**, miR379-410 wt n=53 (male n=26, female n=27), ko n=56 (male n=26, female n=30). Data are presented as mean ± s.e.m.
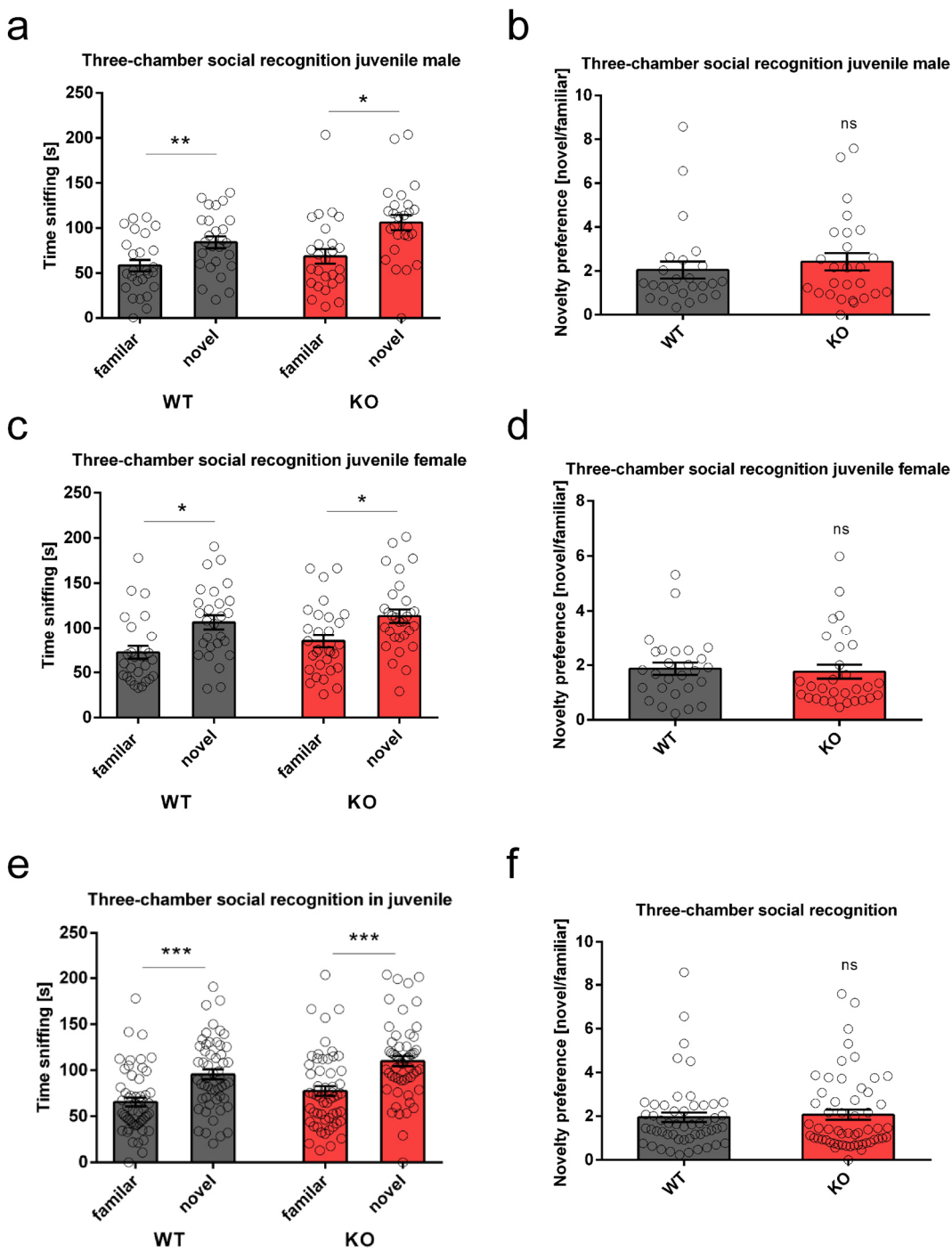
Figure 14: Three-chamber social recognition test in juvenile miR379-410 wt and ko mice. a, c, e, Time sniffing familiar and novel animal is shown. **a,** juvenile male wt **p=0.0072, ko *p=0.0161; paired Student`s t-test. **c,** juvenile female wt *p=0.0101, ko *p=0.0225; paired Student`s t-test. **e,** pooled male and female data, wt ***p<0.0002, ko ***p<0.0008; paired Student`s t-test. **b, d, f,** Novelty preference index - defined as the ratio of time sniffing a novel vs. a familiar mouse - is shown. **b,** juvenile male, ns p=0.4954, unpaired Student`s t-test. miR379-410 wt n=25, ko n=26. **d,** juvenile female, ns p=0.7448; unpaired Student`s t-test. **f,** pooled male and female data, ns p=0.7244, unpaired Student`s t-test. **a, c-f**, miR379-410 wt n=53 (male n=26, female n=27), ko n=56 (male n=26, female n=30). Data are presented as mean ± s.e.m.
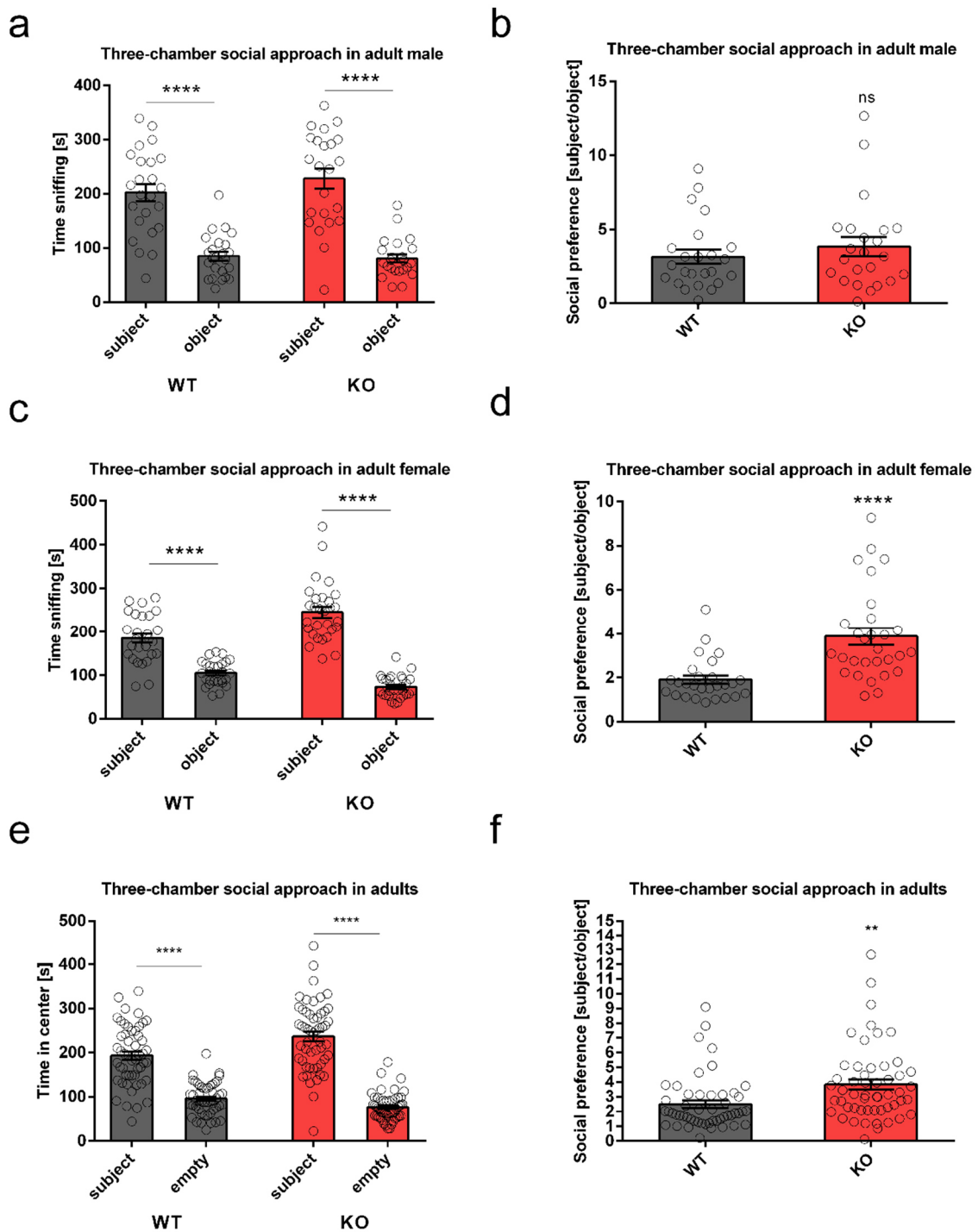
Figure 15: Three-chamber social approach test in adult miR379-410 wt and ko mice. **a, c, e,** Time sniffing subject and object is shown. **a,** adult male, ****p<0.0001, paired Student`s t-test. **c,** adult female, ****p<0.0001, paired Student`s t-test. **e,** pooled adult male and female data, ****p<0.0001, paired Student`s t-test. **b, d, f,** Social preference index - defined as the ratio of time sniffing a stranger mouse vs. an object - is shown. **b,** adult male, ns p=0.3854, unpaired Student`s t-test. **d,** adult female, ****p<0.0001, unpaired Student`s t-test. **f,** pooled adult male and female data, **p=0.0025, unpaired Student`s t-test. **a-f,** miR379-410 wt n=51 (male n=24, female n=27), ko n=52 (male n=23, female n=29). Data are presented as mean ± s.e.m.
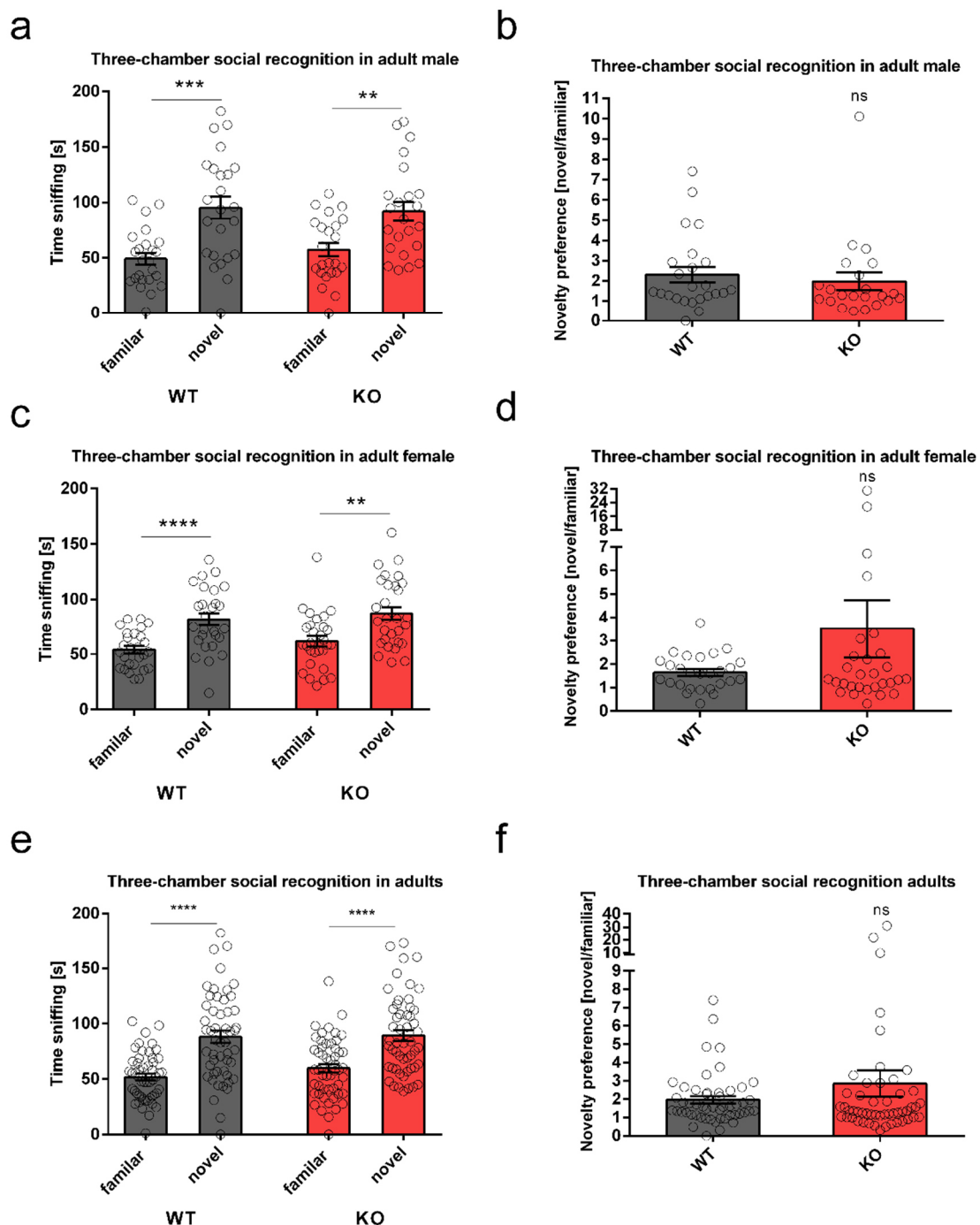
**Figure 16: Three-chamber social recognition test in adult miR379-410 wt and ko mice. a, c, e,** Time sniffing familiar and novel animal is shown. **a,** adult male wt ***p=0.0002, ko **p=0.0085, paired Student`s t-test. **c,** adult female wt ****p<0.0001, ko **p=0.0033, paired Student`s t-test. **e,** pooled adult male and female data, wt ****p<0.0001, ko ****p<0.0001, paired Student`s t-test. **b, d, f,** Novelty preference index - defined as the ratio of time sniffing a novel vs. a familiar mouse - is shown. **b,** adult male, ns p=0.5672, unpaired Student`s t-test. miR379-410 wt n=24, ko n=22. **d,** adult female, ns p=0.1525, unpaired Student`s t-test. **f,** pooled adult male and female data, ns p=0.2400, unpaired Student`s t-test. **a, c-f**, miR379-410 wt n=51 (male n=24, female n=27), ko n=52 (male n=23, female n=29). Data are presented as mean ± s.e.m.

3.6 Loss of miR379-410 expression does not impair novel object recognition in juvenile mice

The novel object recognition test was performed to evaluate non-social memory in juvenile and adult miR379-410 wt and ko mice. Compared to wt mice, juvenile ko male (**Fig. 17a**) and female (**Fig. 17c, e**) mice spent similar time sniffing the objects in both sides of the chamber during the object acquisition task, indicating no object preference. This was additionally reflected by the object preference ratio, calculated as time spent with object 1 divided through time spent with object 2, which was comparable for all three groups (**Fig. 17b, d, f**). During the novel object recognition task, ko males and surprisingly also wt males (**Fig. 18a**) could not distinguish between the novel and the familiar object. This result indicates that the test setup could not reliably detect memory functions, and therefore no further conclusions about potential differences between wt and ko mice can be drawn. As expected, wt female mice preferred the novel over the familiar object during the object recognition task. The same was true for ko female mice (**Fig. 18 b**) and when data from both sexes was pooled (**Fig. 18e**) indicating normal non-social memory function in wt and ko mice. In addition, no difference between the genotypes and sexes was detected for the novelty preference ratio, calculated as time spent with the novel object divided through the time spent with the familiar object. This result indicates that juvenile wt and ko animals have comparable non-social memory functions (**Fig. 18b, d, f**).

The object acquisition and novel object recognition tests were performed again in adult animals to investigate if memory impairments could occur later in life due to the miR379-410 deletion. As in juvenile animals, no object preference is observed when comparing genotypes and sexes (**Fig. 19**) during the object acquisition task. Surprisingly again, male wt controls were not able to distinguish between the novel and familiar object, indicating a problem with the test setup. However, ko males (**Fig. 20a**), and females (**Fig. 20d, e**) were able to distinguish between old and new object. For the novelty preference ratio, no difference between genotype and sexes appeared (**Fig. 20b, d**) except of the pooled data of both sexes, where ko mice (**Fig. 20f**) seemed to perform better in the novel object recognition task compared to the wt controls. In conclusion, non-social memory seems to be intact in adult miR379-410 ko mice.
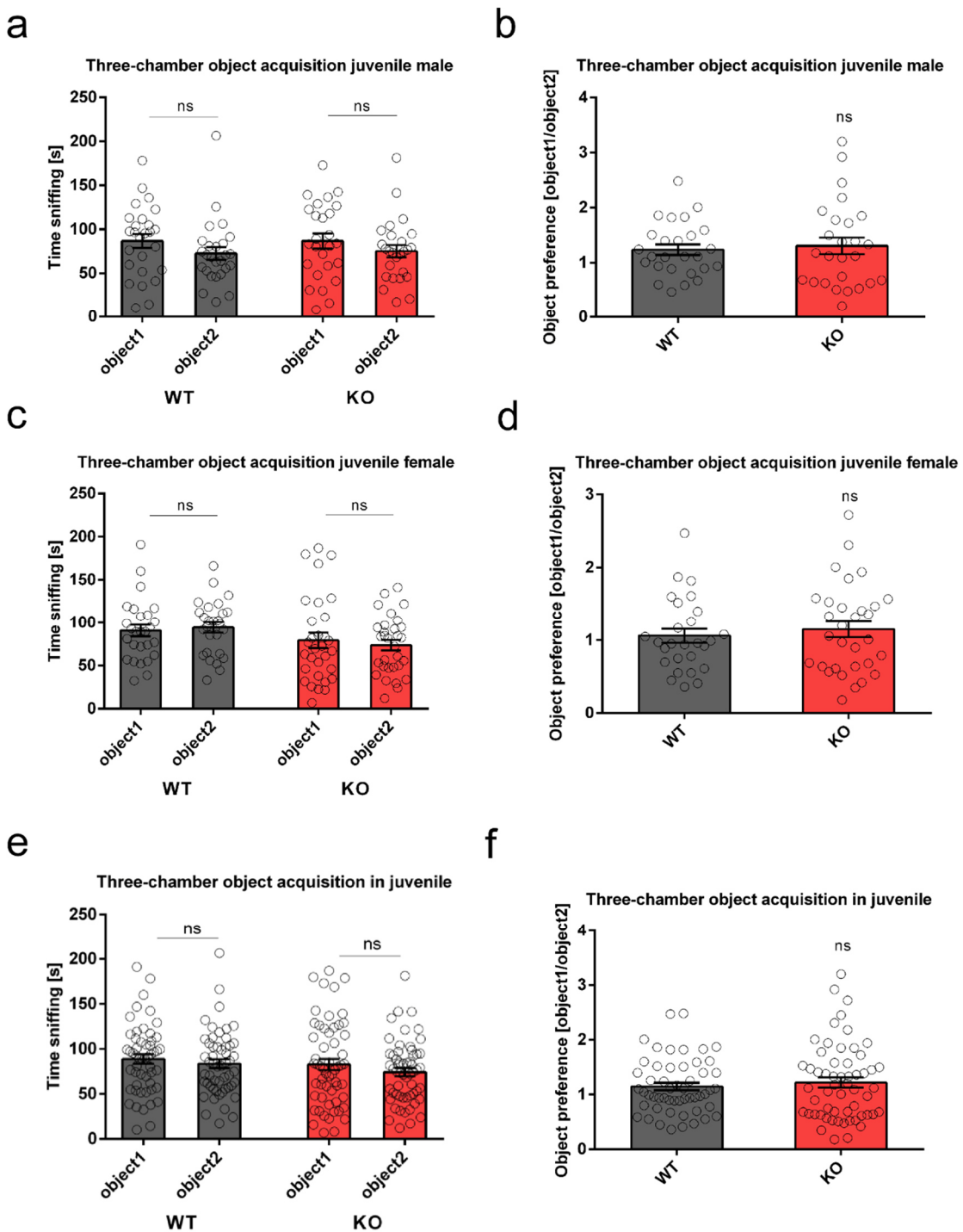
Figure 17: Three-chamber object acquisition test in juvenile miR379-410 wt and ko mice. a, c, e, Time sniffing identical object1 and object2 is shown, **a,** juvenile male wt ns p=0.0797, ko ns p=0.2518, paired Student`s t-test. **c,** juvenile female wt ns p=0.6820, ko ns p=0.4857, paired Student`s t-test. **e,** pooled male and female data, wt ns p=0.3810, ko ns p=0.1846, paired Student`s t-test. **b, d, f,** Object preference index - defined as the ratio of time sniffing object1 vs. object2 - is shown. **b,** juvenile male, ns p=0.7038, unpaired Student`s t-test. **d,** juvenile female, ns p=0.5549, unpaired Student`s t-test. **f,** pooled male and female data, ns p=0.5270, unpaired Student`s t-test. **a-f**, miR379-410 wt n=53 (male n=26, female n=27), ko n=57 (male n=26, female n=31). Data are presented as mean ± s.e.m.
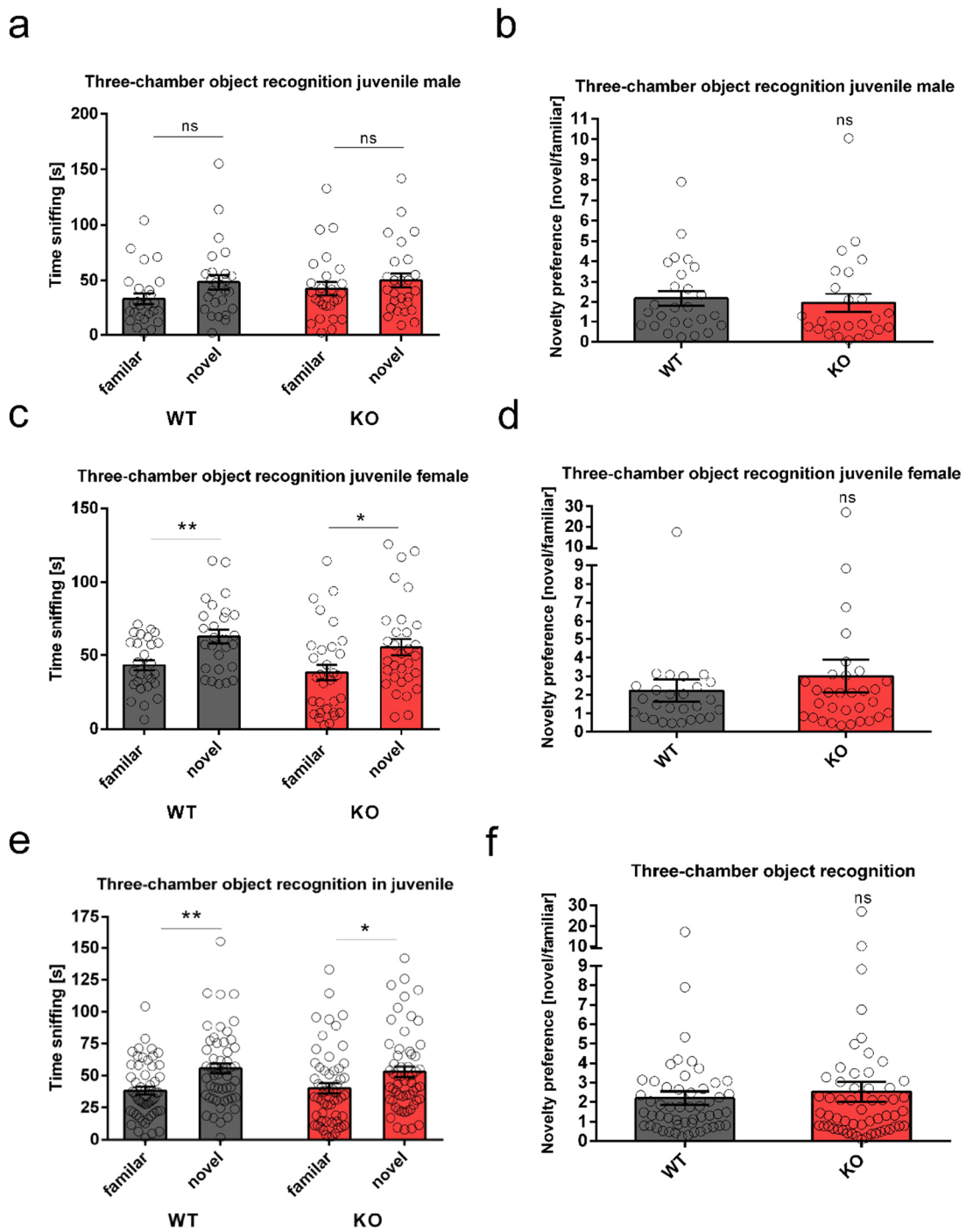
Figure 18: Three-chamber novel object recognition test in juvenile miR379-410 wt and ko mice. a, c, e,
Time sniffing familiar and novel object is shown. **a,** juvenile male wt ns p=0.0821, ko ns p=0.4758, paired
Student`s t-test. **c,** juvenile female wt **p=0.0072, ko *p=0.0303, paired Student`s t-test. **e,** pooled male
and female data, wt **p=0.0018, ko *p=0.0459, paired Student`s t-test. **b, d, f,** Novelty object preference
index - defined as the ratio of time sniffing a novel vs. a familiar object - is shown. **b,** juvenile male, ns
p=0.6951, unpaired Student`s t-test. miR379-410 wt n=26, ko n=25. **d,** juvenile female, ns p=0.4743,
unpaired Student`s t-test. **f,** pooled male and female data, ns p=0.5295, unpaired Student`s t-test. **a, c-f,**
miR379-410 wt n=53 (male n=26, female n=27), ko n=57 (male n=26, female n=31). Data are presented as
mean ± s.e.m.
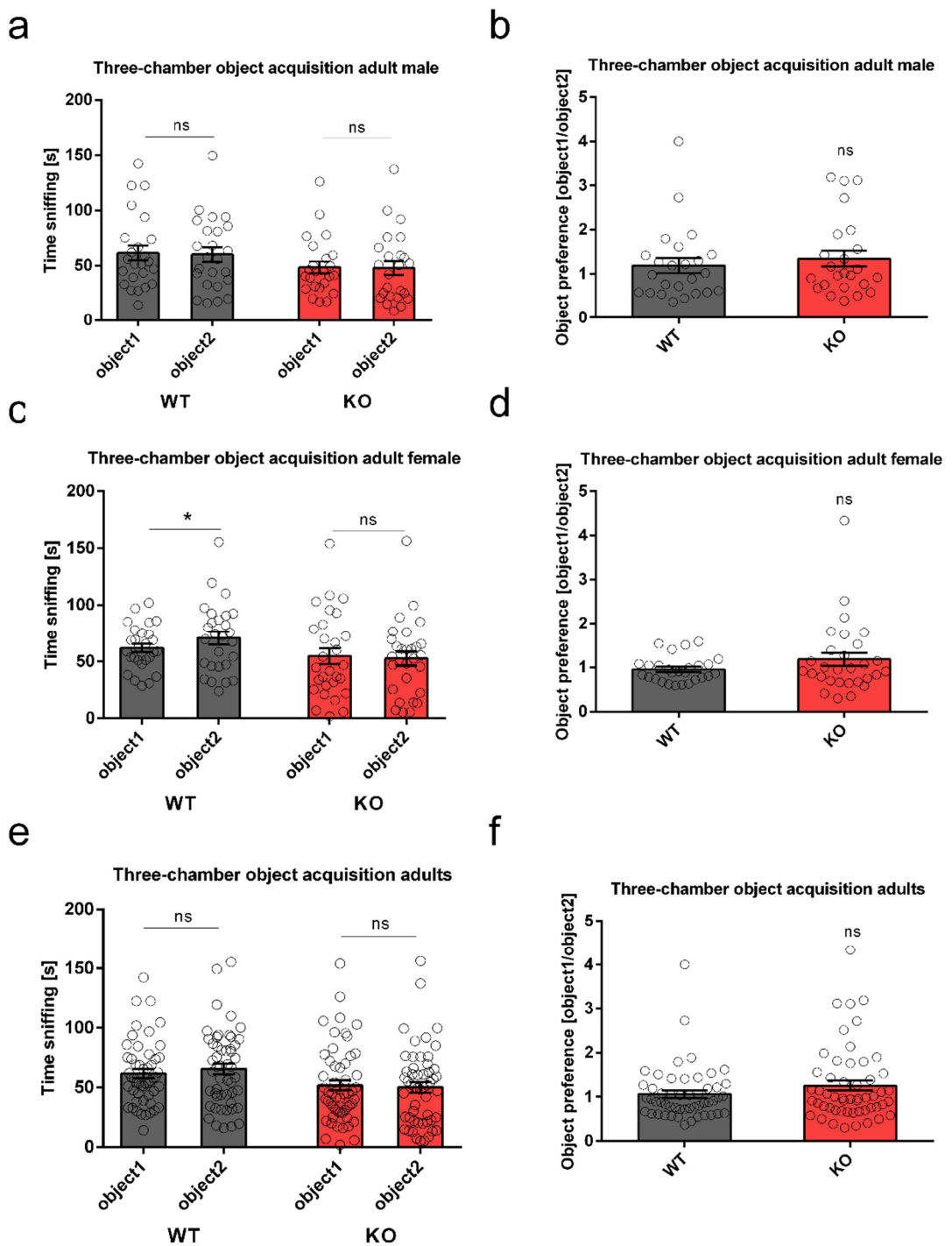
Figure 19: Three-chamber object acquisition test in adult miR379-410 wt and ko mice. a, c, e, Time sniffing identical object1 and object2 is shown, **a,** adult male wt ns p=0.9094, ko ns p=0.8357, paired Student`s t-test. **c,** adult female wt *p=0.0450, ko ns p=0.7758, paired Student`s t-test. **e,** pooled adult male and female data, wt ns p=0.1379, ko ns p=0.7613, paired Student`s t-test. **b, d, f,** Object preference index - defined as the ratio of time sniffing object1 vs. object2 - is shown. **b,** adult male, ns p=0.5249; unpaired Student`s t-test. **d,** adult female, ns p=0.1736, unpaired Student`s t-test. **f,** pooled adult male and female data, ns p=0.1862, unpaired Student`s t-test. **a-f**, miR379-410 wt n=51 (male n=24, female n=27), ko n=53 (male n=24, female n=29). Data are presented as mean ± s.e.m.
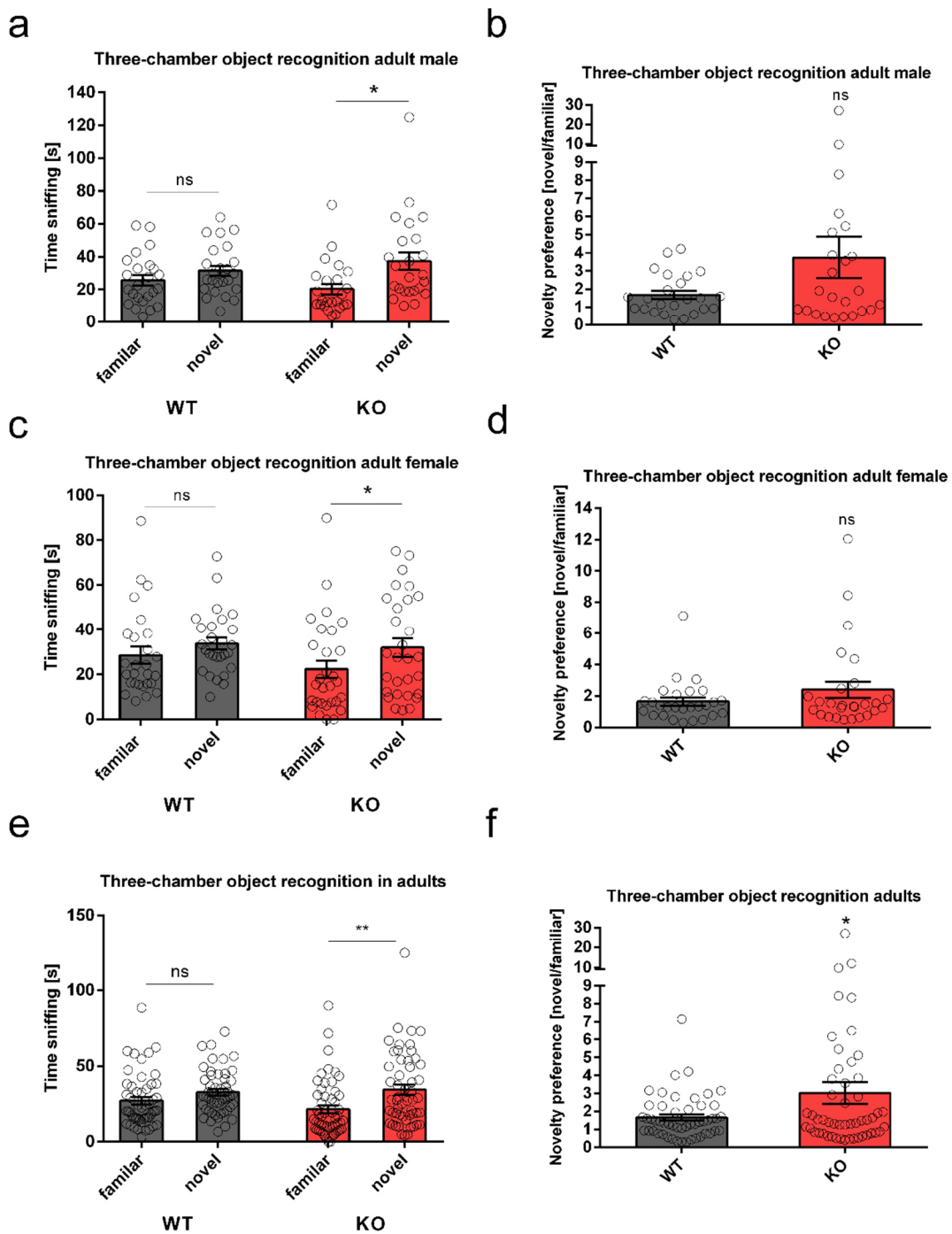
Figure 20: Three-chamber novel object recognition test in adult miR379-410 wt and ko mice. a, c, e, Time sniffing familiar and novel object is shown. **a,** adult male wt ns p=0.1444, ko *p=0.0259, paired Student`s t-test. **c,** adult female wt ns p=0.2352, ko *p=0.0407, paired Student`s t-test. **e,** pooled adult male and female data, wt ns p=0.0617, ko **p=0.0023, paired Student`s t-test. **b, d, f,** Novelty object preference index - defined as the ratio of time sniffing a novel vs. a familiar object - is shown. **b,** adult male, ns p=0.0841, unpaired Student`s t-test. **d,** adult female, ns p=0.1999, unpaired Student`s t-test. miR379-410 wt n=27, ko n=27. **f,** pooled adult male and female data, *p=0.0322, unpaired Student`s t-test. **a-c, e, f,** miR379-410 wt n=51 (male n=24, female n=27), ko n=53 (male n=24, female n=29). Data are presented as mean ± s.e.m.

**3.7 miR379-410 deletion promotes specific anxiety-related behaviours in juvenile and adult mice**

To investigate anxiety in juvenile and adult animals, the open field (OF) task was performed by recording the approach-avoidance behaviour that is typically found in rodents when they explore unfamiliar environments. Anxiety-related behaviour is reflected by the level of avoidance of the central part of the open field arena. Juvenile ko males, females and the pooled data of both sexes spent less time in the center area compared to wt littermate controls (**Fig. 21a, c, e**). Whereas the number of visits into the central area was not reduced in juvenile ko male (**Fig. 21b**) and female mice (**Fig. 21d**), a significant reduction was observed in the pooled data of both sexes (**Fig. 21f**). To confirm the increased avoidance behaviour in older miR379-410 ko mice, the OF test was repeated in adults. The OF test was conducted on two subsequent days. On day one, adult ko male mice did not show reduced time in the center or number of visits (**Fig. 22a-b**) and the same was true on day 2 (**Fig. 23 a-b**) by measuring the animals again. This suggest no approach-avoidance behaviour in adult ko males. Interestingly, approach-avoidance was present in adult ko females, as indicated in reduced time spent in the center and less visits of the center area on day one (**Fig. 22c-d**) and day two (**Fig. 23 c-d**). This result suggests that miR379-410 ko mice are more anxious than wt littermates. By pooling data of both sexes, anxiety-like behaviour was still present in ko mice, as shown by both the reduced time spent in the center and less visits of the center area on day one **(Fig. 22e-f)** and on the subsequent day two **(Fig. 23e-f)**. In addition, spontaneous locomotion in a novel environment was evaluated in ko mice as an indicator of hyperactivity. Hyperactivity in response to novelty / stress is a widely used test in rodent models for positive symptoms associated with SCZ. On day one, the parameter of total distance traveled was reduced in ko males **(Fig. 24a)**, females **(Fig. 24b)** and in the pooled data of both sexes **(Fig. 24c)** compared to wt controls, therefore indicating reduced locomotor activity. On day two, ko males did not differ in the range of total distance traveled **(Fig. 24a),** but reduced locomotor activity was still visible in ko females **(Fig. 24b)** and in the pooled data of both sexes **(Fig. 24c)** in comparison to wt controls. The total locomotor activity between day one and day two was reduced in all wt groups, whereas no difference was observed between the days in the ko groups **(Fig. 24a-c)**. These findings indicate a consistent hypo-activity response of the miR379-410 ko mice to a novel environment.

Next, the elevated plus maze (EPM) test was performed in adult animals **(Fig. 25)** to confirm the increased anxiety-related behaviour observed in the OF. In the EPM, mice were placed

in a plus-shaped apparatus with two open and two (protective) enclosed arms that were elevated from the floor. In ko males, no difference was observed for time spent on the open arms **(Fig. 25a),** but animals displayed a reduced number of visits within the open arms compared to wt males **(Fig. 25b)**. In ko females and in the pooled data of both sexes, a reduction of time spent and number of visits of the open arms was observed **(Fig. 25c-f)**. Thus, our results indicate that miR379-410 ko mice display enhanced anxiety-related behaviour.

To further confirm the result in a third independent anxiety-related task, the light-dark-box (LDB) approach was performed in adult miR379-410 wt and ko animals. The LDB consist of a closed (protective) chamber that is connected with a small passage to an open (unprotected) bright arena. Surprisingly, ko males (**Fig. 26a**), females (**Fig. 26c**) and the pooled data of both sexes (**Fig. 26e**) did not show differences in the number of transitions between the protected and unprotected part when compared to wt controls. Further, ko males (**Fig. 26b**), females (**Fig. 26d**) and the pooled data of both sexes (**Fig. 26 f**) did not show differences in time spent in the open (light) arena compared to wt control mice, indicating that defects in anxiety-related behavioural tasks are limited to the OF and EPM task.
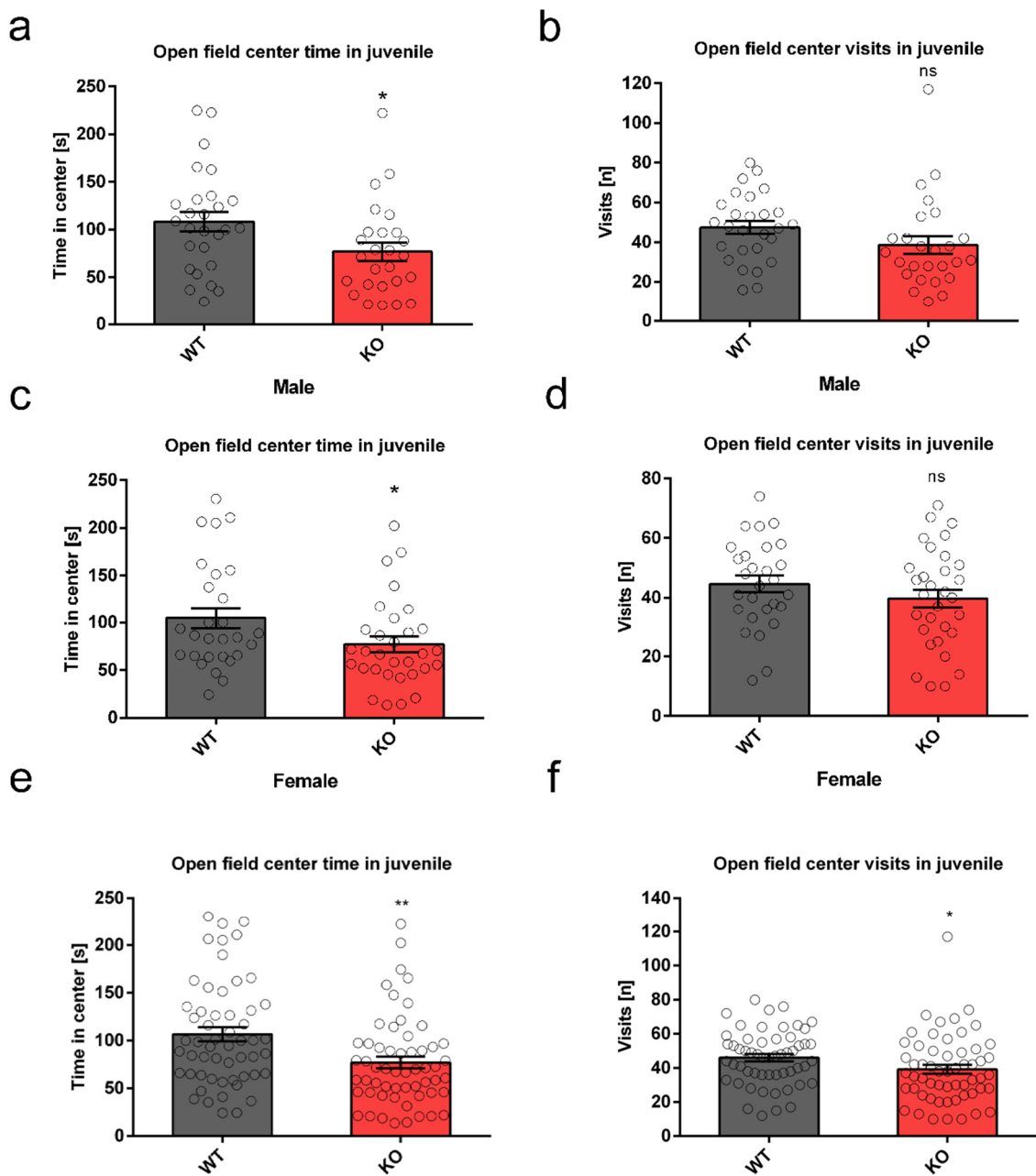
Figure 21: Open field test in juvenile miR379-410 wt and ko mice at Pnd18. a, c, e, Time spent in the central arena was examined. **a,** juvenile male, *p=0.0275. **c,** juvenile female, *p=0.0426. **e,** pooled male and female data, **p=0.0025. **b, d, f,** Center visits in the open field. **b,** juvenile male, ns p=0.1147. **d,** juvenile female, ns p=0.2483. **f,** pooled male and female data, *p=0.0476. **a-f,** miR379-410 wt n=55 (male n=27, female n=28), ko n=57 (male n=26, female n=31), unpaired Student`s t-test. Data are presented as mean ± s.e.m.
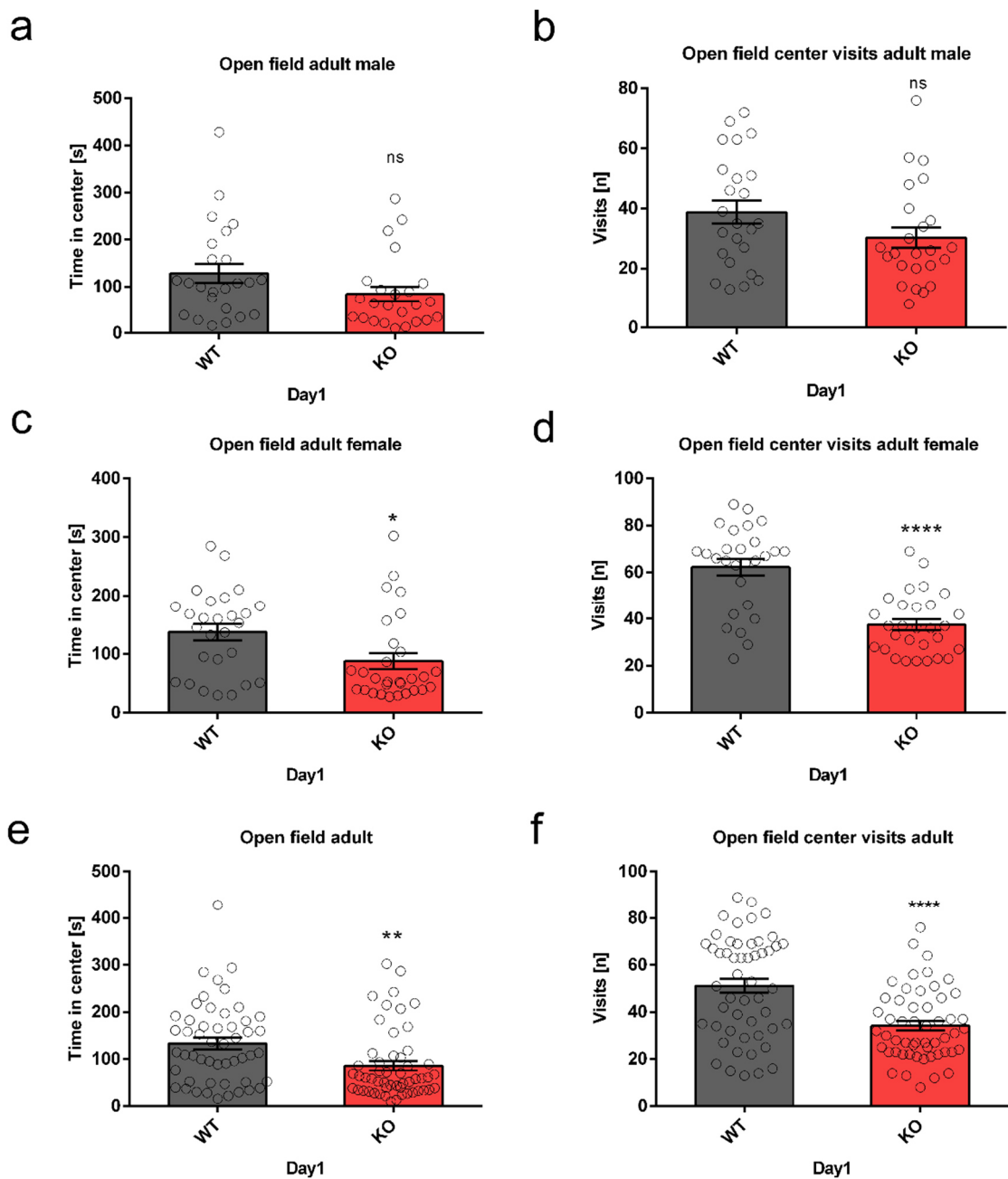
Figure 22: Open field test in adult miR379-410 wt and ko mice measured on day1. **a, c, e,** Time spent in the central arena was examined. **a,** adult male, ns p=0.0902. **c,** adult female, *p=0.0128. **e,** pooled male and female data, **p=0.0032. **b, d, f,** Center visits in the open field. **b,** adult male, ns p=0.1037. **d,** adult female, ****p<0.0001. **f,** pooled male and female data, ****p<0.0001. **a-f**, miR379-410 wt n=53 (male n=24, female n=27), ko n=53 (male n=24, female n=29), unpaired Student`s t-test. Data are presented as mean ± s.e.m.
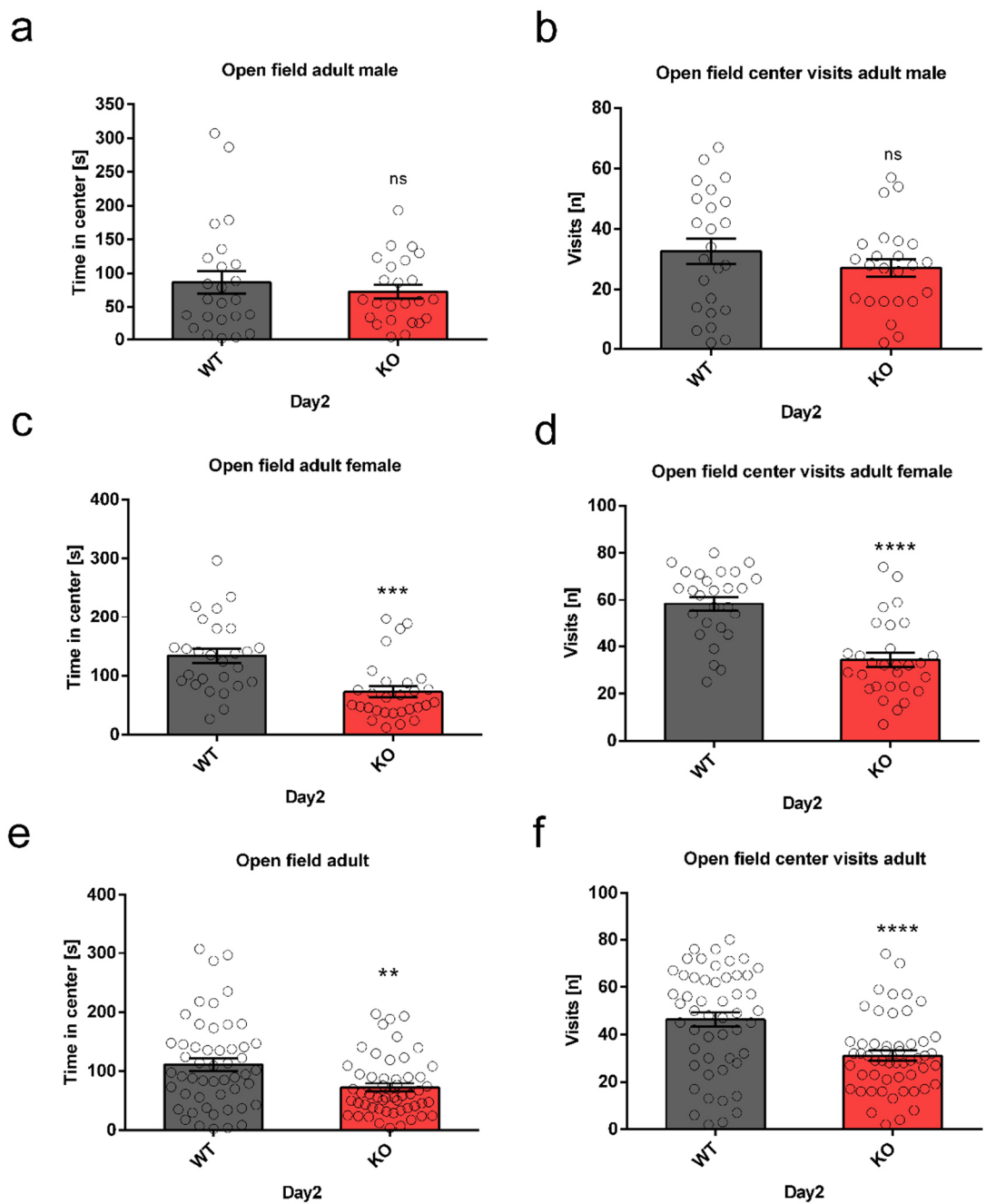
Figure 23: Open field test in adult miR379-410 wt and ko mice measured on day2. a, c, e, Time spent in the central arena was examined. **a,** adult male, ns p=0.4883. **c,** adult female, ***p=0.0001. **e,** pooled male and female data, **p=0.0023. **b, d, f,** Center visits in the open field. **b,** adult male, ns p=0.2835. **d,** adult female, ****p<0.0001. **f,** pooled male and female data, ****p<0.0001. **a-f**, mir379-410 wt n=53 (male n=24, female n=27), ko n=53 (male n=24, female n=29), unpaired Student`s t-test. Data are presented as mean ± s.e.m.
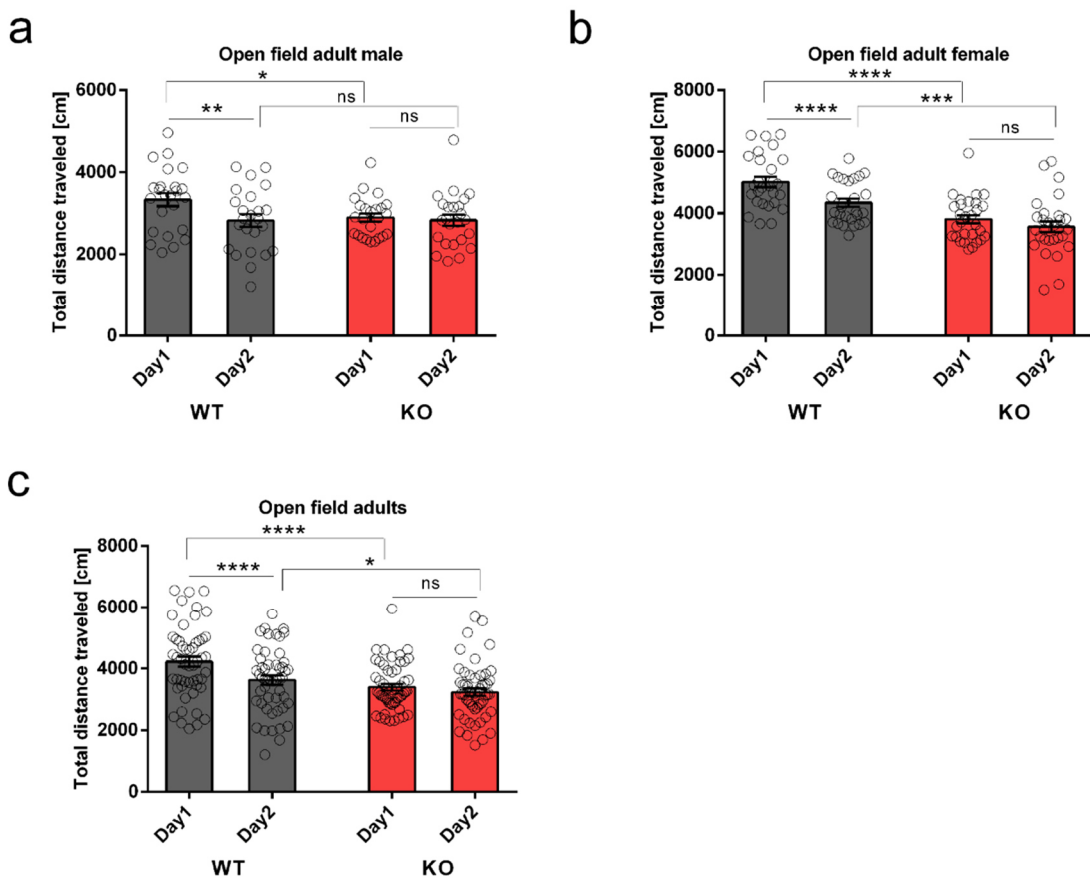
Figure 24: Total distance traveled in the open field test in adult miR379-410 wt and ko mice on two subsequent days. a, b, c, Total distance traveled on day1 and day2 in the open field is shown. **a,** adult male, wt day1 vs. day2 **p=0.0055, ko day1 vs. day2 ns p=0.5617, paired Student`s t-test; wt day1 vs. ko day1 *p=0.0250, wt day2 vs. ko day2 ns p=0.9628; unpaired Student`s t-test. **b,** adult female, wt day1 vs. day2 ****p<0.0001, ko day1 vs. day2 ns p=0.1159, paired Student`s t-test; wt day1 vs. ko day1 ****p<0.0001, wt day2 vs. ko day2 ***p=0.0009, unpaired Student`s t-test. **c,** pooled male and female data, wt day1 vs. day2 ****p<0.0001, ko day1 vs. day2 ns p=0.0959, paired Student`s t-test; wt day1 vs. ko day1 ****p<0.0001, wt day2 vs ko day2 *p=0.0417, unpaired Student`s t-test. **a-c**, mir379-410 wt n=53 (male n=24, female n=27), ko n=53 (male n=24, female n=29). Data are presented as mean ± s.e.m.
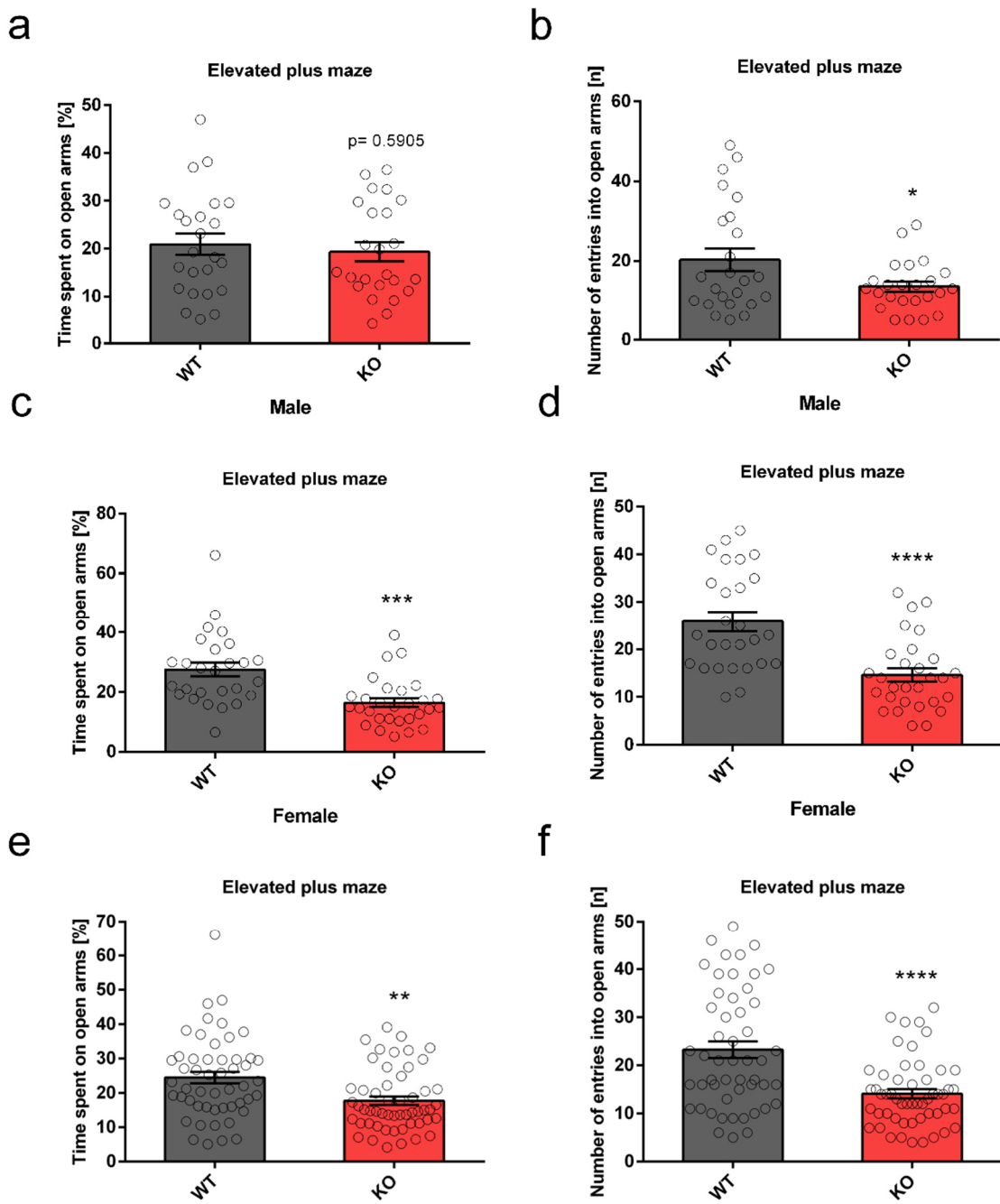
Figure 25: Elevated plus maze test in adult miR379-410 wt and ko mice. a, c, e, Time spent on open arms (percentage) are shown. **a,** adult male, ns p=0.5905. **c,** adult female, ***p=0.0001. **e,** pooled male and female data, **p=0.0015. **b, d, f,** Number of open arm entries was reduced in miR379-410 ko mice. **b,** adult male, *p=0.0326. **d,** adult female, ****p<0.0001. **f,** pooled male and female data, ****p<0.0001. **a-f,** miR379-410 wt n=51 (male n=24, female n=27), ko n=53 (male n=24, female n=29), unpaired Student`s t-test. Data are presented as mean ± s.e.m.
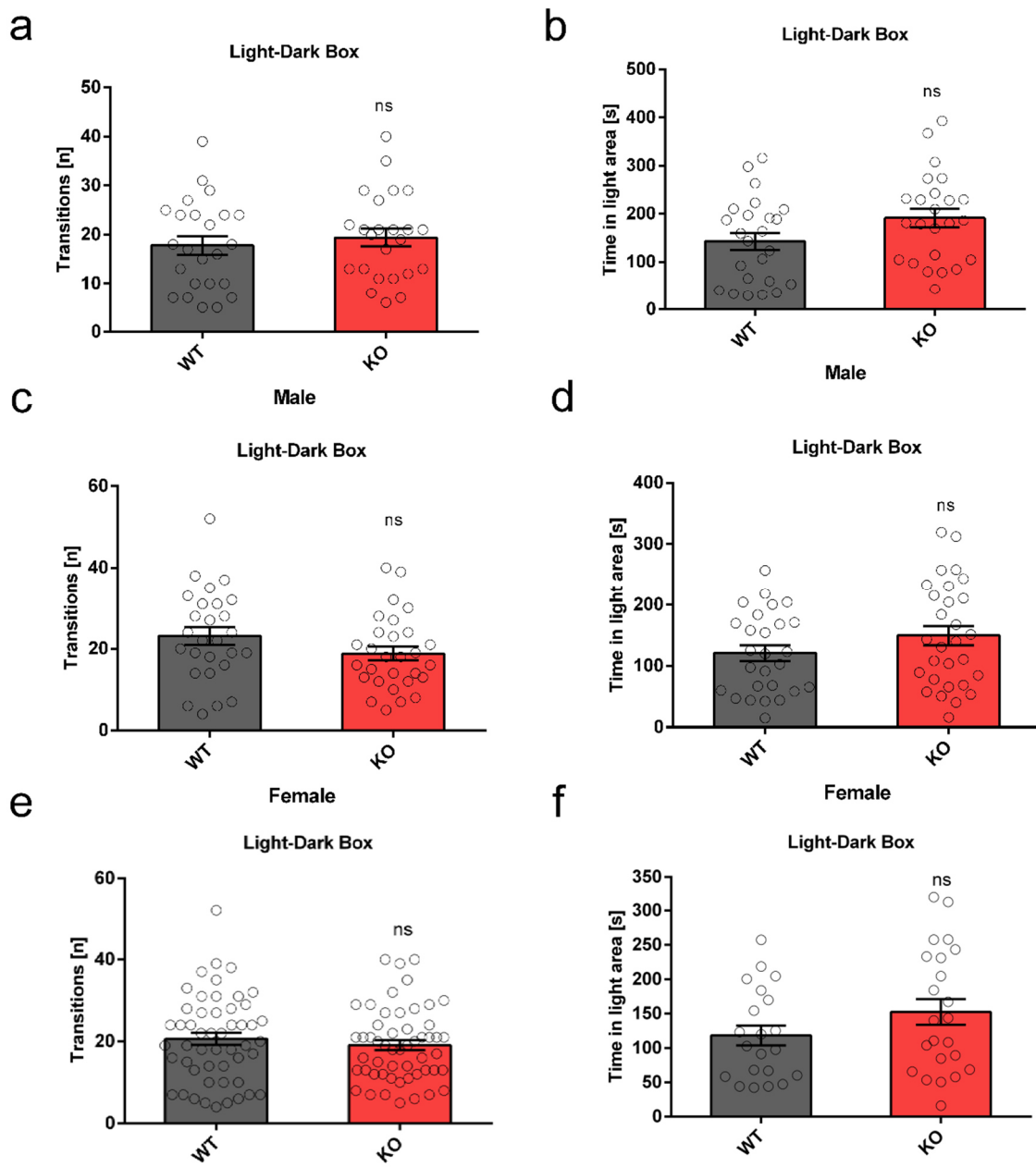
Figure 26: Light-Dark-Box approach in adult miR379-410 wt and ko mice. a, c, e, Transition numbers between dark and light area. **a,** adult male, ns p=0.5367. **c,** adult female, ns p=0.1143. **e,** pooled male and female data, ns p=0.4188. **b, d, f,** Time spent in light area. **b,** adult male, ns p=0.0686. **d,** adult female, ns p=0.1696. **f,** pooled male and female data, ns p=0.1603. **a-f,** miR379-410 wt n=51 (male n=24, female n=27), ko n=53 (male n=24, female n=29), unpaired Student`s t-test. Data are presented as mean ± s.e.m.

**3.8 miR379-410 ko mice display reduced repetitive behaviour**

Beside deficits in social behaviour and communication, one core symptom of ASD is restricted and repetitive behaviour. This can be reliably assessed in rodents with the marble burying test, which was performed in adult miR379-410 wt and ko mice. Marbles were arrayed on the surface of clean bedding and the number of marbles buried were scored after each test session. The number of buried marbles were comparable between ko and wt males (**Fig. 27a**), whereas the number of buried marbles were significantly reduced in ko females (**Fig. 27b**) and in the pooled data of both sexes (**Fig. 27c**) compared to wt controls. This result indicates that repetitive behaviour in miR379-410 ko mice is specifically decreased in ko female mice.
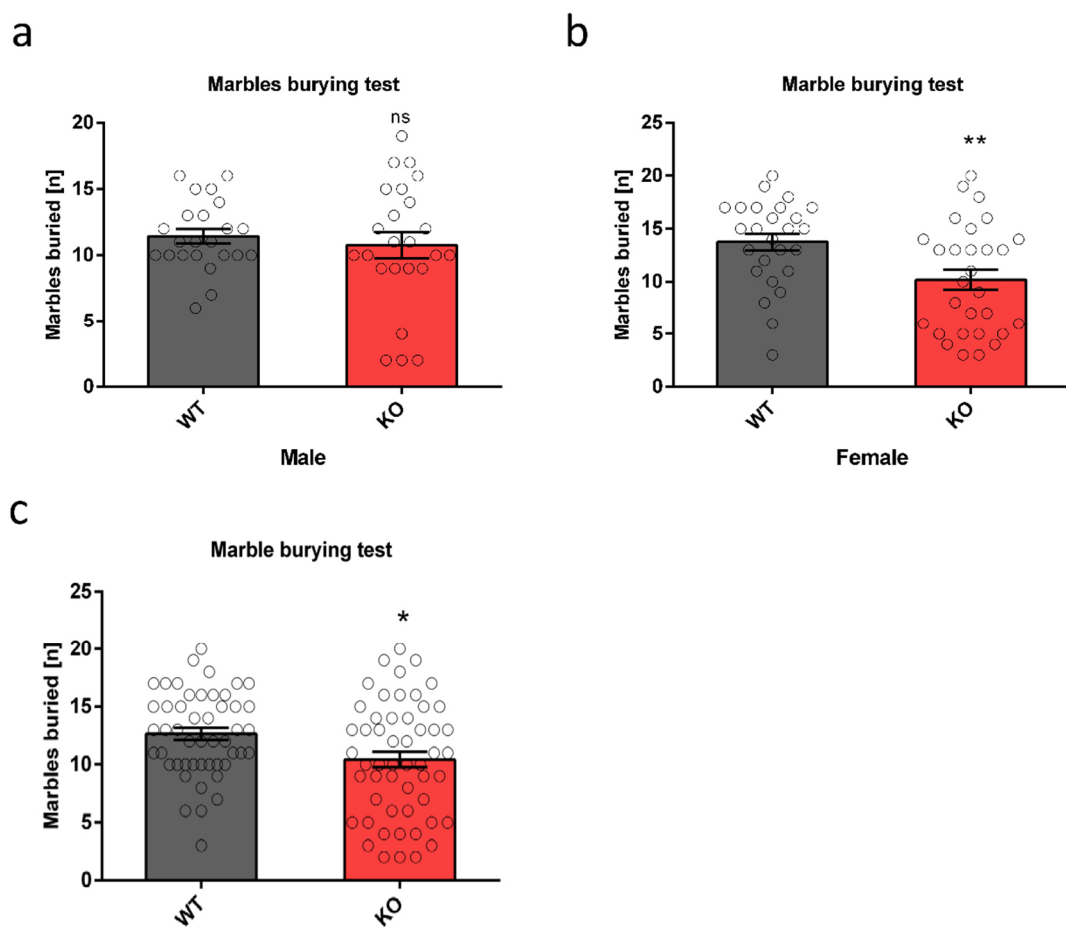
Figure 27: Marbles burying test in adult miR379-410 wt and ko mice. a, b, c Marble burying test as a measure for repetitive behaviour. Total number of marbles (half and completely) buried by adult miR379-410 wt and ko mice is shown. **a,** adult male, ns p=0.5456. **b,** adult female, **p=0.0069. **c,** pooled male and female data, *p=0.0117. **a-c**, miR379-410 wt n=49 (male n=23, female n=26), ko n=53 (male n=24, female n=29), unpaired Student`s t-test. Data are presented as mean ± s.e.m.

**3.9 Deletion of the miR-379-410 cluster interferes with depression-related behaviour in adult mice**

Next, depression-related behaviour was investigated in adult miR379-410 wt and ko mice by using the tail suspension test (TST) in which the animals were suspended by their tails and therefore unable to escape. Time of immobility was evaluated in the animals. As a read-out of despair-related behaviour the time of immobility was measured in the animals. Immobility times between ko males and their wt littermates did not differ **(Fig. 28a)**, whereas a reduced immobility time was visible in ko females **(Fig. 28b)** and in the pooled data of both sexes **(Fig. 28c)** compared to wt controls. Together, these data demonstrate that the deletion of the miR379-410 cluster is associated with reduced depression-like symptoms, mostly in a female-specific manner.
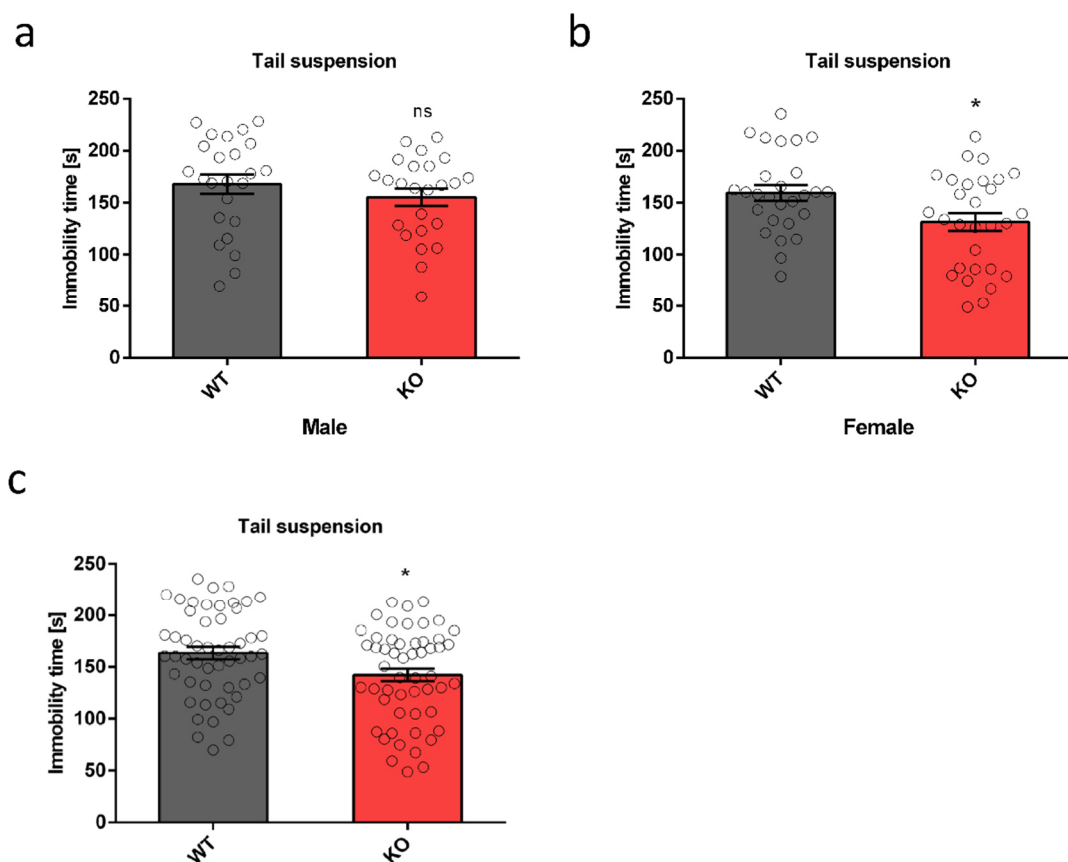
Figure 28: Tail-Suspension test in adult miR379-410 wt and ko mice. a, b, c, Tail suspension test performed in adult mice as a measurement for depression. Time of immobility is indicated. **a,** adult male, ns p=0.3284. **b,** adult female, *p=0.0171. **c,** pooled male and female data, *p=0.0150. **a-c,** miR379-410 wt n=51 (male n=25, female n=26), ko n=53 (male n=24, female n=29), unpaired Student`s t-test. Data are presented as mean ± s.e.m.

3.10 Amphetamine-induced locomotor activity was unaltered in adult miR379-410 ko mice

The pharmacological treatment of mice with amphetamine (amph), a psychostimulant that targets the dopamine transporter (DAT) in mice with a high affinity to dopamine receptor D2, induces hyperlocomotor activity in rodents and can be used to model positive symptoms of neuropsychiatric diseases such as SCZ (reviewed by *van den Buuse, 2010; Helmeste & Seeman, 1982*). Therefore, evaluation of amphetamine-induced locomotor activity in mice can be used to investigate dopaminergic dysfunction in the brain. This experimental part was mainly carried out by Lea Stemmler (**Fig. 29**).
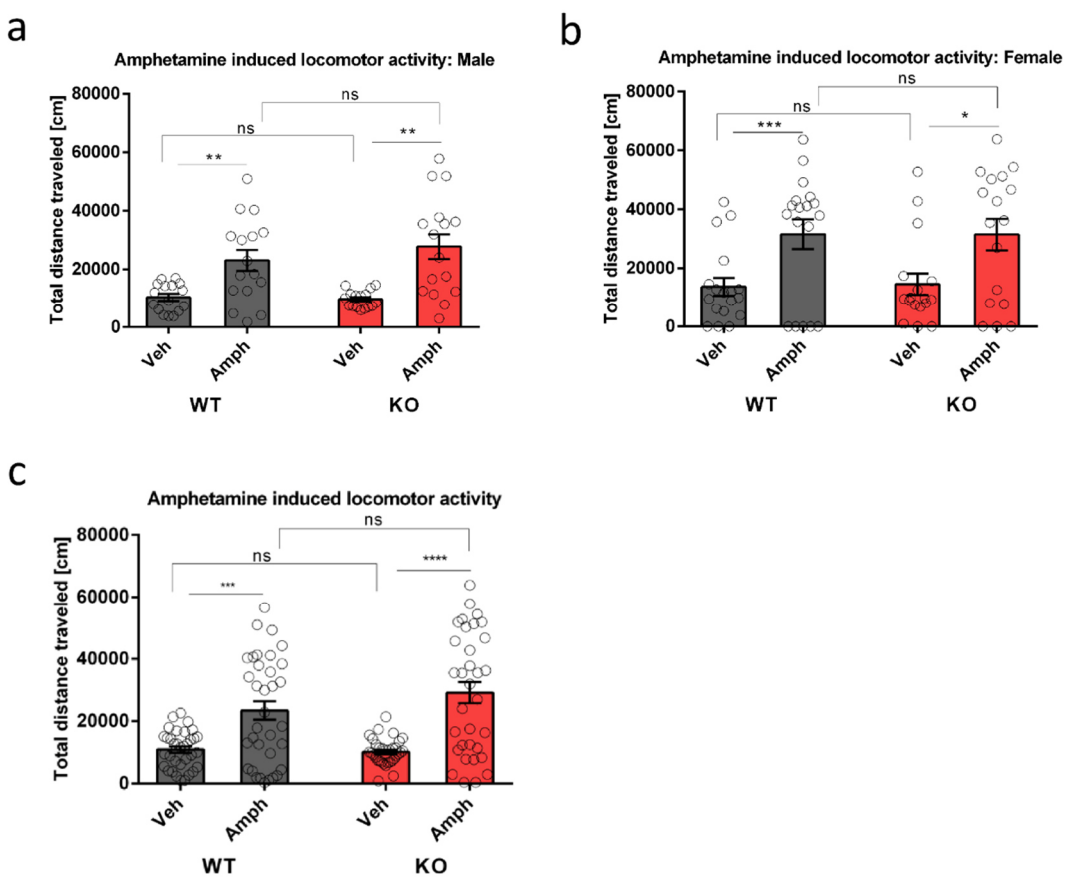
Figure 29: Total distance traveled: Amphetamine-induced locomotor response in adult miR379-410 wt and ko mice (performed by L. Stemmler). **a, b, c,** Total distance traveled within 45 min. after vehicle (veh) or amphetamine (amph) injection. **a,** Adult male wt veh vs. amph **p=0.0093, ko veh vs. amph **p=0.0013, wt veh vs. ko veh ns p=0.6204, wt amph vs. ko amph ns p=0.4026. **b,** Adult female wt veh vs. amph ***p=0.0005, ko veh vs. amph *p=0.0240, wt veh vs. ko veh ns p=0.8604, wt amph vs. ko amph ns p=0.9880. **c,** Pooled male and female data wt veh vs. amph ***p=0.0003, ko veh vs. amph ****p<0.0001, wt veh vs. ko veh ns p=0.5568, wt amph vs. ko amph ns p=0.2108. **a-c,** miR379-410 wt n=34 (male n=16, female n=18), ko n=33 (male n=16, female n=17), unpaired Student`s t-test. Data are presented as mean ± s.e.m.

Adult miR379-410 wt and ko mice were first treated with a saline vehicle (veh) solution given by an intraperitoneal injection, measuring the total distance traveled in an open field. On the subsequent day, animals got an amph injection and locomotor activity was recorded again (**Fig. 29**). Both genotypes and sexes reacted to the amphetamine injection by a significant increase in locomotor activity between veh and amph condition, reflected in the total distanced moved (**Fig. 29a-c**). This indicates a normal dopaminergic response to amphetamine treatment in miR379-410 ko mice. Further, the locomotor activity response by veh and amph injection was not significantly different between the genotypes in males (**Fig. 29a**), females (**Fig. 29b**) and in the pooled data of both sexes (**Fig. 29c**). Overall, these findings indicate that psychosis-like behaviour in miR379-410 ko mice in response to amph treatment is unaffected.

3.11 Reduced locomotor activity during night-phases in adult but not in juvenile miR379-410 ko mice

Hyperlocomotion as well as disturbed activity patterns during day and night phases can be linked to several mental and psychiatric diseases such as attention-deficit/hyperactivity disorder (ADHS) and SCZ. To investigate locomotor activity in a familiar environment (which constitutes reduced anxiety- and stress-levels for the animals) along day and night phases, the home cage activity test was performed in juvenile and adult miR379-410 wt and ko mice (**Fig. 30**). In juvenile ko males (**Fig. 30a-b**), females (**Fig. 30c-d**) and in the pooled data of both sexes (**Fig. 30e-f**) no differences in day- and night-time activity was observed when compared to wt littermates. As expected, activity counts were enhanced in both genotypes and sexes during the night-phases due to the fact that mice are nocturnal animals. Overall, this suggests a normal activity pattern during the typically 12h light/dark phases of juvenile miR379-410 ko mice. To investigate if the activity pattern might be changed later in life, home cage activity was measured again in adult miR379-410 ko mice. Confirming the previous data, ko males showed no difference in activity counts during the day- and night-time compared to wt controls (**Fig. 31a-b**). Interestingly, ko females (**Fig. 31c-d**) and the pooled data of both sexes (**Fig. 31e-f**) displayed reduced activity counts during night- but not during day-time compared to wt controls. These results indicate slightly less activity in adult miR379-410 ko mice, most prominently in ko females during the night-time (dark

phases). Due to the fact that all other behavioural tasks were conducted during day-phases, this phenotype however should not affect any of the outcomes of these other tasks.

Taken together, the behaviour results indicate that the lack of the miR379-410 cluster causes enhanced sociability, anxiety along with reduced repetitive and depressive-like behaviour. Since non-social memory was not affected, at least in juvenile ko mice, loss of miR379-410 appears to specifically impact emotional processing in the mammalian brain.
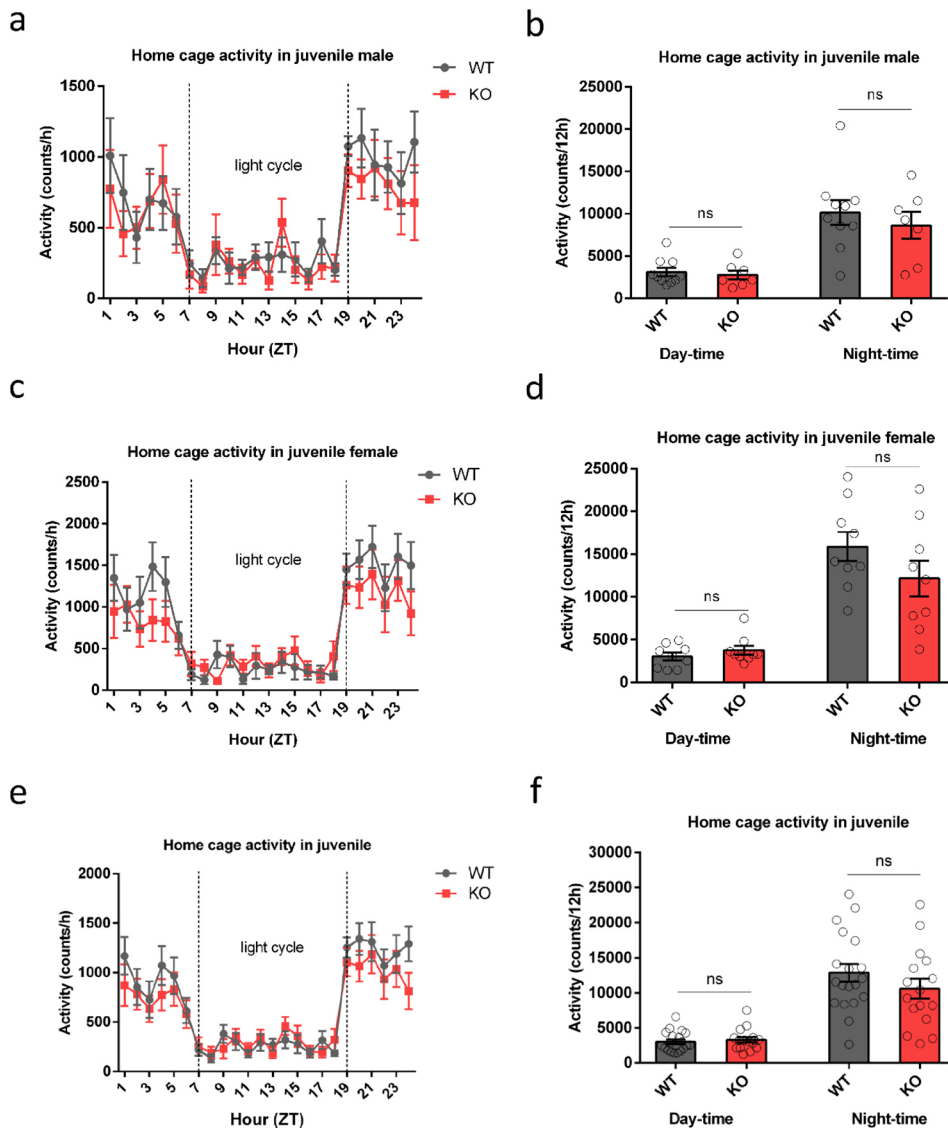
Figure 30: Home cage activity in juvenile miR379-410 wt and ko mice. Number of activity counts in the home cage of juvenile mice during light and dark phases (12h cycle) **a, c, e,** overall counts. **a,** juvenile male. **c,** juvenile female. **e,** pooled male and female data. **b, d, f,** Total activity counts within 12h of light phase (day-time) and dark phase (night-time). **b,** juvenile male, day-time ns p=0.6690, night-time ns p=0.5008; unpaired Student`s t-test. **d,** juvenile female, day-time ns p=0.2977, night-time ns p=0.1864; unpaired Student`s t-test. **f,** pooled male and female data, day-time ns p=0.5924, night-time ns p=0.2436; unpaired Student`s t-test. **a-f,** miR379-410 wt n=19 (male n=10, female n=9), ko n=16 (male n=7, female n=9). Data are presented as mean ± s.e.m.
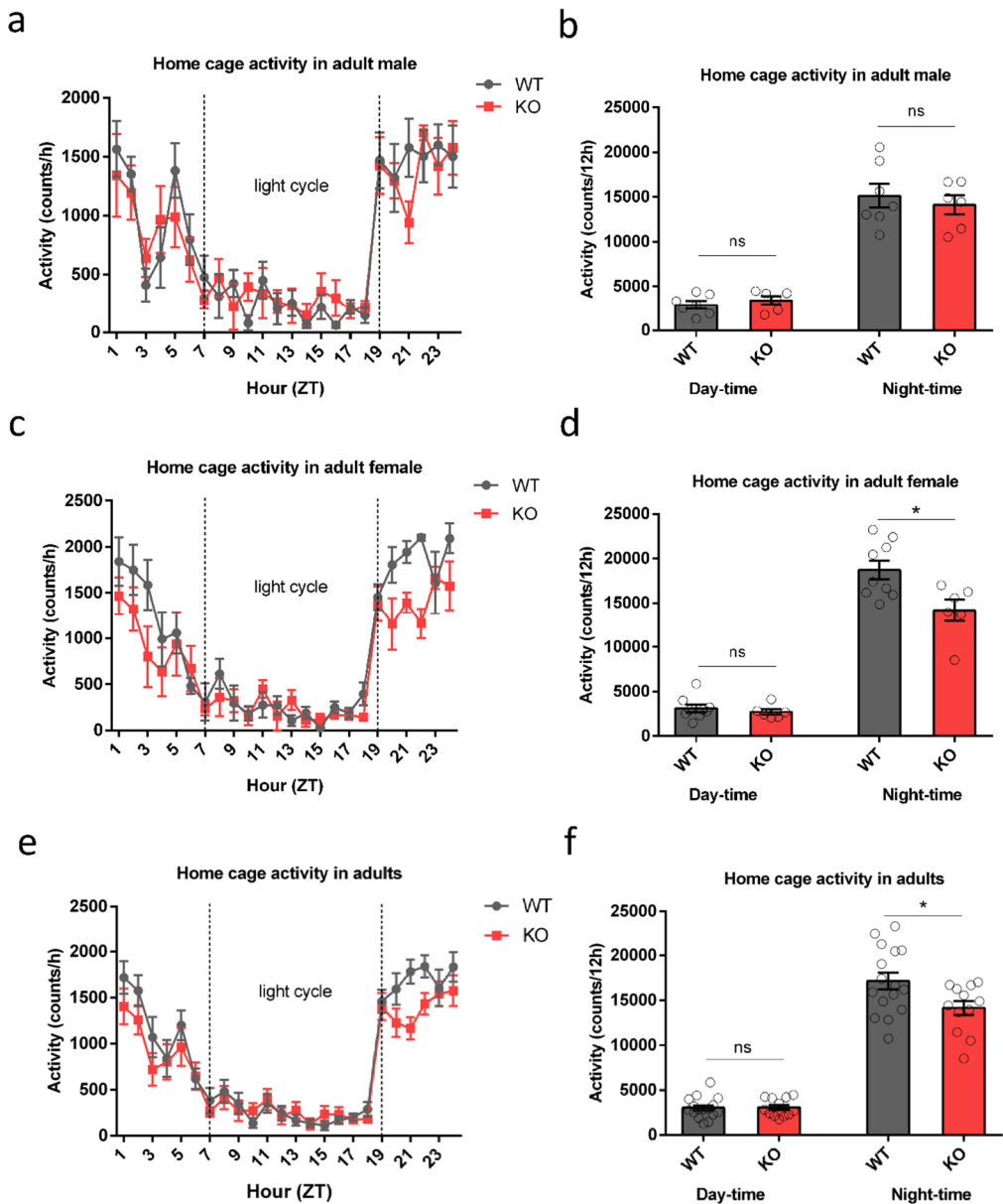
Figure 31: Home cage activity in adult miR379-410 wt and ko mice. Number of activity counts in the home cage of adult mice during light and dark phases (12h cycle) **a, c, e,** overall counts. **a,** adult male. **c,** adult female. **e,** pooled male and female data. **b, d, f,** Total activity counts within 12h of light phase (day-time) and dark phase (night-time). **b,** adult male, day-time ns p=0.4490, night-time ns p=0.5786; unpaired Student`s t-test. **d,** adult female, day-time ns p=0.4912, night-time ns p=0.0156; unpaired Student`s t-test. **f,** pooled male and female data, day-time ns p=0.9326, night-time *p=0.0255; unpaired Student`s t-test. **a-f**, miR379-410 wt n=16 (male n=7, female n=9), ko n=12 (male n=6, female n=6). Data are presented as mean ± s.e.m.

3.12 miR379-410 deletion results in increased excitatory synaptic transmission and dendritic spine density in hippocampal pyramidal neurons

To determine whether behavioural alterations observed upon the lack of miR379-410 are accompanied by cellular and molecular changes within the brain, neuronal physiology and morphology were investigated by different assays. First, Silvia Bicker evaluated the expression of the miR379-410 encoding Mirg gene in mouse hippocampal neuron cultures using single-molecule fluorescent *in situ* hybridization (smFISH) (data not shown). She found that Mirg is strongly expressed in the nucleus and detectable in miR379-410 wt but not ko mouse neurons. Further, she observed that Mirg expression was restricted to MAP2-positive neurons and absent in non-neuronal cells such as glial cells. Next, Reeta Daswani observed by patch-clamp electrophysiological recordings in young mouse hippocampal culture (DIV8-10) a significant increase in miniature excitatory postsynaptic currents (mEPSC) frequency (**Fig. 32a-b**) that was associated with a decrease in average mEPSC amplitudes (**Fig. 32c-d**) in miR379-410 ko neurons. No difference in mEPSC decay time (**Fig. 32e-f**) was observed between the genotypes. Interestingly, Leonie Salzburger (University Braunschweig) could not find any significant difference in patch-clamp electrophysiological recordings in adult male hippocampal miR379-410 ko slices by investigating long-term-potentiation (LTP), excitatory postsynaptic potential (fEPSP) and paired pulse facilitation (PPF) (data not shown). Therefore, the electrophysiology data indicate that basal, but not evoked excitatory transmission is disrupted in hippocampal neurons of miR379-410 ko mice.

Next, neuronal morphology was analyzed by crossing miR379-410 heterozygous mice with a Thy1-GFP reporter line, a transgenic mouse in which only a small subset of neurons expresses GFP, therefore greatly facilitating the analysis of neuronal morphology (*Feng et al., 2000*). Thy1-GFP/miR379-410 ko mice displayed no evident impairments in neuronal structure and dendritic complexity (**Fig. 33a**). In agreement with the patch-clamp mEPSC analysis, CA1 pyramidal neurons in adult Thy1-GFP/miR379-410 ko mice showed a significant increase in dendritic spine density (**Fig. 33c**) and a significant reduction in spine volume (**Fig. 33d**). Together, this data indicates increased excitatory synaptic transmission in CA1 hippocampal pyramidal neurons due to the lack of the miR379-410 cluster.
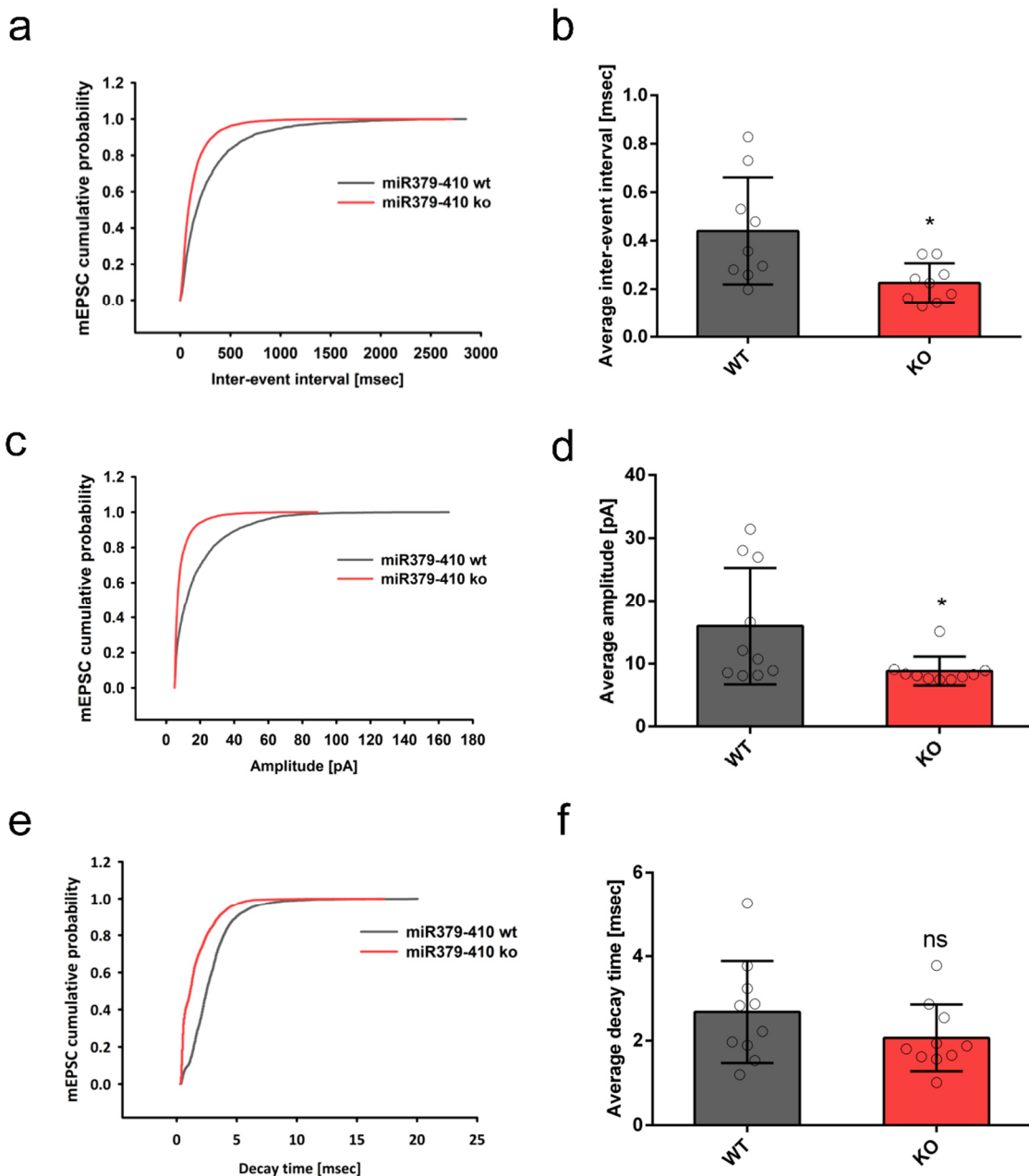
Figure 32: Patch-clamp electrophysiological recordings in young miR379-410 wt and ko mouse cell culture (performed by R. Daswani). **a-f,** Patch-clamp electrophysiological recordings in cultured mouse hippocampal neurons (DIV 8-10) isolated from wt or ko animals (n=3 per group). **a,** Cumulative distribution (D=0.25, ****p<0.0001; KS test) and **b**, mean (*p=0.0146, unpaired Student`s t-test) of mEPSC inter-event intervals; wt n=9, ko n=9 cells analyzed. **c,** Cumulative distribution (D=0.34741, ****p<0.0001, KS test) and **d**, mean (*p=0.0299, unpaired Student`s t-test) of mEPSC amplitudes; wt n=10, ko n=10 cells analyzed. **e,** Cumulative decay time (D=0.00033, ns p>0.9999; KS test) and **f**, Average decay time (ns p=0.1963, unpaired Student`s t-test). **a-f,** Recordings measured in primary hippocampal neurons (DIV8-10) isolated from miR379-410 wt and ko mice, wt n=10, ko n=10. Data are presented as mean ± s.d.
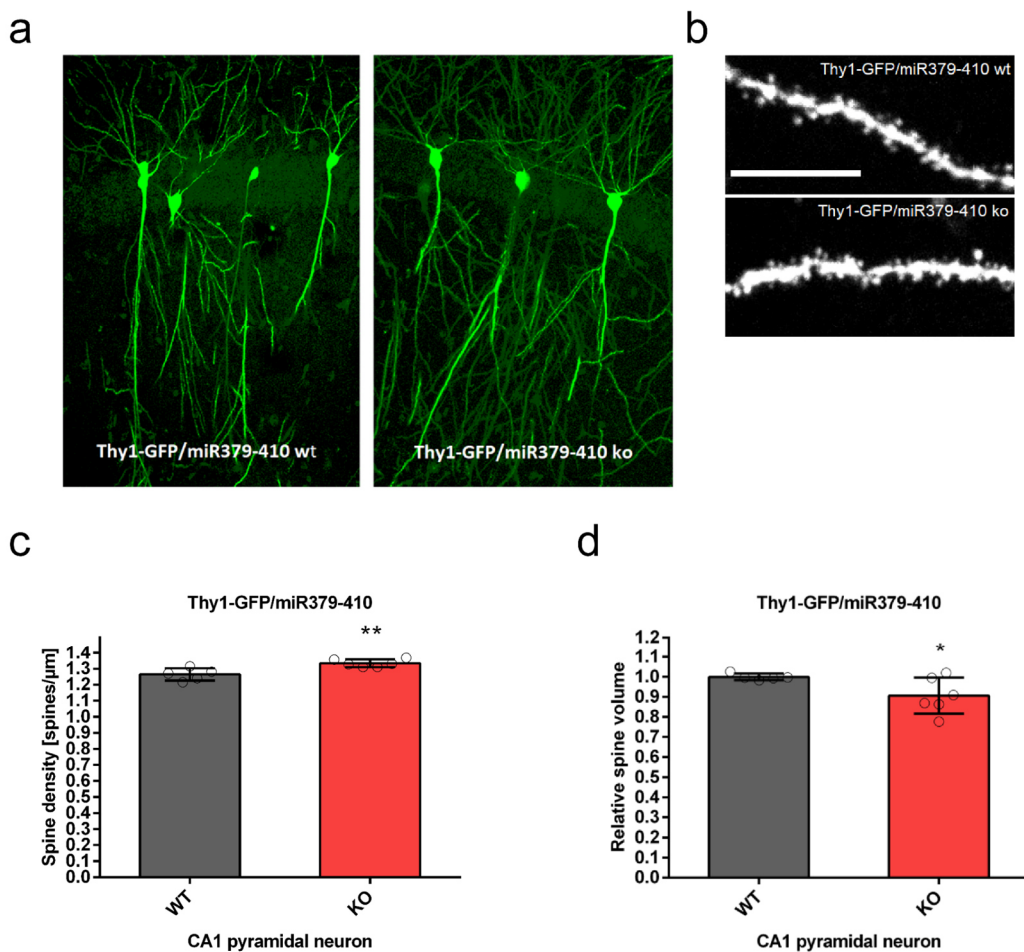
Figure 33: Neuronal morphology in adult male hippocampal Thy1-GFP/miR379-410 wt and ko mice. a, Neuronal health and dendritic complexity of adult hippocampal CA1 regions in male miR379-410 wt or ko mice are shown and were visibly not impaired in adult miR379-410 ko mice. Multiphoton images of Thy1-GFP immunofluorescence were examined over 50 μm-thick coronal sections. **b,** Representative multiphoton images of dendritic spines from the apical dendrites of CA1 pyramidal neuron in adult Thy1-GFP/miR379-410 wt and ko mouse brain. Scale bar: 10 μm. **c,** Spine density in CA1 pyramidal neurons of adult male Thy1-GFP/miR379-410 wt and ko mice; wt n=5, ko n=6 animals. Mean of basal and apical neurons per mouse are shown, **p=0.0052, unpaired Student`s t-test. **d,** Spine volume in CA1 pyramidal neurons of adult Thy1-GFP/miR379-410 wt and ko mice wt n=5, ko n=6 animals. Mean of basal and apical neurons per mouse are shown, *p=0.0497, unpaired Student`s t-test. Data are presented as mean ± s.d.

3.13 qPCR analysis of brain microRNAs and mRNA targets

Next, I asked if the deletion of the large mammalian-specific miR379-410 cluster could be reflected by a general impairment of brain miRNA pathways and changes of known miR-134 targets. Thus, qPCR was performed from hippocampal pnd1 and pnd14 miR379-410 wt and ko mice (**Fig. 34**). First, a selection of brain relevant precursor miRNAs (pre-miR) was

measured in RNA samples isolated from postnatal mice to investigate if the deletion of the largest known mammalian miRNA cluster has a general effect on miRNA biogenesis. As expected, the miR379-410 cluster precursor miRNA pre-miR-134 was not expressed in ko mice at both postnatal days (**Fig. 34a, c**). The precursor miRNAs pre-miR-124, -132 and pre-miR-138.2 expression was unaltered between the hippocampal miR379-410 ko and wt samples on both postnatal days (pnd1, pnd14) (**Fig. 34a, c**). Interestingly, pre-miR-137, an important negative regulator of neuronal maturation (*Smrt et al., 2010*), was reduced on pnd1 but not on pnd14 in miR379-410 ko mice (**Fig. 34a, c**). Next, mRNA expression was measured in ko animal hippocampal samples. Three known and previously validated direct targets of miR-134: Creb1, Limk1 and Pum2 (*Schratt et al., 2006; Fiore et al., 2009; Gao et al., 2010*) were measured in the hippocampal RNA samples. As expected, Creb1 mRNA was significantly upregulated in the miR379-410 ko mice at pnd1 but not at pnd14, whereas mRNA of Limk1 and Pum2 were unaltered between genotypes and postnatal days (**Fig. 34b, d**). Taken together, the majority of pre-miRNAs outside the cluster that were tested here are not differentially expressed in the hippocampus due to the miR379-410 deletion, arguing against a major compensatory effect due to the lack of an entire miRNA cluster. Furthermore, from the validated miR-134 targets, only Creb1 was elevated in the absence of miR379-410, suggesting that loss of miR-134 might affect these targets primarily at the level of mRNA translation.
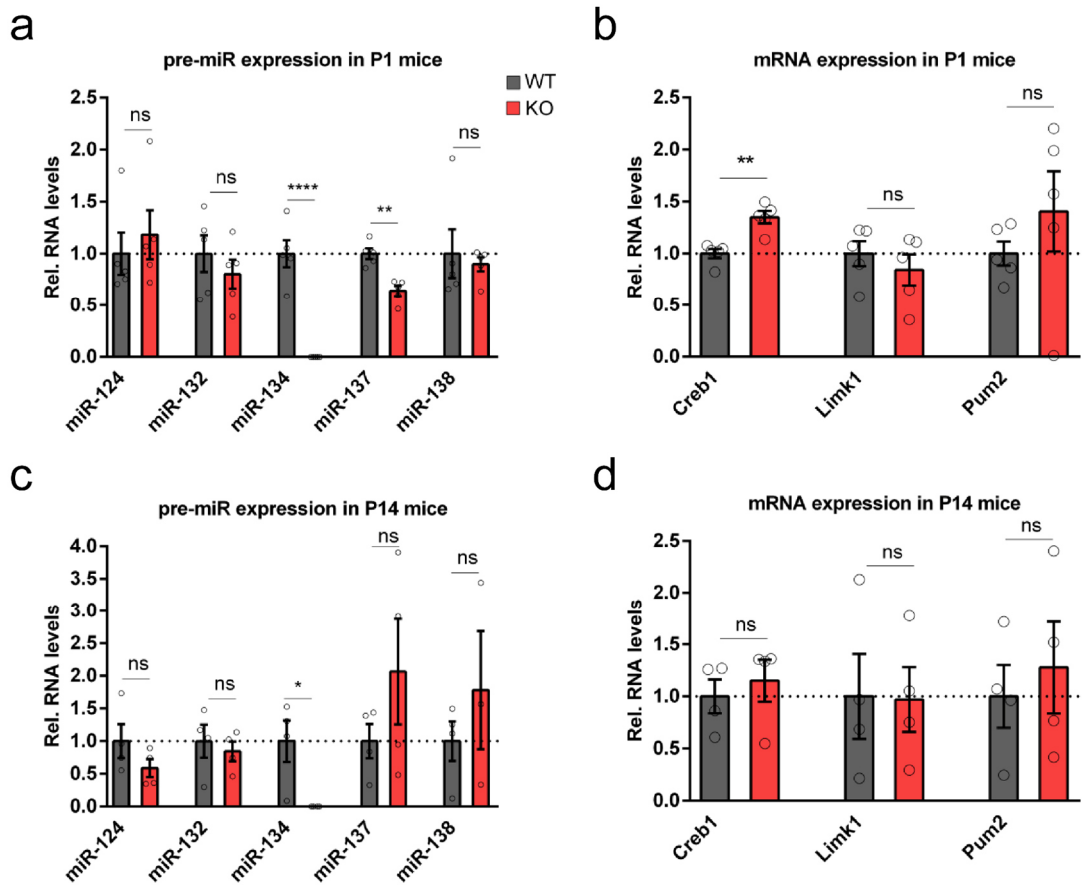
Figure 34: Precursor-miRNA and mRNA expression in hippocampal pnd1 and pnd14 miR379-410 wt and ko mice by qPCR. a, Expression of pre-miRNAs in Pnd1 pups without the miR379-410 cluster: pre-miR-124 ns p=0.5748; pre-miR-132 ns p=0.4076; pre-miR-137 **p=0.0010; pre-miR-138.2 ns p=0.6894; and from the miR379-410 cluster: pre-miR-134 ****p<0.0001. miR379-410 wt n=5, ko n=5. **b,** Expression in Pnd1 pups of known miR379-410-cluster targets: mRNA Creb1 **p=0.0016; mRNA Limk1 ns p=0.3453 and mRNA Pum2 ns p=0.3436. miR379-410 wt n=5, ko n=5. **c,** Expression of pre-miRNAs in Pnd14 juvenile without the miR379-410 cluster: pre-miR-124 ns p=0.2093; pre-miR-132 ns p=0.6120; pre-miR-137 ns p=0.2578; pre-miR-138.2 ns p=0.3932; and from the miR379-410-cluster: pre-miR-134 *p=0.0198. mir379-410 wt n=4, ko n=4. **d,** Expression in Pnd14 juvenile of known miR379-410-cluster targets: mRNA Creb1 ns p=0.5798; mRNA Limk1 ns p=0.9543 and mRNA Pum2 ns p=0.6219. miR379-410 wt n=4, ko n=4. **a-d**, Unpaired Student`s t-test. Data are presented as mean ± s.e.m.

3.14 Comprehensive transcriptome analysis of miR379-410 ko mice reveals key microRNAs from the cluster

The miR379-410 cluster represents the largest known mammalian miRNA clusters that hosts 38 miRNAs. Therefore, it can be expected that other targets than Creb1, Limk1 and Pum2 are changed through the cluster deletion. To gain insight into the molecular pathways,

affected by the deletion of this cluster, a comparative transcriptome analysis of the hippocampus of adult male miR379-410 wt and ko mice was performed using RNAseq. This data was analyzed by Christoph Dieterich (University Heidelberg) and Michael Soutschek. The deletion of the miR379-410 cluster caused extensive changes in the hippocampal transcriptome: n=3068 of differentially expressed genes (DEG) were detected, of those 2170 were upregulated and 898 downregulated (**Fig. 35a**). Next, Gene Ontology (GO) term enrichment analysis revealed a number of significant terms associated with synaptic cellular components in the brain (**Fig. 35b**), which is consistent with the cellular phenotypes observed by electrophysiological recordings (cp. **Fig. 32**) and spine morphology analysis (cp. **Fig. 33**). Clustering of synaptic GO terms led to the identification of an extensive network comprising mainly ionotropic glutamatergic and GABAergic receptor complexes (data not shown). Interestingly, a large number of positive regulators of ionotropic glutamate receptor complexes like Cacng4/7/8, Grin2c/d, Homer3 and Shank1/3 were upregulated, whereas negative regulators such as Fmr1 and Homer1 were downregulated due to miR379-410 deficiency (**Fig. 36a**).

To identify direct miR379-410 targets I focused on the upregulated genes, since the negative effect of miRNAs on transcript levels, in particular in brain and at the synapse, is well established (reviewed by *Schratt, 2009; McNeil and Van Vactor, 2012*). First, an enrichment analysis of cluster binding motifs showed five cluster miRNAs (miR-134-5p, miR-329-3p, miR-377-3p, miR-381-3p and miR-485-5p) that were overrepresented in the upregulated genes (**Fig. 36b**). Notably, four of these miRNAs of the miR379-410 cluster, miR-134-5p/miR-485-5p and miR-377-3p/miR-329-3p, share similar seed sequences (**Fig. 36c**). This suggests, that the target spectrum of these miRNAs could be at least partially overlapping. Next, the investigation of 3'UTR sequences of DEG encoding for components of ionotropic glutamate receptor complexes highlighted several genes that contain at least one conserved miRNA binding site for these five "hub" microRNAs and miR-299-3p (**Fig. 36d**).

By using qPCR technique, I could validate selected upregulated components found by RNAseq, including Cnih2, Dlgap3, Prr7, Prr12, Shank3 and Src (**Fig. 37a**). Neurl1a or Rgs14 expression was not significantly different between the genotypes, possibly due to the high variability of the data from independent animals (**Fig. 37b**). Together, our results suggest that the lack of miRNAs from the miR379-410 cluster could largely explain the coordinated upregulation of ionotropic glutamate receptor components in miR379-410 ko hippocampal neurons. Interestingly, these qPCR verified synaptic targets have at least one miRNA binding

site from the five "hub" miRNAs, namely miR-134, -381, -485, -328 and miR-377, or miRNA miR-299 **(Fig. 36d)** that might be act as key miRNAs from the cluster.
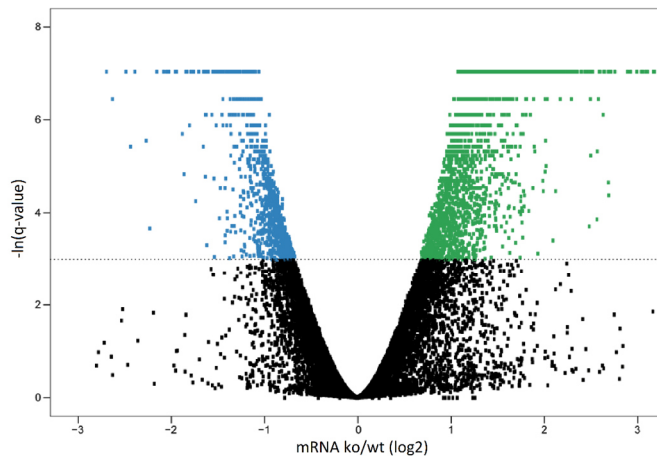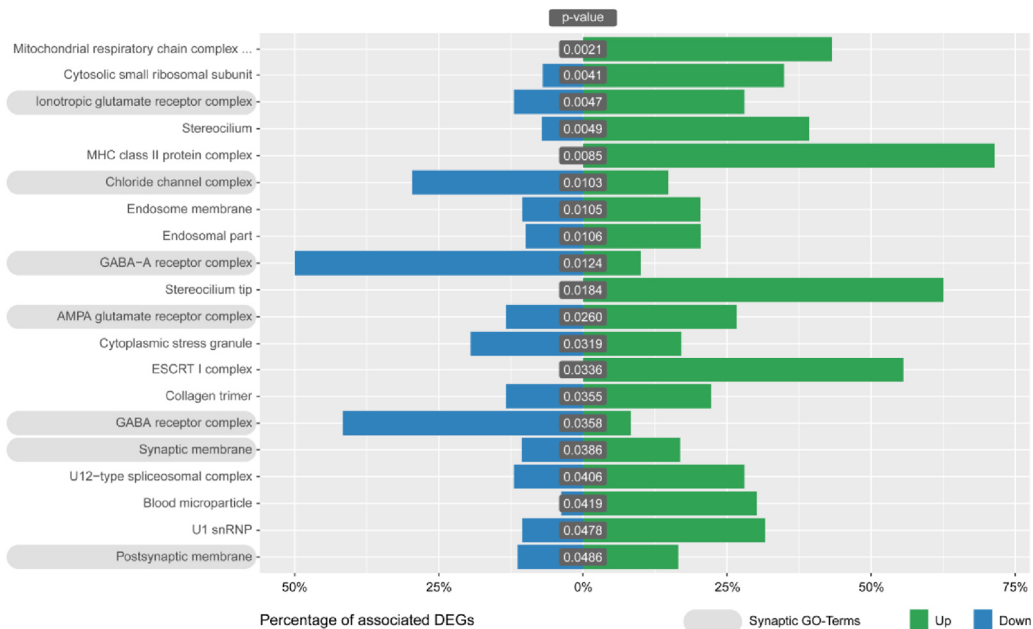
Figure 35: RNA sequencing analysis in adult male hippocampus of miR379-410 wt and ko mice (performed by M. Soutschek and C. Dieterich). **a,** RNAseq differentially expressed gene (DEG) analysis in the adult hippocampus of miR379-410 wt and ko mice. Up- (green) and down- (blue) regulated DEG are indicated by average changes in mRNA levels (ko/wt; log2) (n=3; q-values represent FDR-corrected P-values; *q<0.05); 2170/898 genes were significantly up- and downregulated in miR379-410 ko mice, respectively. **b,** GO-Term enrichment analysis of DEG reveals several synaptic cellular components (highlighted in grey). Green and blue bars indicate the percentage of significantly up- and downregulated genes associated with specific GO-Terms, respectively. GO-Terms with more than 300 annotated genes are not shown.

Figure 36: Enrichment analysis of miR379-410 cluster miRNA binding motifs (performed by M. Soutschek and C. Dieterich). **a,** String-Database protein interaction network. The network is built including String-DB parameters Experiments, Databases and Textmining. Clusters associated with synaptic transmission are enlarged. Green and blue borders indicate significantly up- and downregulated genes, respectively. **b,** Enrichment analysis of cluster miRNA binding motifs (TargetScan v7.1). miRNAs overrepresented in DEG are highlighted in green and blue, respectively. Shown is the natural logarithm of the ratio of BS in DEG. Bubble sizes correspond to RPM values in the mouse brain. Continued on p101.

Figure 36. c, miRNAs of the miR379-410 cluster sharing similar seed regions: miR485-5p/miR-134-5p and miR-377-3p/miR-329-3p. Seed region (nucleotide 2-8) are highlighted in bigger letters, conserved nucleotides in red and those that allow wobble base pairing in blue. **d,** List of synaptic targets among DEG containing conserved binding sites for indicated miRNAs based on TargetScan v7.1. Abbreviations: Binding Sites (BS), Differentially Expressed Gene (DEG), Reads Per Million (RPM).
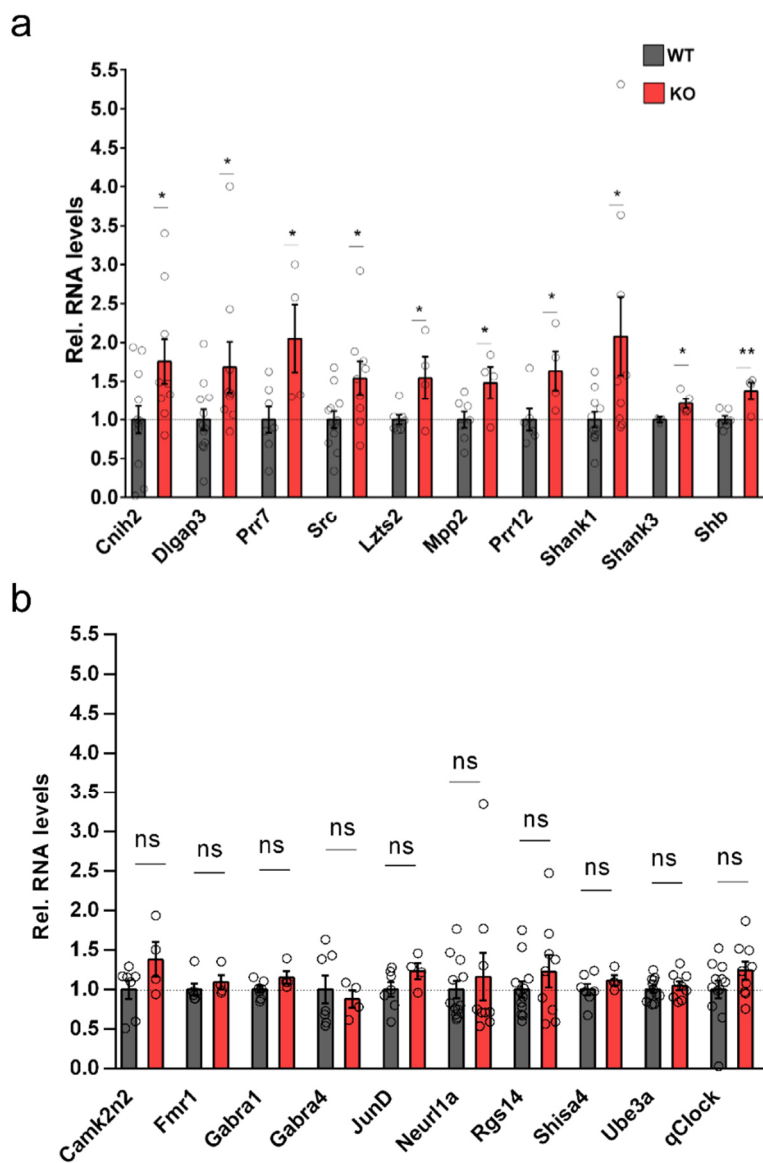
Figure 37: qPCR validation of candidate direct miR379-410 targets. a, qPCR validation of predicted direct miR379-410 targets using RNA from hippocampi of juvenile (Pnd22-24) or for Shank3 adult (3-month-old) miR-379-410 wt and ko animals. If not indicated, both, male and female samples were used. Cnih2 (wt n=12, ko n=9, *p=0.0301), Dlgap3 (wt n=12, ko n=9, *p=0.0467), Prr7 (male wt n=7, ko n=4, *p=0.0236), Src (wt n=12, ko n=9, *p=0.0263), Lzts2 (male wt n=7, ko n=4, *p=0.0310), Mpp2 (male wt n=7, ko n=4, *p=0.0420), Prr12 (wt n=6, ko n=4, *p=0.0449), Shank1 (wt n=11, ko n=9, *p=0.0329), Shb (male wt n=6, ko n=4, **p=0.0087) and Shank3 (adult male wt n=3, ko n=5, *p=0.0442). Continued on p102.

Figure 37. b, qRT-PCR of predicted miR379-410 targets that could not be validated using RNA from hippocampi of juvenile (Pnd22-24) wt and ko animals. If not indicated, both, male and female samples were used. Camk2n2 (male wt n=7, ko n=4, ns p=0.1253), Fmr1 (male wt n=6, ko n=4, ns p=0.4581), Gabra1 (male wt n=7, ko n=4, ns p=0.0889), Gabra4 (male wt n=7, ko n=4, ns p=0.6379), JunD (male wt n=7, ko n=4, ns p=0.1502), Neurl1a (wt n=12, ko n=9, ns p=0.5843), Rgs14 (wt n=12, ko n=9, ns p=0.2955), Shisa4 (male wt n=7, ko n=4, ns p=0.3015), Ube3a (wt n=12, ko n=9, ns p=0.4917), qClock (wt n=12, ko n=9, ns p=0.1560). **a-b**, Unpaired Student`s t-test. Data are presented as mean ± s.e.m.

3.15 Validation of direct miR379-410 targets by luciferase 3'UTR reporter gene assays

To validate direct regulation of candidate targets by specific miRNAs from the miR379-410 cluster that are predicted by Targetscan (cp. **Fig 36d**), 3'UTR luciferase reporter gene assays were performed in primary rat cortical and hippocampal neurons. First, the effect of miRNA mimics (overexpression) on wildtype (wt) and mutant (mut) reporter genes was evaluated. In cortical neurons, the transfection of miR-485-5p mimics down-regulated the expression of the homologous rat Cnih2 and Src wildtype-UTR, but not the corresponding mutant 3'UTR reporter genes which carry point mutations within the predicted miR-485-5p binding sites (**Fig. 38a-b**). Furthermore, transfection of miR-329-3p and miR-411-3p, but not miR-377-3p or miR-495-3p mimics downregulated the Prr7 wt-UTR reporter gene. In contrast, the corresponding mut-UTR reporter did not react to all of the mimics, demonstrating miRNA specificity (**Fig. 38c**). Similarly, transfection of miR-299-3p mimics downregulated the Dlgap3 wt-UTR but not the mut-UTR reporter gene (**Fig. 38d**). Interestingly and consistent with the qPCR data (cp. **Fig. 37b**)**,** transfection of miR-485-5p mimics did not affect the JunD or Rgs14 wt-UTR reporter genes that also contain predicted miR-485-5p binding sites within their 3'UTRs (**Fig. 38e-f**). Together, these findings demonstrate the functionality of a subset of miR379-410 binding sites within the 3'UTRs of candidate genes identified by RNAseq. To further address the relevance of selected endogenous miRNAs for target gene regulation, primary rat hippocampal neurons were transfected with locked nucleic acid (LNA)-modified antisense oligonucleotides (anti-miRNAs) (**Fig. 39**). It was previously shown that picrotoxin (PTX), a GABA-A receptor blocker, upregulates several members of the miR379-410 cluster. In addition, it was recently demonstrated that miR-134 was required for PTX-dependent homeostatic synaptic downscaling, indicating that members of the cluster have an effect on homeostatic plasticity at the synapse (*Fiore et al., 2014; Rajman et al., 2017*). Thus, after transfection with specific LNAs, hippocampal neurons were treated for 48h with PTX. When

hippocampal neurons were transfected with scramble negative control anti-miRNA (CTR), Cnih2 and Src wt-UTR but not mut-UTR gene reporter were downregulated by PTX. The effect of PTX on wt reporters was abrogated by the transfection of anti-miRNA miR-485 (**Fig. 39a-b**). The same was true for the expression of the wt Prr7 3'UTR reporter when the cognate anti-miRNA (anti-miR-329/495 cocktail) was co-transfected (**Fig. 39c**). PTX induced down-regulation was also observed for the Dlgap3 3'UTR in a miR-299-3p binding site dependent manner (**Fig. 39d**). Consistent with the previous experiments (cp **Fig. 37b, 38e-f**), JunD and Rgs14 wt-UTR reporter genes did not react to PTX treatment (**Fig. 39e-f**). Taken together, these findings validate several new direct miR379-410 cluster target genes (Cnih2, Dlgap3, Prr7, Src) that encode for components of ionotropic glutamate receptor complexes in neurons.
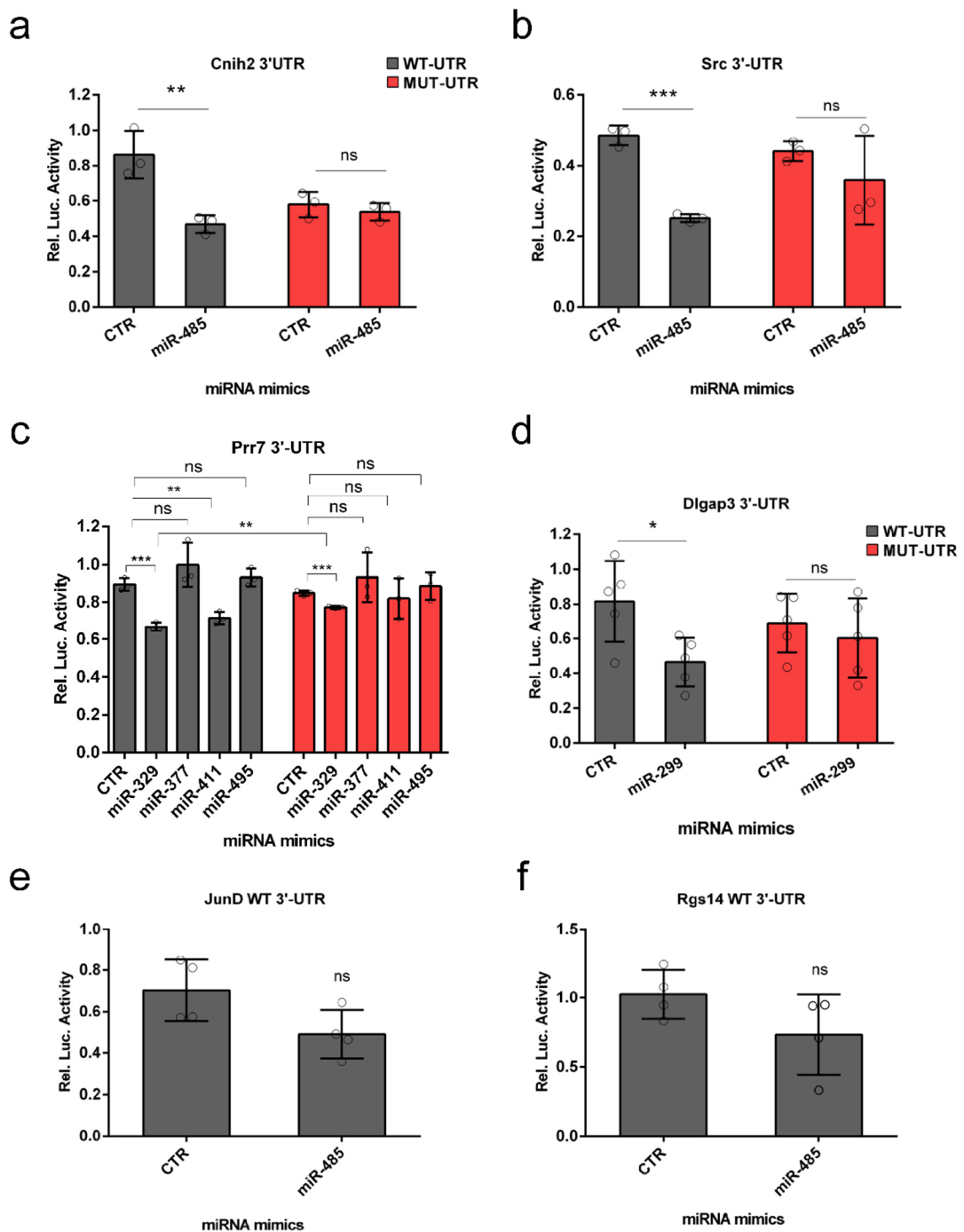
Figure 38: Validation of direct miR379-410 targets using miRNA mimics in 3'UTR luciferase reporter assays. Cnih2, Src, Prr7 and Dlgap3 but not JunD and Rgs14 are direct miR-379-410 target mRNAs. 3'UTR luciferase reporter gene assays in cultured (DIV15) rat cortical neurons transfected with the indicated 3'UTR reporter genes (wt or seed mutant) together with specific miRNA mimics. **a,** Cnih2: (n=3 per group; wt: **p=0.0093; mut: ns p=0.4512). **b,** Src (n=3 per group; wt: ***p=0.0002; mut: ns p=0.3330). **c,** Prr7 (n=3 per group; wt: ***p=0.0006; mut: ***p=0.0008; wt vs. mut mimic miR329: **p=0.0013). **d,** Dlgap3 (n=5 per group; wt: *p=0.0201; mut: ns p=0.5188). **e,** JunD (n=4 per group, wt: ns p=0.0671). **f,** Rgs14 (n=4 per group, wt: ns p=0.1371). **a-f,** Unpaired Student`s t-test. Data are presented as mean ± s.d.
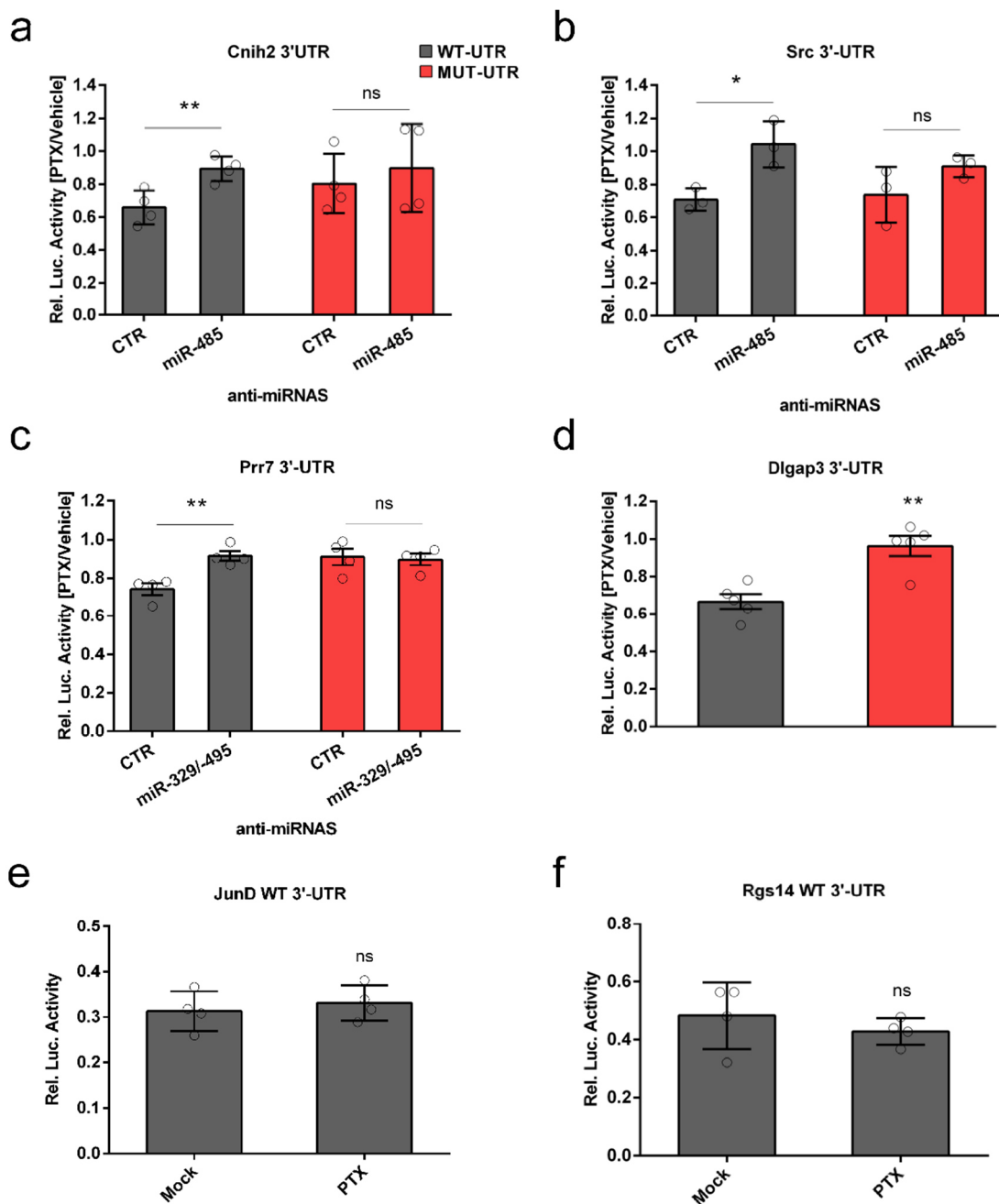
Figure 39: Validation of direct miR379-410 targets using anti-miRNAs in 3'UTR luciferase reporter assays. Cnih2, Src, Prr7 and Dlgap3 but not JunD and Rgs14 are direct miR-379-410 target mRNAs. 3'UTR luciferase reporter gene assays in cultured (DIV20) rat hippocampal neurons after 48h of PTX stimulation using the indicated 3'UTR reporter genes (wt or seed mutant), **a-c** together with specific anti-miRNAs (pLNAs). **a,** Cnih2: (n=4 per group; wt: **p=0.0098; mut: ns p=0.5803). **b,** Src (n=3 per group; wt: *p=0.0209; mut: ns p=0.1745). **c,** Prr7 (n=4 per group; wt: **p=0.0045; mut: ns p=0.8105). **d,** Dlgap3 (n=5 per group; wt vs mut: **p=0.0023). **e,** JunD (n=4 per group, wt mock vs ptx: ns p=0.5490). **f,** Rgs14 (n=4 per group, wt mock vs ptx: ns p=0.4102). **a-f,** Unpaired Student`s t-test. Data are presented as mean ± s.d.

3.16 Protein expression in hippocampal neurons were mostly unaffected by the lack of miR379-410

To investigate if altered mRNA expression of validated miR379-410 targets translated into corresponding changes in protein abundance, I first performed miRNA loss-of-function experiments in primary hippocampal neurons (**Fig. 40**). Therefore, corresponding anti-miRNAs were transfected in DIV17 primary rat hippocampal neurons, proteins were extracted on DIV20 and Western blotting was performed. Relative protein levels were determined by measuring band intensities of the target protein relative to an internal loading control (tubulin). The protein expression of Dlgap3 was significantly increased upon transfection of 400nM anti-miR-299 (2x) compared to 400 nM of control (scrambled) LNA (CTR) , whereas 200nM anti-miR-299 had no effect (**Fig. 40a-b**). Surprisingly, anti-miR-329 transfection did not change protein level of Prr7, which was validated before as direct miR-329 target (**Fig. 40a, c**). Also, the transfection of anti-miR-329, anti-miR-485 and the combination of both did not change the protein level of the validated miR-485 target Src (**Fig. 40a, d**) in hippocampal neurons. Together, these results suggest that, at least for the anti-miRNA concentrations used here, only inhibition of miR-299-3p resulted in an increase in protein expression of the corresponding direct target Dlgap3. Next, we asked if protein expression of direct miR379-410 targets was altered in adult ko mice. Therefore, expression of the two candidates Cnih2 and Prr7 was analyzed in hippocampus protein lysate of 3-month old male miR379-410 wt and ko animals by Western blot (performed by M. Soutscheck) (**Fig. 41**). The quantification of band intensities for Cnih2 (**Fig. 41b**) and Prr7 (**Fig. 41d**) from multiple experiments showed a trend for upregulation of both proteins in the hippocampus of miR379-410 ko mice, although these changes did not reach statistical significance. In the last few years, the ventral hippocampus, through the projections from the basolateral amygdala, has been implicated in the modulation of anxiety-related and social behaviour (*Felix-Oritz & Tye, 2014; Allsop et al., 2014*). Therefore, to increase spatial resolution and to focus our attention on juvenile animals which show a more robust social behavioural phenotype, protein extracts from dorsal and ventral hippocampus of juvenile male miR379-410 wt and ko mice were analyzed by Western blot using antibodies against Cnih2, Dlgap3, Prr7 and Src (**Fig. 42**). However, no significant changes in the expression of any of these proteins between juvenile miR379-410 ko or wt mice could be observed either in dorsal hippocampus (**Fig. 42b**) or in ventral hippocampus (**Fig. 42c**). Taken together, these results indicate that for the investigated direct miR379-410 targets, observed mRNA

changes between miR379-410 ko and wt animals translate only into very subtle, if any changes at the level of endogenous protein expression.
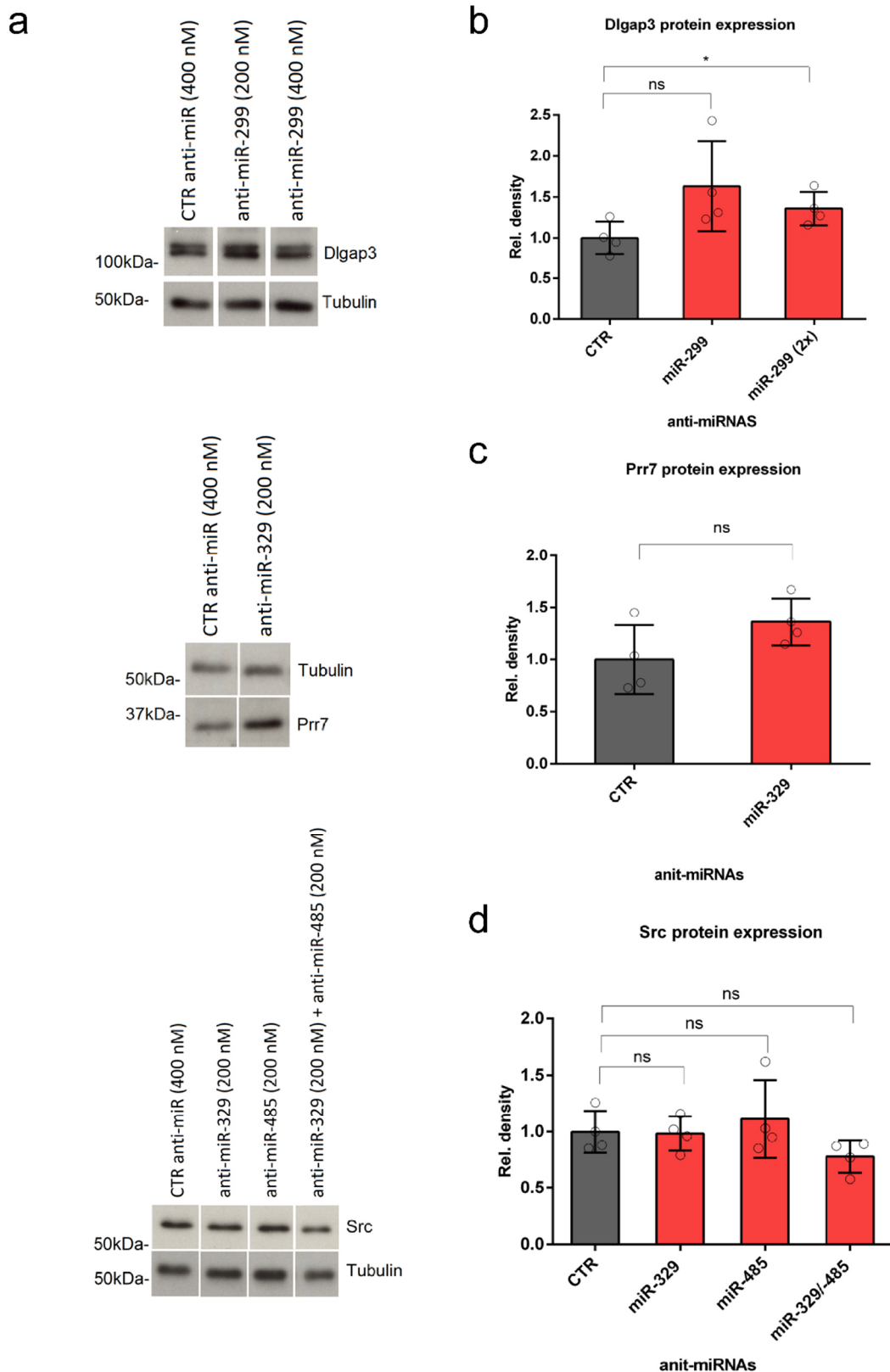

Figure 40: Validation experiment of direct miR379-410 targets with anti-miRNAs by Western blot analysis. Continued on p108.

Figure 40: a, Representative Western blots. Dlgap3, Prr7 and Src protein expression in hippocampal DIV20 neurons that were transfected with anti-miRNas (pLNAs) as indicated. Tubulin was used as loading control. **b-d,** Quantification of Western blots. **b,** Dlgap3 (n=4 per group, ctr 400nM vs 200nM anti-miR-299: ns p=0.0737; ctr 400nM vs 400nM anti-miR-299 (2x): *p=0.0464), unpaired Student`s t-test. **c,** Prr7 (n=4 per group, ctr 400nM vs anti-miR-329 200nM: ns p=0.1206), unpaired Student`s t-test. **d,** Src (n=4 per group, ctr 400nM vs anti-miR-329 200nM: ns p=0.9052, ctr 400nM vs anti-miR-485 200nM: ns p=0.5800, ctr 400nM vs 200nM anti-miR-329+ 200nM anti-miR-485: ns p=0.1095), unpaired Student`s t-test. Data are presented as mean ± s.d.
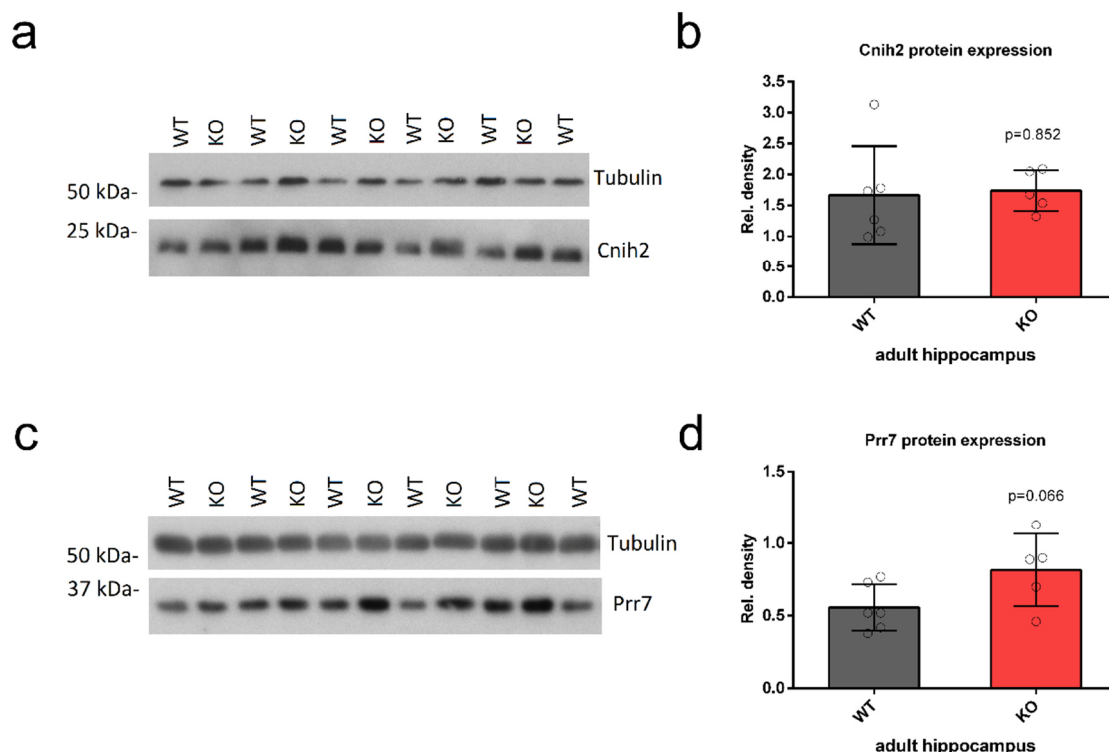
Figure 41: Protein expression in hippocampus of 3-month old male miR379-410 wt and ko mice (blot performed by M. Soutscheck)**. a, c,** Representative Western blots of Cnih2 and Prr7 protein expression in hippocampus of adult male mice. Tubulin was used as loading control. **c,** Western blot quantification of Cnih2, wt n=6, ko n=5, ns p=0.852, unpaired Student`s t-test. **d,** Western blot quantification of Prr7, wt n=6, ko n=5, ns p=0.066, unpaired Student`s t-test. Data are presented as mean ± s.d.
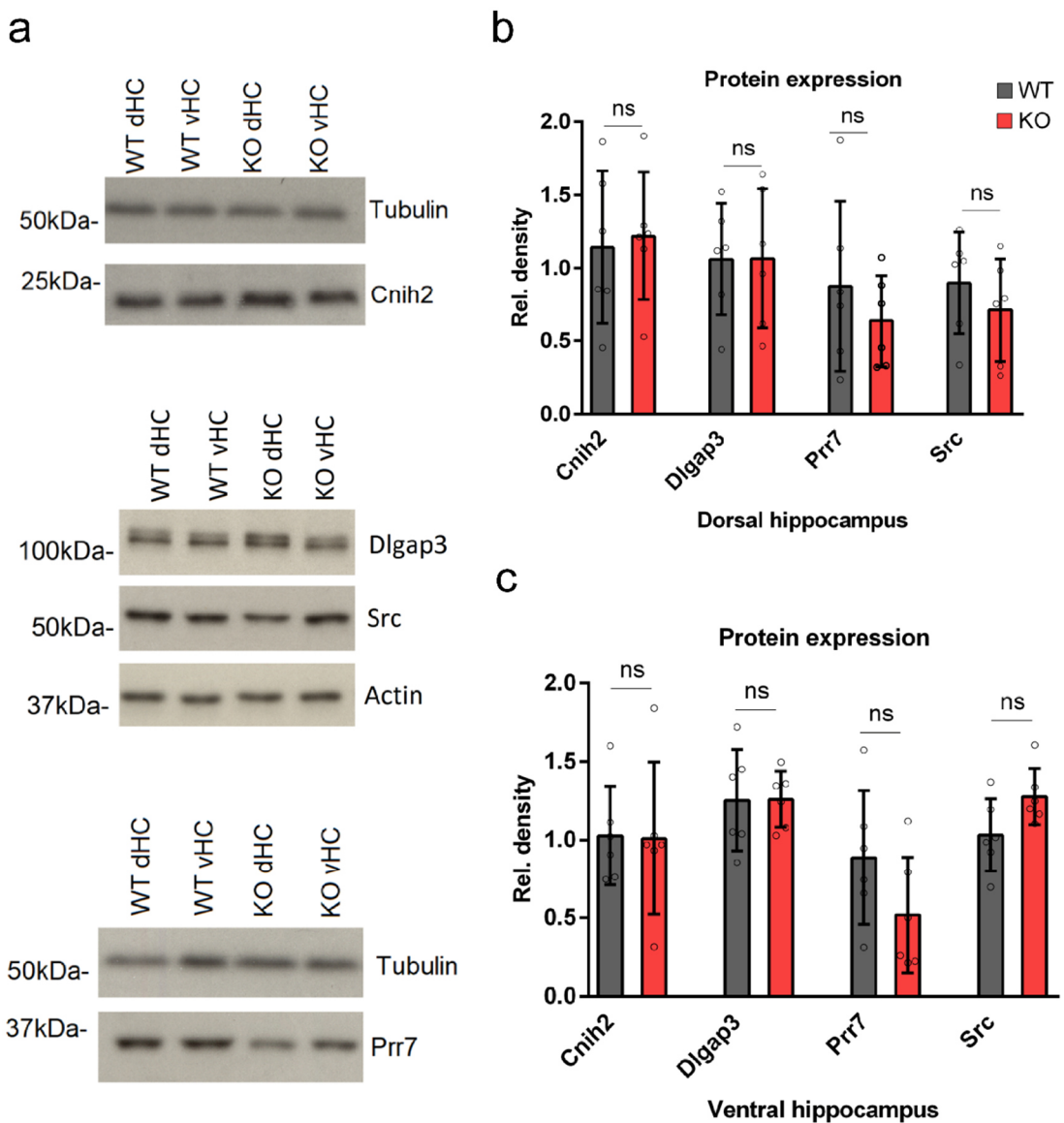
Figure 42: Protein expression in dorsal and ventral hippocampus of 3-4 weeks old juvenile male miR379-410 wt and ko mice. a, Representative Western blots. Cnih2, Dlgap3, Prr7 and Src protein expression in dorsal and ventral hippocampus of juvenile mice. Tubulin and actin were used as loading controls. **b,** Western blot quantification of dorsal hippocampus: Cnih2 (wt n=6, ko n=6, ns p=0.7920), Dlgap3 (wt n=6, ko n=6, ns p=0.9857), Prr7 (wt n=6, ko n=6, ns p=0.3964), Src (wt n=6, ko n=6, ns p=0.3770), unpaired Student`s t-test. **c,** Western blot quantification of ventral hippocampus: Cnih2 (wt n=6, ko n=6, ns p=0.9455), Dlgap3 (wt n=6, ko n=6, ns p=0.9709), Prr7 (wt n=6, ko n=6, ns p=0.1425), Src (wt n=6, ko n=6, ns p=0.0668), unpaired Student`s t-test. Data are presented as mean ± s.d.

4. Discussion

Whereas the function of miRNAs in neuronal development and plasticity is well established, the role of miRNA-dependent post-transcriptional gene regulation in higher brain functions, such as cognition and emotion, is still not well characterized. This is an important issue since neurodevelopmental and psychiatric diseases such as ASD and SCZ are often associated with behavioural deficits, most notably social impairments and withdrawal. However, the underlying cellular and molecular causes remain poorly understood. My work provides first evidence that the miR379-410 miRNA cluster acts as a regulator of social and anxiety-like behaviours in mice and that deficits in ionotropic glutamatergic transmission might underlie these phenotypes.

4.1 Deletion of the miR379-410 cluster leads to phenotypes in social and anxiety-like behaviours

Mice lacking the miR379-410 cluster display normal postnatal development and memory function but increased social behaviour accompanied by more pronounced anxiety-like behaviour across the entire lifespan. The hypersocial phenotype was revealed by the measurement of increased USV calls when miR379-410 ko pups were separated from their mother and later in juvenile mice during social interaction behaviour with conspecifics. In line with that, social interaction time and social approach behaviour in juvenile and adult miR379-410 ko animals were found to be enhanced.

A first direct link between miRNA function and the control of sociability came from a study performed by *Gascon et al. (2014).* The authors could restore social deficits in a genetic mouse model of frontotemporal dementia (FTD) by virus-mediated overexpression of miR-124. The rescue of pro-social behaviour in older animals through miR-124 overexpression was mediated by suppression of the calcium impermeable AMPA-type glutamate receptor subunit GluA2 (*Gascon et al., 2014*). Intriguingly, GluA2 mRNA levels were downregulated in the miR379-410 ko hippocampus, suggesting that the GluA2 levels could predict the degree of sociability. However, it should be noted that this study relied on miRNA overexpression and was performed in older animals suffering from FTD, raising the

possibility that cognitive impairments associated with this model could have a secondary impact on social behaviour. Comorbidity is a frequent phenomenon in neurodevelopmental and psychiatric disorders. Main comorbid conditions, including anxiety and depression, are often apparent in patients. In the last years further miRNAs beside miR-124, including miR-155 and the miR379-410 cluster were identified to control emotional responses such as anxiety- and depressive-like behaviour (*Higuchi et al., 2016; Fonken et al., 2015; Marty et al., 2016*). However, the role of miRNAs in sociability and the implications to neurodevelopmental and psychiatric disorders is still elusive.

Interestingly, pro-social behaviour in miR379-410 ko mice was associated with increased anxiety behaviour in juvenile and adult animals as judged by results obtained from the OF and EPM tests. The important function of the miR379-410 cluster for emotional responses in mice, notably for anxiety-related behaviour, was recently shown. *Marty et al. (2016)* observed in their miR379-410 ko model a strong anxiety phenotype in adult male mice with normal memory function and social approach behaviour. In their study, the spatial (Morris water maze) and non-spatial (fear conditioning) memory test demonstrated no cognitive impairments in miR379-410 ko mice. That agrees with my behavioural results in the three-chamber assay where juvenile ko animals showed normal memory function. In line with the previous study, I found that juvenile and adult male and female miR379-410 ko mice displayed increased anxiety-like behaviour, consistently over multiple tasks. Interestingly, in the LDB task which is another conflict-based anxiety test, genotypes displayed no differences. Thus, the observed anxiety-related phenotype in miR379-410 ko mice suggests a specific non-social anxiety in response to environmental novelty. It is important to mention that these behavioural assays measure different types of anxiety and therefore results have to be interpreted differently. For instance, the OF test evaluates agoraphobia-induced anxiety (fear of open spaces) whereas the EPM measures acrophobia-induced anxiety (fear of height) and the LDB evaluates photophobia-induced anxiety (repulsion for light). Therefore, my findings highly indicate that miR379-410 ko mice display an agoraphobia- and acrophobia-induced anxiety with the absence of anxiety to light and social environment. It seems unlikely that the observed anxiety-related avoidance of stressful environments is caused and dominated by non-emotional factors. Exploratory locomotion, home cage activity during daytime and learning and memory remained for the main part unaltered in juvenile and adult miR379-410 ko mice of both sexes. The recent demonstration in a restraint stress test, that the hypothalamic–pituitary–adrenal (HPA) axis

and thereby the cortisol release in response to stress is not impaired in miR379-410 ko mice gives another hint that the displayed anxiety is an emotional response (*Marty et al., 2016*). Thus, the observed anxiety-related phenotype in my thesis can be likely interpreted as a short-term, maladaptive response to a novel stressful environment rather than a permanent habit caused by chronically enhanced cortisol levels in the mice (*Marty et al., 2016; Belzung & Griebel, 2001*).

At first glance, the observed anxiety phenotype in miR379-410 ko mice seems to be at odds with an hypersocial phenotype, since anxiety is usually associated with hyposociabilty, as nicely illustrated by the high anxiety comorbidity (around 40%) in ASD patients (reviewed in *Zaboski & Storch, 2018*). On the other hand, a combination of hypersocial and anxiety-like behaviour is observed in patients suffering from the rare neurodevelopmental disorders AS and Williams-Beuren-Syndrome (WBS) (*Stoppel & Anderson, 2017; Meyer-Lindenberg et al., 2005*). This suggests that specific deficiencies in neural circuits, presumably involving the amygdala and hippocampus, can lead to a simultaneous upregulation of anxiety and sociability. Intriguingly, candidate genes for AS and WBS are Ube3a and Limk1, respectively. Both represent validated targets of the miR379-410 cluster miRNA miR-134, raising the possibility that impaired expression of these genes might also be involved in the aetiology of AS and WBS (*Schratt et al., 2006; Valluy et al., 2015*). Thus, miR379-410 ko mice could serve as a valuable model to study the mechanisms underlying increased sociablity and anxiety in AS and WBS.

Although my results are mostly in line with the ones reported by *Marty et al. (2016)*, there are some discrepancies worth mentioning. For instance, I observed enhanced social approach behaviour in juvenile and adult ko females and in the pooled data of both sexes. However, this effect was most prominent in ko females and not significantly changed in ko males, whereas *Marty et al. (2016)* only measured adult male mice, providing a possible explanation for these disparate findings. In support of this assumption, I observed anti-depressive-like symptoms in miR379-410 ko females based on a tail-suspension test (TST), whereas *Marty et al (2016)* did not see differences in their mouse model. Although *Marty et al. (2016)* was the first group that demonstrated the role of miR379-410 on higher brain function and emotion, their study is still superficial in places. First, in their study only male subjects were used in behavioural tests. Second, the testing of animals was only performed in adulthood and third, stereotype behaviour was not investigated. Since several miRNAs from the miR379-410 cluster were already linked to neurodevelopmental processes and

related diseases such as ASD and SCZ, age of behavioural testing and selection of appropriate assays might indeed be very important (*Schratt et al., 2006, Fiore et al., 2009; Cohen et al., 2011; Rago et al., 2014; Wu et al., 2016; Gardiner et al., 2011; Sukoff Rizzo & Crawley, 2017*).

Another unexpected finding in my thesis work was the apparent strong sex-dependance of many of the performed behavioural tasks. In particular, adult miR379-410 ko females displayed a stronger behavioural phenotype when compared to ko males in the tasks for social approach, anxiety, repetitive and depressive-like behaviour. It is well known that female behavioural data can be highly influenced by the status of the estrus cycle (*Meziane et al., 2007*). Therefore, to keep the inter- and intra-animal variability on a low level, it is important to study adult female mice with synchronized estrus cycle for a better comparison. Further, sexual dimorphism, as it is observed and discussed in ASD and SCZ cases, could be another explanation for the observed discrepancies between male and female data (*Werling & Geschwind, 2013; Mendrek & Stip, 2011*). Overall, it cannot be ruled out that altered levels of sexual steroid hormones, for instance estrogen and testosterone, could have a strong impact on behavioural results. This is an important issue that has to be investigated in the future, since it is getting more and more obvious that gender differences can have a strong impact on the outcome of behavioural experiments (*McCullough et al., 2014; An et al., 2011*).

4.2. Relevance for neurodevelopmental diseases: Focus on Autism

ASD is a prevalent neurodevelopmental disease that involves early postnatal symptoms and delayed developmental milestones within the first years of life. In several mouse models of ASD, delayed developmental milestones were observed. For instance, mice lacking the postsynaptic cell adhesion protein Neuroligin2 or the synaptic scaffolding protein Shank1 are characterized by delayed postnatal development (*Wöhr et al., 2013; Wöhr et al., 2011*). Communication deficits are belonging to one of the core symptoms of autism and are observed in several mouse models related to ASD (reviewed in *Wöhr & Scattoni, 2013*). For example, Shank1-3 ko and Neuroligin4 deficient mice displayed reduced USV calls in early development and/or adulthood (*Sungur et al., 2016; Won et al., 2012; Wang et al., 2016; Jamain et al., 2008*). The second core symptom of ASD is impaired social behaviour. For

instance, reduced social interaction behaviour was observed in Shank1 ko (*Silverman et al., 2011*), Shank3A ko (*Wang et al., 2011*) and BTBR mice, a strain that has been used as an animal model of core behavioural deficits in autism (*Yang et al., 2012; Silverman et al., 2015*). The third core symptom of ASD is repetitive and stereotyped behaviour. In mouse models related to ASD, increased repetitive behaviour was found, such as in BTBR and Fmr1 ko mice (*McFarlane et al., 2008; Gholizadeh et al., 2014*). Intriguingly, the phenotypes of miR379-410 ko mice in these three domains are opposite to those of known autism models, which points me to suggest that loss of the miR379-410 cluster could lead to an "anti-autistic" behaviour.

However, important experiments are necessary to strengthen this hypothesis. First, the novel object recognition test has to be performed in a different setup, since wt mice used as a "positive control" did not show the expected preference index. Second, since miR379-410 ko mice displayed also a strong anxiety phenotype in the OF and EPM task, it cannot be ruled out that the decreased number of marbles buried are results from an anxiety dependent object avoidance, instead of a stereotypical phenotype. However, juvenile and adult miR379-410 ko mice displayed normal object acquisition behaviour in the three-chamber assay when compared to wt controls, indicating no object avoidance. In summary, further assays have to be carried out in miR379-410 ko mice to evaluate stereotypies and repetitive behaviour in more detail, like repetitive self-grooming or stereotyped jumping and circling behaviour to confirm my findings in the marble burying test (*Rizzo & Crawly, 2017*). Finally, demonstrating that loss of miR379-410 expression could reverse autism-related phenotypes in established autism mouse models would provide strong support for "anti-autistic" function of the miR379-410 cluster and point to a potential therapeutic value. For instance, cross breeding experiments of miR379-410 ko with Shank3 deficient mice could be a promising rescue approach. Although Shank3 was only validated by qPCR in my thesis and might not represent a direct target of the miR379-410 cluster, its deficiency is one of the best characterized and replicated genetic defects associated with autism in humans (*Cochoy et al., 2015; Zhao et al., 2017*). Furthermore, Shank3 mouse models display strong core symptoms of ASD, making them ideal candidate models for such rescue experiments (*Peca et al., 2011; Wang, 2011; Won et al., 2012*). One would speculate that ASD-related behavioural phenotypes are attenuated in Shank3$^{+/-}$/miR379-410 ko mice due to the upregulation of Shank3 expression in the absence of the inhibitory constrain exerted by miR379-410 miRNAs. Furthermore, Shank3$^{-/-}$/miR379-410 ko mice could be used as

negative controls to determine whether the deletion of the miR379-410 cluster mediated rescue is specifically linked to Shank3 upregulation. A second rescue approach could be represented by the stereotactic injection of specific anti-miRNAs. In this rescue strategy Shank3$^{+/-}$ mice can be treated with anti-miRNAs miR-134, -329 and -485 alone or in combination, to induce specific miRNA depletion which again would be expected to boost Shank3 expression from the remaining intact allele.

4.3 Altered spine morphology and increased excitatory synaptic transmission upon deletion of the miR379-410 cluster

The hypersocial and anxiety-like behaviour in miR379-410 ko mice was accompanied by changes in basal excitatory transmission in hippocampal pyramidal neurons as judged by increased mEPSC frequency and decreased mEPSC amplitudes in ko mouse culture. Together, these findings from cultured neurons could be an indication of increased excitatory synaptic transmission within the hippocampus. In the future, additional recordings should be conducted in brain slices (*ex vivo*) and/or in anaesthetized and awake mice (*in vivo*) to study the role of miR379-410 in synaptic transmission within intact neural circuits (*Tao et al., 2015; Lee & Lee, 2017*). Furthermore, we still have limited knowledge about the morphology of excitatory synapses. For instance, determining the density and exact localization of AMPA and NMDA receptors via immunostainings could be a valuable strategy to address the composition of ionotropic glutamate synapses in miR379-410 ko mice in more detail. Moreover, the ultrastructural analyses of pre- and postsynaptic specializations, e.g. by Cryo-EM, can provide useful information about excitatory synapse morphology and function (*Tao et al., 2018*). In agreement with our results from patch-clamp recordings, high-resolution fluorescence multiphoton imaging in dorsal hippocampal CA1 pyramidal neurons of adult miR379-410 ko mice revealed increased spine density and reduced dendritic spine volume. Previously, a number of *in vitro* and *ex vivo* studies showed that manipulation of the cluster miRNA miR-134 impairs dendritic spine morphology, dendritic outgrowth and long-term potentiation in the hippocampus (*Schratt et al., 2006; Fiore et al., 2009; Gao et al., 2010; Jimenez-Mateos et al., 2012; Jimenez-Mateos et al., 2015).* However, some of these results are somehow at odds with the results presented in my thesis. For instance, inhibition of miR-134 led to increased spine volume in hippocampal

pyramidal neurons in culture (*Schratt et al., 2006*) and *in vivo* (*Jimenez-Mateos et al., 2015*). Furthermore, it was shown that miR-134 inhibition *in vivo* decreases spine density in the hippocampus (*Jimenez-Mateos et al., 2012*). On the other hand, *Cohen et al. (2011)* demonstrated through inhibition of miR-485 that it negatively regulates dendritic spine density in hippocampal culture. Several possible reasons might explain these discrepancies. First, the complete absence of the large miR379-410 cluster might be less perturbing to neuromorphology than down-regulation of a single miRNA (e.g. miR-134, -485), since other members of the cluster could have an opposite effect on spine morphology and therefore compensate for the loss of miR-134. Second, previous investigations were performed in young animals or in cell culture mostly during development, whereas my results were obtained in adult mice. Therefore, one could speculate that compensatory mechanisms alleviate potential cellular and molecular synaptic defects over the course of the animal's development. Finally, previous studies were performed in the CA3 region or in mixed hippocampal cultures and can therefore not be directly compared to my findings from the CA1 region.

The observed alterations in neurotransmission and morphology could provide additional links between miR379-410 and neurodevelopmental diseases such as AS, ASD, FXS, SCZ and RTT, that are characterized by dendrite and spine defects in brain regions including the cerebral cortex, mainly the prefrontal cortex (PFC), and the hippocampus (reviewed in *Martinez-Cerdeno, 2017; Phillips & Pozzo-Miller, 2015*). Although subtle changes in spine morphology were observed in miR379-410 ko mice, it should be noted that the determination of spine density and volume was performed in neurons of the dorsal hippocampus. However, several studies have revealed molecular, structural and functional differences within subregions of the hippocampus (*Fanselow & Dong, 2010; Lee et al., 2017; Bannerman et al., 2014*). For example, there is emerging evidence that, whereas the dorsal region is mostly involved in cognitive performances, the ventral region is regulating emotional processing. Considering that I found phenotypes in the social but not cognitive domain, it is plausible that the effect size of differences in spine morphology might actually be higher in the ventral compared to the dorsal part of the hippocampus. miR379-410 ko mice displayed normal non-social and social memory function. The observation that adult male ko mice express normal LTP in the Schäffer-collateral pathway of the hippocampus based on electrophysiological field recordings performed by L. Salzburger (data not shown) further suggests intact memory function upon miR379-410 deletion. These results are also

in line with data from *Marty et al. (2016)*, who did not find alterations in learning and memory behaviour in their miR379-410 ko mouse line. Taken together, we conclude that the dorsal hippocampal region in general (CA1-3) is not strongly affected by miR379-410 deficiency (*Farovik et al., 2009; Moser, 1998; Hitti & Siegelbaum, 2014*). On the other hand, it is also important to note that changes in dendritic spine morphology do not necessarily result in cognitive disabilities. For instance, inhibiting miR-134 by the use of antagomirs increases CA3 hippocampal pyramidal neuron spine volume *in vivo*, yet it does not affect the performance of mice in the novel object location test (*Jimenez-Mateos et al., 2015*). In conclusion, the complete lack of the miR379-410 cluster over the entire course of neuronal development leads to subtle, yet significant alterations in synapse physiology and morphology that do not solely represent a sum of the effects of individual miRNA loss-of-function phenotypes, but rather represent a system-wide response to the absence of a large post-transcriptional regulatory layer.

4.4 The contribution of specific microRNAs to gene expression changes in the miR379-410 ko hippocampus

Comprehensive hippocampal transcriptome and bioinformatic analysis performed in my thesis by C. Dieterich and M. Soutschek suggests that loss of a small subgroup of related miRNAs from the miR379-410 cluster might explain to a large extent the upregulation of key synaptic proteins. Interestingly, two of these miRNA-combinations (miR-134-5p/miR-485-5p and miR-329-3p/miR-377-3p) share similar seed regions and might therefore regulate overlapping target gene sets. This assumption is supported by previous results that miR-134-5p and miR-485-5p are both essential for homeostatic synaptic downscaling (*Fiore et al., 2014; Cohen et al., 2011*), although the target genes implicated in this phenotype were different between the two miRNAs. Transcriptome analysis in my study reveals a large number of positive regulators of ionotropic glutamate receptor complexes that were upregulated in miR379-410 ko mice. Therefore, it is likely that enhanced excitation in miR379-410 ko neurons could be the result of inefficient homeostatic compensation. Abnormalities in genes encoding components of synaptic glutamate receptor complexes can trigger excitatory/inhibitory (E/I) imbalance that finally could lead to neurodevelopmental disorders (reviewed in *Carnitano & Pallagrosi, 2017*). Indeed, several mouse models with

genetic mutations related to ASD, such as Fmr1 (*Hanson & Madison, 2007*), Mecp2 (*Zhang et al., 2014*), Neuroligin3 (*Etherton et al., 2011*) and Shank3 (*Wang et al., 2011; Bozdagi et al., 2010; Han et al., 2013*), display excitatory dysfunction in the hippocampus. However, further investigations are needed to define the exact contribution of key microRNAs to the behavioural, cellular and molecular phenotypes observed in the miR379-410 ko mice. For instance, specific deletion by germline transgenic approaches (e.g. CRISPR-Cas system) or inhibition of individual miRNAs from the cluster by stereotactic injections with anti-miRNAs or lentiviral miRNA knockdown will be useful tools to depict single miRNAs and their contribution in the brain *(Issler & Chen, 2015)*. It should be mentioned that the transcriptional analysis of differentially expressed genes (DEG) was based on whole hippocampal tissue from only three individual animals per genotype. Although all mice used in this experiment had the same sex, age, cohort history and were taken from different litters, it can not be excluded that the DEG study is underpowered due to the low number of biological replicates and the high inter-animal variability (*Schurch et al., 2016*). Moreover, it was shown by in situ experiments from S. Bicker (data not shown) that miR379-410 expression is restricted to neurons and absent from other cell types, e.g. glia cells. Therefore, single cell RNAseq, preferably from different hippocampal regions (e.g. dorsal vs. ventral hippocampus), could provide the spatial resolution necessary to yield robustly regulated genes in hippocampal neurons of miR379-410 ko animals. Another approach to evaluate a more homogenous RNA lysate would be a neuron-enriched high-throughput sequencing of RNA isolated by crosslinking immunoprecipitation (HITS-CLIPS) analysis in neuronal cell culture. In this approach the mitotic inhibitor fluorodeoxyuridine (FUdR) can be used to inhibit non-neuronal cells (e.g. glia cells) in the cell culture before HITS-CLIPS is performed. Overall, these approaches can help to identify direct miRNA target genes that are responsible for initiating neuronal changes that result in the observed behavioural, cellular and molecular phenotypes.

4.5 Deletion of the miR379-410 cluster upregulates a large number of excitatory synaptic genes

Glutamate is the major excitatory neurotransmitter in the brain and acts on two types of receptors: metabotropic and ionotropic receptors. The latter type consists mainly of AMPA- and NMDA-type glutamate receptors (AMPA-R, NMDA-R), and to a lesser extent kainate

receptors. They are organized as multiprotein complexes in the postsynaptic density (PSD) of central neurons. qPCR analysis of juvenile hippocampal miR379-410 ko tissue confirmed upregulation of several genes involved in the structure and function of AMPA-R and NMDA-R (Cnih2, Src, Prr7) complexes in the PSD (Dlgap3, Lzts2, Mpp2 and Shank3). Furthermore, four genes (Cnih2, Src, Prr7 and Dlgap3) were validated as direct targets of cluster miRNAs by using specific luciferase reporter gene assays. miR-485-5p targets Cnih2, a subunit of the ionotropic glutamate receptor that is involved in the regulation of AMPA-R trafficking. Conditional Cnih2/3 ko mice exhibit reduced AMPA-R synaptic transmission in the hippocampus through a selective loss of surface GluA1/A2 heterodimers (*Herring et al., 2013*). Thus, elevated Cnih2 levels in miR379-410 ko mice might contribute to enhanced excitation. Other validated upregulated genes that promote NMDA-R function are Prr7, which has a target site for miR-329-3p and Src, which has a target site for miR-485-5p (*Kravchick et al., 2016; Ali & Salter, 2001*). It was shown that, on the one hand, Prr7 is enriched in the nucleus of hippocampal neurons, where it regulates c-Jun transcriptional activity and mediates NMDA-R-dependent excitotoxicity. On the other hand, Src binds to scaffolding proteins in the NMDA-R complex and acts on this occasion as a common step in signaling cascades important for excitatory synaptic transmission and plasticity (*Ali & Salter, 2001*). These findings indicate that upregulated Prr7 and Src genes can enhance NMDA-R activity and thus might contribute to the cellular and behavioural phenotype found in miR379-410 ko mice. In agreement with these findings, animal studies have shown a contribution of NMDA-R hypofunction to ASD-associated behaviour (*Duffney et al., 2013; Gandal et al., 2012; Eadie et al., 2010*). Another validated miR379-410 target gene is the disks large associated protein Dlgap3, which is localized at the PSD and was identified as direct target of miR-299-3p. The Dlgap gene family has been found to interact with PSD-95 and Shank. Further, they are supposed to control synaptic scaling as a result of NMDA-R, AMPA-R and group I mGluR activation (reviewed in *Rasmussen et al., 2017*). Interestingly, Dlgap3 ko mice displayed high levels of stereotypies with extreme self-grooming behaviour, leading to facial hair loss and skin lesions in these animals (*Welch et al., 2007*). Furthermore, variations within the human Dlgap3 gene were found to be associated with obsessive compulsive disorder (OCD), including symptoms of pathologic nail biting, skin picking and trichotillomania (*Bienvenu et al., 2009*). In another study, *Coba et al. (2018)* observed a loss of connectivity between core scaffolding proteins and reduced sociability in Dlgap1 ko mice.

These results could explain that miR379-410 ko mice show an opposite phenotype, since the expression of the Dlgap family member Dlgap3 is increased in these mice.

Since miRNAs are regulating gene expression at the level of mRNA translation, it was expected that increased levels of miR379-410 target mRNAs are accompanied by corresponding increases in protein expression. However, results obtained from Western blot in general turned out to be very variable. Dlgap3 was one of the strongest validated candidates according to my Western blot results. However, since only the dosage of 400 nM anti-miRNAs miR-299 displayed a significant upregulation of the Dlgap3 protein, it is most likely that the 200 nM concentration used for Prr7 and Src blots was just too low. Therefore, further experiments have to be conducted, in addition with a proper amount of CTR LNA, to validate these targets at the protein level. Furthermore, Cnih2 and Prr7 protein expression was slightly, although not significantly elevated in the adult miR379-410 ko compared to wt hippocampus. This data might be solidified by increasing the number of biological replicates.

Since molecular and behavioural data was most robust in juvenile animals, the absence of significant effects on protein expression of direct miR379-410 targets at this developmental stage was rather surprising. This may suggest that the used method for protein detection (Western blotting) was not sensitive enough to pick up the expected small changes in protein levels as a result of the low mRNA fold changes (max. 1.5-fold). More quantitative technologies, such as mass spectrometry (MS), could help to more accurately quantify proteins in complex samples and thereby get a more reliable validation of target genes regulated by specific miRNAs (*Aebersold et al., 2013*). Another elegant approach that could be employed in the future to close the gap between mRNA and protein is ribosome profiling by deep sequencing (Ribo-Seq). Ribo-Seq is highly quantitative and can give a snapshot of the translatome with high temporal resolution (reviewed in *Dermit et al., 2017; Ingolia et al., 2011*). Nevertheless, beside the high costs and the high amount of starting material required, this method has the disadvantage that it infers mRNA translation from ribosome occupancy, which is not always the case.

Once new miR379-410 targets have been convincingly validated, the next step will be to demonstrate if they are functionally important. Normalization of gene expression of specific targets at the excitatory synapse in the miR379-410 ko model by using knock-down approaches, e.g. gene silencing by siRNAs or antisense-oligonucleotide (ASO) injections, will be required to demonstrate a functional involvement of the presented targets Cnih2, Src, Prr7 and Dlgap3 in the regulation of behavioural phenotypes. For instance, *Sztainberg et al.*

(2015) demonstrated successful application of ASOs in a transgenic Mecp2 duplication mice (Mecp2-TG). In this study, intracerebral injection of ASO reversed social deficits and anxiety-like behaviour in adult Mecp2-TG mice. Thus, ASOs could provide an excellent tool to validate the functional importance of the here identified direct miR379-410 target genes in social behaviour and anxiety.

4.6 Conclusions and Remarks

The aim of my project was to unravel the physiological relevance of the largest known placental mammalian-specific miRNA cluster, miR-379-410, in the regulation of higher brain functions using a constitutive ko mouse model. Besides performing comprehensive behavioural tests, a detailed cellular and molecular characterization of the miR379-410 ko mouse model was included in an attempt to explain the mechanisms that might underlie behavioural phenotypes. This characterization revealed profound alterations in excitatory synapse structure and function, as well as neuronal gene expression. In conclusion, my thesis demonstrates that loss of the miR379-410 miRNA cluster results in a hypersocial and anxiety-related phenotype as judged by increased USVs, social interaction, social approach, anxiety and decreased repetitive behaviour in ko mice. These animals also present increased frequency of excitatory synaptic transmission and number of dendritic spines in the hippocampus. Further, this work identified a small miR379-410 subgroup of key miRNAs, namely miR-134 -299, -329, -377 and miR-485, that repress ionotropic glutamate receptor components and members of the postsynaptic density (PSD) that might promote excitatory synapse formation and function in hippocampal neurons. Moreover, several upregulated components of the ionotropic glutamate receptors (Cnih2, Src, Prr7) and PSD scaffolds (Dlgap3) could be validated as direct targets of miR379-410, thereby strengthening our hypothesis of an increased excitatory synaptic phenotype. Based on these results, it can be speculated that the excitatory upregulation could lead to a shift in the E/I ratio, an important parameter of network stability that is often disrupted in neurodevelopmental diseases, towards excitation. However, precise determination of E/I ratio requires further characterization of inhibitory transmission in miR379-410 ko neurons. This includes immunofluorescent staining with specific markers for inhibitory synapses (e.g. vGAT,

GAD65/67), patch-clamp recordings of miniature inhibitory postsynaptic currents (mIPSCs) and the exact number (ratio) of excitatory and inhibitory neurons within the hippocampus. While my results advance our understanding of the function of the miR379-410 cluster in the mammalian brain and provide interesting links to neurodevelopmental diseases, such as ASD, many questions for follow-up studies remain. Above all, what are the (brain) regions that are responsible for the observed behavioural phenotypes? In my studies, I used a constitutive miR379-410 ko model and focused almost exclusively on the hippocampal region. We made this decision based on results from our previous *in vitro* studies in hippocampal neurons and previous behavioural studies about emotional and cognitive processing performed by others. However, it cannot be ruled out that deficits outside the brain might be involved in the manifestation of behavioural phenotypes. For instance, *Labialle et al. (2014)* showed that miR379-410 expression during postnatal development and adulthood is mostly restricted to the brain, however cluster expression is also present, although to a lower degree, at E18.5 in the liver, lung, skin and small intestine. In agreement with this expression profile, they observed defects in the maintenance of energy homeostasis in miR379-410 ko mice due to metabolic deficits in the liver. To address the function of miR379-410 in the brain more directly, the use of a conditional miR379-410 ko mouse model could be a valuable strategy. Cre-mediated deletion of miR379-410 at different time points and in specific brain regions can provide spatio-temporal information about the cluster`s role in neurodevelopmental processes of the brain. In the last years, several studies performed in mice and humans provided ample evidence for the importance of brain regions outside the hippocampus, including the PFC, striatum, ventral tegmental area (VTA), nucleus accumbens (NAc) and (basolateral) amygdala, for the control of social behaviour (*Kim et al., 2015*; reviewed in *Ko et al., 2017*; *Báez-Mendoza & Schultz, 2013*) and anxiety (*Adhikari et al., 2015; reviewed in Martin et al., 2009; Duval et al., 2015*). Thus, there is a high chance that alterations in various brain regions and circuits contribute to the observed hypersocial and anxiety-like phenotype in miR379-410 ko mice. For instance, *Guanydin et al. (2014)* demonstrated, using a combination of optogenetics and fiber photometry recordings in freely moving mice, that increased activity in the VTA to NAc projection is responsible for enhanced social interaction behaviour. Moreover, it was shown by optogenetics that projections from the basolateral amygdala (BLA) to the ventral hippocampus CA1 (vCA1) are responsible for the modulation of anxiety-related behaviour and social interaction in mice (*Felix-Ortiz & Tye, 2014*). In a follow up study *Felix-Ortiz et al.*

(2016) demonstrated that, through Channelrhodopsin-2 (ChR2)-mediated activation of BLA projections to the mPFC, mice became more anxious in the EPM and OF task, whereas halorhodopsin (NpHR)-mediated inhibition caused anxiolytic effects in these animals. Interestingly, activation of the BLA-mPFC pathway reduced social interaction behaviour, while inhibition of the pathway increased sociability (*Felix-Ortiz et al., 2016*). Recently, optogenetic experiments in adolescent mice identified a pathway between the prelimbic cortex (PL), which is part of the mPFC, and NAc that is involved in social-spatial learning (*Murugan et al., 2017*). Here, activation of PL-NAc neurons resulted in decreased social investigation. More recently, *Jimenez et al. (2018)* identified "anxiety cells" in the vHPC region by a combination of calcium imaging and optogenetic approaches in freely moving mice. These "anxiety cells" were located in the vCA1 and projected to the lateral hypothalamic area (LHA). By switching these cells "on" and "off" they could elegantly demonstrate that vCA1 outputs to the LHA control anxiety-related behaviour. These studies attractively highlighted the functional role of the vHPC, BLA, NAc and mPFC connection for social and anxiety-related behaviour in mice. Taken together, state-of-the-art techniques, such as calcium imaging and optogenetics in freely moving mice, can help to obtain detailed information about local brain function, or in other words from "which" gene to "where" in the brain and "when" during development this change leads to neuronal circuit dysfunction. Since hypersocial and anxiety-like behaviour are strong hallmarks in the miR379-410 ko phenotype, one interesting optogenetic approach in juvenile and adult ko mice could be performed by ChR2-mediated neuronal activation and NpHR-mediated neuronal inactivation of the vCA1-BLA and BLA-mPFC projections. This experimental design could be carried out by stereotaxic injections in the specific brain regions with two different adeno-associated viral vectors (AAVs) which encode a light-sensitive cation-pump ChR2 and a light-sensitive chloride-pump NpHR, respectively. If performed in the context of social interaction or anxiety-related tasks, such experiments could help to identify circuits whose disruption contributes to enhanced sociablity/anxiety in miR379-410 ko mice. Such optogenetic investigations shoud be accompanied by the collection of more molecular and cellular information about these brain regions, using high-resolution imaging, genomics and proteomics. In addition, rescue experiments performed *in vivo* and *in vitro* by using ASOs to knock-down candidate target genes can help to further understand the cellular and molecular mechanisms underlying the observed phenotype. Rodent models have proven to be a suitable system to study miRNA functions in the mammalian brain both *in vitro* and *in*

vivo. Nonetheless, to follow-up cellular phenotypes that are identified in miR379-410 ko rodent models, the development of human induced pluripotent stem cell (hiPSC) models could help to enhance our knowledge about the cluster and its function in humans. For example, monolayer culture or complex spatially organized 3D organoid cultures might be appropriate tools to investigate the cellular phenotype in hiPSCs (reviewed in *Ardhanareeswaran et al., 2017*). This approach could be complemented with hiPSCs derived from individuals suffering from neurodevelopmental or psychiatric diseases with monogenic (*Marchetto et al., 2010; Nageshappa et al., 2016, Doers et al., 2014; Sheridan et al., 2011*) or complex genetic origin (*Mariani et al., 2015, Chailangkarn et al., 2016; Khattak et al., 2015*). Thereby, hiPSC models could help to decipher the disease-altered trajectory of human brain development related to the expression of miR379-410 cluster members. Overall, such a model system in a dish could drive the translational approach from animals to human with a real potential for therapeutic advances in the future.

5. References

Aebersold, R., Burlingame, A.L., Bradshaw, R.A. (2013). Western Blots versus Selected Reaction Monitoring Assays: Time to Turn the Tables? *Mol Cell Proteomics* **12**, 2381–2382.

Adhikari, A., Lerner, T.N., Finkelstein, J., Pak, S., Jennings, J.H., Davidson, T.J., Ferenczi, E., Gunaydin, L.A., Mirzabekov, J.J., Ye, L., Kim, S.Y., Lei, A., Deisseroth, K. (2015). Basomedial amygdala mediates top-down control of anxiety and fear. *Nature* **527**, 179-185.

Agarwal, V., Bell, G.W., Nam, J.W., Bartel, D.P. (2015). Predicting effective microRNA target sites in mammalian mRNAs. *eLife* **4**, e05005.

Aibar, S., Fontanillo, C., Droste, C., De Las Rivas, J. (2015). Functional Gene Networks: R/Bioc package to generate and analyse gene networks derived from functional enrichment and clustering. *Bioinformatics* **31**, 1686–1688.

Alexa, A., Rahnenführer, J., Lengauer, T. (2006). Improved scoring of functional groups from gene expression data by decorrelating GO graph structure. *Bioinformatics* **22**, 1600-1607.

Ali, D.W., Salter, M.W. (2001). NMDA receptor regulation by Src kinase signalling in excitatory synaptic transmission and plasticity. *Curr Opin Neurobiol.* **11**, 336-342.

Allsop, A.S., Weele, C.M.V., Wichmann, R., Tye, K.M. (2014). Optogenetic insights on the relationship between anxiety-related behaviors and social deficits. *Front Behav Neurosci.* **8**, 241.

An, X.L., Zou, J.X., Wu, R.Y., Yang, Y., Tai, F.D., Zeng, S.Y., Jia, R., Zhang, X., Liu, E.Q., Broders, H. (2011). Strain and sex differences in anxiety-like and social behaviors in C57BL/6J and BALB/cJ mice. *Exp Anim.* **60**, 111-123.

Angoa-Pérez, M., Kane, M.J., Briggs, D.I., Francescutti, D.M., Kuhn, D.M. (2013). *J Vis Exp.* **82**, 50978**.**

Ambros, V., Bartel, B., Bartel, D.P., Burge, C.B., Carrington, J.C., Chen, X., Dreyfuss, G., Eddy, S.R., Griffiths-Jones, S., Marshall, M., Matzke, M., Ruvkun, G., Tuschl, T. (2003). A uniform system for microRNA annotation. *RNA* **9**, 277-279.

Ardhanareeswaran, K., Mariani, J., Coppola, G., Abyzov, A., Vaccarino, F.M. (2017). Human induced pluripotent stem cells for modelling neurodevelopmental disorders. *Nat Rev Neurol.* **13**, 265-278.

Báez-Mendoza, R., Schultz, W. (2013). The role of the striatum in social behavior. *Front Neurosci.* **7**:233.

Baladrón, V., Ruiz-Hidalgo, M.J., Nueda, M.L., Díaz-Guerra, M.J., García-Ramírez, J.J., Bonvini, E., Gubina, E., Laborda, J. (2005). dlk acts as a negative regulator of Notch1 activation through interactions with specific EGF-like repeats. *Exp Cell Res.* **303**, 343-359.

Banerjee, S., Neveu, P., and Kosik, K.S. (2009). A coordinated local translational control point at the synapse involving relief from silencing and MOV10 degradation. *Neuron* **64**, 871–884

Bannerman, D.M., Sprengel, R., Sanderson, D., McHugh, S.B., Rawlins, J.N., Monyer, H., Seeburg, P.H. (2014). Hippocampal synaptic plasticity, spatial memory and anxiety. *Nat Rev Neurosci.* **15**, 181-192.

Barak, B., Feng, G. (2016). Neurobiology of social behavior abnormalities in autism and Williams syndrome. *Nat Neurosci.* **19**, 647-655.

Barnes, T.D., Rieger, M.A., Dougherty, J.D., Holy, T.E. (2017). Group and Individual Variability in Mouse Pup Isolation Calls Recorded on the Same Day Show Stability. *Front Behav Neurosci*. **11**, 243.

Baroncelli, L., Braschi, C., Spolidoro, M., Begenisic, T., Maffei, L., Sale, A. (2011). Brain plasticity and disease: a matter of inhibition. *Neural Plast.* 2011:286073.

Bartel, D.P. (2009). MicroRNAs: target recognition and regulatory functions. *Cell* **136**, 215-233.

Bartel, D.P. (2018). Metazoan MicroRNAs. *Cell* **22**;20-51.

Baskerville, S., Bartel, D.P. (2005). Microarray profiling of microRNAs reveals frequent coexpression with neighboring miRNAs and host genes. *RNA* **11**, 241-247.

Bauman, M.D., Schumann, C.M. (2018). Advances in nonhuman primate models of autism: Integrating neuroscience and behavior. *Exp Neurol.* **299**, 252-265.

Bekkers, J.M., Stevens, C.F. (1989). NMDA and non-NMDA receptors are co-localized at individual excitatory synapses in cultured rat hippocampus. *Nature* **341**, 230-233.

Belzung, C., Griebel, G. (2001). Measuring normal and pathological anxiety-like behaviour in mice: a review. *Behav Brain Res.* **125**, 141-149.

Bernstein E., Kim S.Y., Carmell, M.A., Murchison, E.P., Alcorn, H., Li, M.Z., Mills, A.A., Elledge, S.J., Anderson, K.V., Hannon, G.J. (2003). Dicer is essential for mouse development. *Nat Genet.* **35**, 215-217.

Bicker, S., Khudayberdiev, S., Weiß, K., Zocher, K., Baumeister, S., Schratt, G. (2013). The DEAH-box helicase DHX36 mediates dendritic localization of the neuronal precursor-microRNA-134. *Genes Dev.* **27**, 991–996.

Bicker, S., Lackinger, M., Weiß, K., Schratt, G. (2014). MicroRNA-132, -134, and -138: a microRNA troika rules in neuronal dendrites. *Cell Mol Life Sci.* **71**, 3987-4005.

Bienvenu, O.J., Wang, Y., Shugart, Y.Y., Welch, J.M., Grados, M.A., Fyer, A.J., Rauch, S.L., McCracken, J.T., Rasmussen, S.A., Murphy, D.L., Cullen, B., Valle, D., Hoehn-Saric, R., Greenberg, B.D., Pinto, A., Knowles, J.A., Piacentini, J., Pauls, D.L., Liang, K.Y., Willour, V.L., Riddle, M., Samuels, J.F., Feng, G., Nestadt, G. (2009). Sapap3 and pathological grooming in humans: Results from the OCD collaborative genetics study. *Am J Med Genet B Neuropsychiatr Genet.* **150B**, 710-720.

Birling, M.C., Herault, Y., Pavlovic, G. (2017). Modeling human disease in rodents by CRISPR/Cas9 genome editing. *Mamm Genome* **28**, 291–301.

Boeckers, T.M., Bockmann, J., Kreutz, M.R., Gundelfinger, E.D. (2002). ProSAP/Shank proteins - a family of higher order organizing molecules of the postsynaptic density with an emerging role in human neurological disease. *J Neurochem.* **81**, 903-910.

Bozdagi, O., Sakurai, T., Papapetrou, D., Wang, X., Dickstein, D.L., Takahashi, N., Kajiwara, Y., Yang, M., Katz, A.M., Scattoni, M.L., Harris, M.J., Saxena, R., Silverman, J.L., Crawley, J.N., Zhou, Q., Hof, P.R., Buxbaum, J.D. (2010). Haploinsufficiency of the autism-associated Shank3 gene leads to deficits in synaptic function, social interaction, and social communication. *Mol Autism* **1**, 1-15.

Branchi, I., Santucci, D., Vitale, A., Alleva, E. (1998). Ultrasonic vocalizations by infant laboratory mice: a preliminary spectrographic characterization under different conditions. *Dev Psychobiol.* **33**, 249-56.

Brandt, J., Veith, A.M., Volff, J.N. (2005). A family of neofunctionalized Ty3/gypsy retrotransposon genes in mammalian genomes. *Cytogenet Genome Res.* **110**, 307–317.

Brandt, R., Hundelt, M., Shahani, N. (2005). Tau alteration and neuronal degeneration in tauopathies: mechanisms and models. *Biochim. Biophys. Acta.* **1739**, 331-354.

Can, A., Dao, D.T., Terrillion, C.E., Piantadosi, S.C., Bhat, S., Gould, T.D. (2012). The Tail Suspension Test. *J Vis Exp.* **59**, 3769.

Canitano, R., Pallagrosi, M. (2017). Autism Spectrum Disorders and Schizophrenia Spectrum Disorders: Excitation/Inhibition Imbalance and Developmental Trajectories. *Front Psychiatry* **8**, 69.

Castren, E., Elgersma, Y., Maffei, L., Hagerman, R. (2012). Treatment of neurodevelopmental disorders in adulthood. *J. Neurosci.* **32**, 14074–14079.

Chailangkarn, T., Trujillo, C.A., Freitas, B.C., Hrvoj-Mihic, B., Herai, R.H., Yu, D.X., Brown, T.T., Marchetto, M.C., Bardy, C., McHenry, L., Stefanacci, L., Järvinen, A., Searcy, Y.M., DeWitt, M., Wong, W., Lai, P., Ard, M.C., Hanson, K.L., Romero, S., Jacobs, B., Dale, A.M., Dai, L., Korenberg, J.R., Gage, F.H., Bellugi, U., Halgren, E., Semendeferi, K., Muotri, A.R. (2016). A human neurodevelopmental model for Williams syndrome. *Nature* **536**, 338-343.

Chattopadhyaya, B., Cristo, G.D. (2012). GABAergic circuit dysfunctions in neurodevelopmental disorders. *Front Psychiatry* **3**, 51.

Cheng, L.C., Pastrana, E., Tavazoie, M., Doetsch, F. (2009). miR-124 regulates adult neurogenesis in the subventricular zone stem cell niche. *Nat. Neurosci.* **12**, 399-408.

Chen, C.H., Huang, C.C., Cheng, M.C., Chiu, Y.N., Tsai, W.C., Wu, Y.Y., Liu, S.K., Gau, S.S. (2014). Genetic analysis of GABRB3 as a candidate gene of autism spectrum disorders. *Mol Autism* **25,** 36.

Chen, P., Hong, W. (2018). Neural Circuit Mechanisms of Social Behavior. *Neuron* 98, 16-30.

Chiang, H.R., Schoenfeld, L.W., Ruby, J.G., Auyeung, V.C., Spies, N., Baek, D., Johnston, W.K., Russ, C., Luo, S., Babiarz, J.E., Blelloch, R., Schroth, G.P., Nusbaum, C., Bartel, D.P. (2010). Mammalian microRNAs: experimental evaluation of novel and previously annotated genes. *Genes Dev.* **24**, 992-1009.

Christensen, M., Larsen, L.A., Kauppinen, S., Schratt, G.M. (2010). Recombinant adeno-associated virus-mediated microRNA delivery into the postnatal mouse brain reveals a role for miR-134 in dendritogenesis in vivo. *Front Neural Circuits*. **3**, 1-10.

Coba, M.P., Ramaker, M.J., Ho, E.V., Thompson, S.L., Komiyama, N.H., Grant, S.G., Knowles, J.A., Dulawa, S.C. (2018). Dlgap1 knockout mice exhibit alterations of the postsynaptic density and selective reductions in sociability*. Sci Rep.***8**, 2281.

Cochoy, D.M., Kolevzon, A., Kajiwara Y., Schoen, M., Pascual-Lucas, M., Lurie, S., Buxbaum, J.D., Boeckers, T.M., Schmeisser, M.J. (2015). Phenotypic and functional analysis of SHANK3 stop mutations identified in individuals with ASD and/or ID. *Mol Autism*. **6**:23.

Cohen, S., Greenberg, M.E. (2008). Communication between the synapse and the nucleus in neuronal development, plasticity, and disease. *Annu Rev Cell Dev Biol.* **24**, 183-209.

Cohen, J.E., Lee, P.R., Chen, S., Li W., Fields, R.D. (2011). MicroRNA regulation of homeostatic synaptic plasticity. *Proc Natl Acad Sci U S A*. **108**, 11650-11655.

D'Amato, F.R., Scalera, E., Sarli, C., Moles, A. (2005). Pups call, mothers rush: does maternal responsiveness affect the amount of ultrasonic vocalizations in mouse pups? *Behav Genet.* **35**, 103-112.

Davis, T.H., Cuellar, T.L., Koch, S.M., Barker, A.J., Harfe, B.D., McManus, M.T., Ullian, E.M. (2008). Conditional loss of Dicer disrupts cellular and tissue morphogenesis in the cortex and hippocampus. *J. Neurosci.* **28**, 4322-4330.

da Rocha, S.T., Edwards, C.A., Ito, M., Ogata, T., Ferguson-Smith, A.C. (2008). Genomic imprinting at the mammalian Dlk1-Dio3 domain. *Trends Genet.* **24**, 306-316.

Dermit, M., Dodel, M., Mardakheh, F.K. (2017). Methods for monitoring and measurement of protein translation in time and space. *Mol Biosyst.* **13**, 2477–2488.

Diamantopoulou, A., Sun, Z., Mukai, J., Xu, B., Fenelon, K., Karayiorgou, M., Gogosb, J.A. (2017). Loss-of-function mutation in Mirta22/Emc10 rescues specific schizophrenia-related phenotypes in a mouse model of the 22q11.2 deletion. *Proc Natl Acad Sci USA* **114**, 6127–6136.

Doers, M.E., Musser, M.T., Nichol, R., Berndt, E.R., Baker, M., Gomez, T.M., Zhang, S.C., Abbeduto, L., Bhattacharyya, A. (2014). iPSC-derived forebrain neurons from FXS individuals show defects in initial neurite outgrowth. *Stem Cells Dev.* **23**, 1777-1787.

Duffney, L.J., Wei, J., Cheng, J., Liu, W., Smith, K.R., Kittler, J.T., Yan, Z. (2013). Shank3 Deficiency Induces NMDA Receptor Hypofunction via an Actin-Dependent Mechanism. *J Neurosci.* **33**, 15767–15778.

Duval, E.R., Javanbakht, A., Liberzon, I. (2015). Neural circuits in anxiety and stress disorders: a focused review. *Ther Clin Risk Manag.* **11**, 115–126.

Eadie, B.D., Cushman, J., Kannangara, T.S., Fanselow, M.S., Christie, B.R. (2010). NMDA receptor hypofunction in the dentate gyrus and impaired context discrimination in adult Fmr1 knockout mice. *Hippocampus* **22**, 241-254.

Ebert, D.H., Greenberg, M.E. (2013). Activity-dependent neuronal signalling and autism spectrum disorder. *Nature* **493**, 327-337.

Edbauer, D, Neilson, J.R., Foster, K.A., Wang, C.F., Seeburg, D.P., Batterton, M.N., Tada, T., Dolan, B.M., Sharp, P.A., Sheng, M. (2010). Regulation of synaptic structure and function by FMRP-associated microRNAs miR-125b and miR-132. *Neuron* **65**, 373-384.

Etherton, M., Földy, C., Sharma, M., Tabuchi, K., Liu, X, Shamloo, M., Malenka, R.C., Südhof, T.C. (2011). Autism-linked neuroligin-3 R451C mutation differentially alters hippocampal and cortical synaptic function. *Proc Natl Acad Sci USA* **108**, 13764-13769.

Fabian, M.R., Sonenberg, N. (2012). The mechanics of miRNA-mediated gene silencing: a look under the hood of miRISC. *Nat Struct Mol Biol.* **19**, 586-93.

Fanselow, M.S., Dong, H.W. (2010). Are the dorsal and ventral hippocampus functionally distinct structures? *Neuron* **65**, 7-19.

Farovik, A., Dupont, L.M., Eichenbaum, H. (2009). Distinct roles for dorsal CA3 and CA1 in memory for sequential nonspatial events. *Learn Mem.* **17**, 12-17.

Felix-Ortiz, A.C., Tye, K.M. (2014). Amygdala inputs to the ventral hippocampus bidirectionally modulate social behavior. *J Neurosci.* **34**, 586-595.

Felix-Ortiz, A.C., Burgos-Robles, A., Bhagat, N.D., Leppla, C.A., Tye, K.M. (2016). Bidirectional modulation of anxiety-related and social behaviors by amygdala projections to the medial prefrontal cortex. *Neuroscience* **321**, 197-209.

Feng, G., Mellor, R.H., Bernstein, M., Keller-Peck, C., Nguyen, Q.T., Wallace, M., Nerbonne, J.M., Lichtman, J.W., Sanes, J.R. (2000). Imaging neuronal subsets in transgenic mice expressing multiple spectral variants of GFP. *Neuron* **28**, 41-51.

Ferguson, J.N., Young, L.J., Hearn, E.F., Matzuk, M.M., Insel, T.R., Winslow, J.T. (2000). Social amnesia in mice lacking the oxytocin gene. *Nat Genet.* **25**, 284-288.

Fineberg, S.K., Ross, D.A. (2017). Oxytocin and the Social Brain. *Biol Psychiatry* **81**, e19–e21.

Fiore, R., Khudayberdiev, S., Christensen, M., Siegel, G., Flavell, S.W., Kim, T.K., Greenberg, M.E., Schratt, G.M. (2009). Mef2-mediated transcription of the miR379-410 cluster regulates activity-dependent dendritogenesis by fine-tuning Pumilio2 protein levels. *EMBO J.* **28**, 697-710.

Fiore, R., Rajman, M., Schwale, C., Bicker, S., Antoniou, A., Bruehl, C., Draguhn, A., Schratt, G. (2014). MiR-134-dependent regulation of Pumilio-2 is necessary for homeostatic synaptic depression. *EMBO J.* **33**, 2231–2246.

Fonken, L.K., Gaudet, A.D., Gaier, K.R., Nelson, R.J., Popovich, P.G. (2015). MicroRNA-155 deletion reduces anxiety- and depressive-like behaviors in mice. *Psychoneuroendocrinology* **63**, 362-369.

Frith, C.D. (2007). The social brain? *Philos Trans R Soc Lond B Biol Sci.* **362**, 671-678.

Fritschy, J.M., Brünig, I. (2003). Formation and plasticity of GABAergic synapses: physiological mechanisms and pathophysiological implications. *Pharmacol Ther.* **98**, 299-323.

Galton, V.A., Martinez, E., Hernandez, A., St Germain, E.A., Bates, J.M., St Germain, D.L. (1999). Pregnant rat uterus expresses high levels of the type 3 iodothyronine deiodinase. *J Clin Invest* **103**, 979-987.

Gandal, M.J., Sisti, J., Klook, K., Ortinski, P.I., Leitman, V., Liang, Y., Thieu, T., Anderson, R., Pierce, R.C., Jonak, G., Gur, R.E., Carlson, G., Siegel, S.J. (2012). GABAB-mediated rescue of altered excitatory-inhibitory balance, gamma synchrony and behavioral deficits following constitutive NMDAR-hypofunction. *Transl Psychiatry* **2**, e142.

Gao, J., Wang, W.Y., Mao, Y.W., Graff, J., Guan, J.S., Pan, L., Mak, G., Kim, D., Su, S.C., Tsai, L.H. (2010). A novel pathway regulates memory and plasticity via SIRT1 and miR-134. *Nature* **466**, 1105–1109.

Gao, R., Penzes, P. (2015). Common mechanisms of excitatory and inhibitory imbalance in schizophrenia and autism spectrum disorders. *Curr Mol Med.* **15**, 146-167.

Gardiner, E., Beveridge, N.J., Wu, J.Q., Carr, V., Scott, R.J., Tooney, P.A., Cairns, M.J. (2012). Imprinted DLK1-DIO3 region of 14q32 defines a schizophrenia-associated miRNA signature in peripheral blood mononuclear cells. *Mol Psychiatry* **17**, 827-840.

Garner, J.P., Meehan, C.L., Mench, J.A. (2003). Stereotypies in caged parrots, schizophrenia and autism: evidence for a common mechanism. *Behav Brain Res.* **145**, 125-34.

Gascon, E., Lynch, K., Ruan, H., Almeida, S., Verheyden, J.M., Seeley, W.W., Dickson, D.W., Petrucelli, L., Sun, D., Jiao, J., Zhou, H., Jakovcevski, M., Akbarian, S., Yao, W.D., Gao, F.B. (2014). Alterations in microRNA-124 and AMPA receptors contribute to social behavioral deficits in frontotemporal dementia. *Nat Med.* **20**, 1444-1451.

Gatto, C.L., Broadie, K. (2010). Genetic Controls Balancing Excitatory and Inhibitory Synaptogenesis in Neurodevelopmental Disorder Models. *Front Synaptic Neurosci.***2**: 4.

Gholizadeh, S., Arsenault, J., Xuan, I.C.Y., Pacey, L.K., Hampson, D.R. (2014). Reduced Phenotypic Severity Following Adeno-Associated Virus-Mediated Fmr1 Gene Delivery in Fragile X Mice. *Neuropsychopharmacology* **39**, 3100–3111.

Giraldez, A.J., Cinalli, R.M., Glasner, M.E., Enright, A.J., Thomson, J.M., Baskerville, S., Hammond, S.M., Bartel, D.P., Schier, A.F. (2005). MicroRNAs regulate brain morphogenesis in zebrafish. *Science* **308**, 833-838.

Glausier, J.R., Lewis, D.A. (2013). Dendritic spine pathology in schizophrenia. *Neuroscience* **251**, 90-107.

Gogolla, N., Takesian, A.E., Feng, G., Fagiolini, M., Hensch, T.K. (2014). Sensory integration in mouse insular cortex reflects GABA circuit maturation. *Neuron* **83**, 894-905.

Gu, Z., Eils, R., Schlesner, M. (2016). Complex heatmaps reveal patterns and correlations in multidimensional genomic data. *Bioinformatics* **32**, 2847-2849.

Guilmatre, A., Huguet, G., Delorme, R., Bourgeron, T. (2014). The emerging role of SHANK genes in neuropsychiatric disorders. *Dev Neurobiol.* **74**, 113–122.

Gunaydin, L.A., Grosenick, L., Finkelstein, J.C, Kauvar, I.V., Fenno, L.E., Adhikari, A., Lammel, S., Mirzabekov, J.J., Airan, R.D., Zalocusky, K.A., Tye, K.M., Anikeeva, P., Malenka, R.C., Deisseroth, K. (2014). Natural neural projection dynamics underlying social behavior. *Cell* **157**, 1535–1551.

Grün, D., Wang, Y.L., Langenberger, D., Gunsalus, K.C., Rajewsky, N. (2005). microRNA Target Predictions across Seven Drosophila Species and Comparison to Mammalian Targets. *PLoS Comput Biol.*, **1**(1): e13.

Ha, M., Kim, V.N. (2014). Regulation of microRNA biogenesis. *Nat Rev Mol Cell Biol.* **15**, 509-524.

Han, K., Holder, J.L., Schaaf, C.P., Lu, H., Chen, H., Kang, H., Tang, J., Wu, Z., Hao, S., Cheung, S.W., Yu, P., Sun, H., Breman, A.M., Patel, A., Lu, H.C., Zoghbi, H.Y. (2013). SHANK3 overexpression causes manic-like behaviour with unique pharmacogenetic properties. *Nature* **503**, 72-77.

Hansen, K.F., Sakamoto, K., Wayman, G.A., Impey, S., Obrietan, K. (2010). Transgenic miR132 alters neuronal spine density and impairs novel object recognition memory. *PLoS One* **5**, e15497.

Hanson, J.E., Madison, D.V. (2007). Presynaptic FMR1 genotype influences the degree of synaptic connectivity in a mosaic mouse model of fragile X syndrome. *J Neurosci.* **27**, 4014-4018.

He, L. and Hannon, G.J. (2004). MicroRNAs: small RNAs with a big role in gene regulation. *Nat. Rev. Genet*. **5**, 522-531.

Hébert, S.S., Papadopoulou, A.S., Smith, P., Galas, M.C., Planel, E., Silahtaroglu, A.N., Sergeant, N., Buée, L., De Strooper, B. (2010). Genetic ablation of Dicer in adult forebrain neurons results in abnormal tau hyperphosphorylation and neurodegeneration. *Hum. Mol. Genet.* **19**, 3959-3969.

Heinrichs, M., von Dawans, B., Domes, G. (2009). Oxytocin, vasopressin, and human social behavior. *Front Neuroendocrinol.* **30**, 548-557.

Helmeste, D.M., Seeman, P. (1982). Amphetamine-induced hypolocomotion in mice with more brain D2 dopamine receptors. *Psychiatry Res.* **7,** 351-359.

Hernandez, A., Park, J.P., Lyon, G.J., Mohandas, T.K., St. Germain, D.L. (1998). Localization of the type 3 iodothyronine deiodinase (DIO3) gene to human chromosome 14q32 and mouse chromosome 12F1. *Genomics* **53**, 119-121

Herring, B.E., Shi, Y., Suh, Y.H., Zheng, C.Y., Blankenship, S.M., Roche, K.W., Nicoll, R.A. (2013). Cornichon proteins determine the subunit composition of synaptic AMPA receptors. *Neuron* **77**, 1083-1096.

Higuchi, F., Uchida, S., Yamagata, H., Abe-Higuchi, N., Hobara, T., Hara, K., Kobayashi, A., Shintaku, T., Itoh, Y., Suzuki, T., Watanabe, Y. (2016). Hippocampal MicroRNA-124 Enhances Chronic Stress Resilience in Mice. *J Neurosci.* **36**, 7253-7267.

Hitti, F.L., Siegelbaum, S.A. (2014). The hippocampal CA2 region is essential for social memory. *Nature* **508**, 88-92.

Huang, T., Liu, Y., Huang, M., Zhao, X., Cheng, L. (2010). Wnt1-cre-mediated conditional loss of Dicer results in malformation of the midbrain and cerebellum and failure of neural crest and dopaminergic differentiation in mice. *J. Mol. Cell Biol.* **2**, 152-163

Hutsler, J.J., Zhang, H. (2010). Increased dendritic spine densities on cortical projection neurons in autism spectrum disorders. *Brain Res.* **1309**, 83-94.

Ingolia, N.T., Lareau, L.F., Weissman J.S. (2011). Ribosome profiling of mouse embryonic stem cells reveals the complexity and dynamics of mammalian proteomes. *Cell* **147**, 789-802.

Jamain, S., Radyushkin, K., Hammerschmidt, K., Granon, S., Boretius, S., Varoqueaux, F., Ramanantsoa, N., Gallego, J., Ronnenberg, A., Winter, D., Frahm, J., Fischer, J., Bourgeron, T., Ehrenreich, H., Brose, N. (2008). Reduced social interaction and ultrasonic communication in a mouse model of monogenic heritable autism. *Proc Natl Acad Sci USA* **105**, 1710-1715.

Jasińska, M., Miłek, J., Cymerman, I.A., Łęski, S., Kaczmarek, L., Dziembowska, M. (2016). miR-132 Regulates Dendritic Spine Structure by Direct Targeting of Matrix Metalloproteinase 9 mRNA. *Mol Neurobiol.* **53**, 4701-4712.

Jeste, S. S., Tuchman, R. (2015). Autism Spectrum Disorder and Epilepsy: Two Sides of the Same Coin*? J Child Neurol.* **30**, 1963–1971.

Jiang, Y.H., Ehlers, M.D. (2013). Modeling autism by SHANK gene mutations in mice. *Neuron* **78**, 8-27.

Jimenez-Mateos, E.M., Engel, T., Merino-Serrais, P., Mc Kiernan, R.C., Tanaka, K., Mouri, G., Sano, T., O'Tuathaigh, C., Waddington, J.L., Prenter, S., Delanty, N., Farrell, M.A., O'Brien, D.F., Conroy RM, Stallings, R.L., Defelipe, J., Henshall, D.C. (2012). Silencing microRNA-134 produces neuroprotective and prolonged seizure-suppressive effects. *Nat. Med.* **10**.

Jimenez, J.C., Su, K., Goldberg, A.R., Luna, V.M., Biane, J.S., Ordek, G., Zhou, P., Ong, S.K., Wright, M.A., Zweifel, L., Paninski, L., Hen, R., Kheirbek, M.A. (2018). Anxiety Cells in a Hippocampal-Hypothalamic Circuit. *Neuron* **97**, 670-683.

Jimenez-Mateos, E.M., Engel, T., Merino-Serrais, P., Fernaud-Espinosa, I., Rodriguez-Alvarez, N., Reynolds, J., Reschke, C.R., Conroy, R.M., McKiernan, R.C., de Felipe, J., Henshall, D.C. (2015). Antagomirs targeting microRNA-134 increase hippocampal pyramidal neuron spine volume in vivo and protect against pilocarpine-induced status epilepticus. *Brain Struct Funct.* **220**, 2387-2399.

Jonas, S., Izaurralde, E. (2015). Towards a molecular understanding of microRNA-mediated gene silencing. *Nat Rev Genet.* **16**, 421-433.

Jung, E.M., Moffat, J.J., Liu, J., Dravid, S.M., Gurumurthy, C.B., Kim, W.Y. (2017). Arid1b haploinsufficiency disrupts cortical interneuron development and mouse behavior. *Nat Neurosci.* **20**, 1694-1707.

Kandel, E.R., Schwartz, J.H., Jessell, T.M. (2012). Principles of neural science, 5th Edition. New York: *McGraw-Hill Education Ltd.*

Karayiorgou, M., Morris, M.A., Morrow, B., Shprintzen, R.J., Goldberg, R., Borrow, J., Gos, A., Nestadt, G., Wolyniec, P.S., Lasseter, V.K., et al. (1995). Schizophrenia susceptibility associated with interstitial deletions of chromosome 22q11. *Proc Natl Acad Sci USA* **92**, 7612-7616.

Kapsimali, M., Kloosterman, W.P., de Bruijn, E., Rosa, F., Plasterk, R.H., Wilson, S.W. (2007). MicroRNAs show a wide diversity of expression profiles in the developing and mature central nervous system. *Genome Biol.* **8**, R173.

Khudayberdiev, S.A., Zampa, F., Rajman, M., Schratt, G. (2013). A comprehensive characterization of the nuclear microRNA repertoire of post-mitotic neurons. *Front Mol Neurosci.* **6**, 43.

Kim, Y., Venkataraju, K.U., Pradhan, K., Mende, C., Taranda, J., Turaga, S.C., Arganda-Carreras, I., Ng, L., Hawrylycz, M.J., Rockland, K.S., Seung, H.S., Osten, P. (2015). Mapping social behavior-induced brain activation at cellular resolution in the mouse. *Cell Rep.* **10**, 292-305.

Kim, H., Lim, C.S., Kaang, B.K. (2016). Neuronal mechanisms and circuits underlying repetitive behaviors in mouse models of autism spectrum disorder. *Behav Brain Funct*. **12**, 3.

Kircher, M., Bock, C., Paulsen, M (2008). Structural conservation versus functional divergence of maternally expressed microRNAs in the Dlk1/Gtl2 imprinting region. *BMC Genomics* **9**, 346.

Khattak, S., Brimble, E., Zhang, W., Zaslavsky, K., Strong, E., Ross, P.J., Hendry, J., Mital, S., Salter, M.W., Osborne, L.R., Ellis, J. (2015). Human induced pluripotent stem cell derived neurons as a model for Williams-Beuren syndrome. *Mol Brain.* **8**, 77.

Ko, J. (2017). Neuroanatomical Substrates of Rodent Social Behavior: The Medial Prefrontal Cortex and Its Projection Patterns. *Front Neural Circuits*. **11**: 41.

Konopka, W., Kiryk, A., Novak, M., Herwerth, M., Parkitna, J.R., Wawrzyniak, M., Kowarsch, A., Michaluk, P., Dzwonek, J., Arnsperger, T., Wilczynski, G., Merkenschlager, M., Theis, F.J., Köhr, G., Kaczmarek, L., Schütz, G. (2010). MicroRNA loss enhances learning and memory in mice. *J. Neurosci.* **30**, 14835-14842.

Kravchick, D.O., Karpova, A., Hrdinka, M., Lopez-Rojas, J., Iacobas, S., Carbonell, A.U., Iacobas, D.A., Kreutz, M.R., Jordan, B.A. (2016). Synaptonuclear messenger PRR7 inhibits c-Jun ubiquitination and regulates NMDA-mediated excitotoxicity. *EMBO J.* **35**, 1923-1934.

Kosik, K.S. (2006). The neuronal microRNA system. *Nat. Rev. Neurosci.* **7**, 911-920.

Kozomara, A. and Griffiths-Jones, S. (2011). miRBase: integrating microRNA annotation and deep-sequencing data. *Nucleic. Acids Res.* **39**, D152-157.

Krol, J., Busskamp, V., Markiewicz, I., Stadler, M.B., Ribi, S., Richter, J., Duebel, J., Bicker, S., Fehling, H.J., Schübeler, D., Oertner, T.G., Schratt, G., Bibel, M., Roska, B., Filipowicz, W. (2010). Characterizing light-regulated retinal microRNAs reveals rapid turnover as a common property of neuronal microRNAs. *Cell* **14**, 618-631.

Labialle, S., Marty, V., Bortolin-Cavaillé, M.L., Hoareau-Osman, M., Pradère, JP., Valet, P., Martin, P.G.P., Cavaillé, J. (2014). The miR-379/miR-410 cluster at the imprinted Dlk1-Dio3 domain controls neonatal metabolic adaptation. *EMBO J.* **33**, 2216–2230.

Lee, D., Lee, A.K. (2017). In Vivo Patch-Clamp Recording in Awake Head-Fixed Rodents. *Cold Spring Harb Protoc.* **4**:pdb.prot095802.

Li, M. et al. (2013). Role of the Prefrontal Cortex (PFC) on Processing the Social Statistical Information: An fMRI Study. In: Imamura K., Usui S., Shirao T., Kasamatsu T., Schwabe L., Zhong N. (eds) *Brain and Health Informatics*. BHI 2013. Lecture Notes in Computer Science, vol **8211**. Springer, Cham

Liu, C, Teng, Z.Q., Santistevan, N.J., Szulwach, K.E., Guo, W., Jin, P., Zhao, X. (2010). Epigenetic regulation of miR-184 by MBD1 governs neural stem cell proliferation and differentiation. *Cell Stem Cell.* **7**, 433-444.

Lee, A.R., Kim, J.H., Cho, E., Kim, M., Park, M. (2017). Dorsal and Ventral Hippocampus Differentiate in Functional Pathways and Differentially Associate with Neurological Disease-Related Genes during Postnatal Development. *Front Mol Neurosci.* **10**, 331.

Lord, C., Bishop, S.L. (2015). Recent advances in autism research as reflected in DSM-5 criteria for autism spectrum disorder. *Annu. Rev. Clin. Psychol.* **11**, 53–70.

Luikart, B.W., Bensen, A.L., Washburn, E.K., Perederiy, J.V., Su, K.G., Li, Y., Kernie, S.G., Parada, L.F., Westbrook, G.L. (2011). miR-132 mediates the integration of newborn neurons into the adult dentate gyrus. *PLos One* **6**, e19077.

Lynch, J.W. (2004). Molecular structure and function of the glycine receptor chloride channel. *Physiol Rev.* **84**, 1051-1095.

Mariani, J., Coppola, G., Zhang, P., Abyzov, A., Provini, L., Tomasini, L., Amenduni, M., Szekely, A., Palejev, D., Wilson, M., Gerstein, M., Grigorenko, E.L., Chawarska, K., Pelphrey, K.A., Howe, J.R., Vaccarino, F.M. (2015). FOXG1-Dependent Dysregulation of GABA/Glutamate Neuron Differentiation in Autism Spectrum Disorders. *Cell* **162**, 375-390.

McFarlane, H.G., Kusek, G.K., Yang, M., Phoenix, J.L., Bolivar, V.J., Crawley, J.N. (2008). Autism-like behavioral phenotypes in BTBR T+tf/J mice. *Genes Brain Behav.* **7**, 152-163.

Marchetto, M.C., Carromeu, C., Acab, A., Yu, D., Yeo, G.W., Mu, Y., Chen, G., Gage, F.H., Muotri, A.R. (2010). A model for neural development and treatment of Rett syndrome using human induced pluripotent stem cells. *Cell* **143**, 527-539.

Martin, E.I., Ressler, K.J., Binder, E., Nemeroff, C.B. (2009). The Neurobiology of Anxiety Disorders: Brain Imaging, Genetics, and Psychoneuroendocrinology. *Psychiatr Clin North Am.* **32**, 549–575.

Martínez-Cerdeño, V. (2017). Dendrite and spine modifications in autism and related neurodevelopmental disorders in patients and animal models. *Dev Neurobiol.* **77**, 393-404.

Marty, V., Labialle, S., Bortolin-Cavaillé, M.L., Ferreira De Medeiros, G., Moisan, M.P., Florian, C., Cavaillé, J. (2016). Deletion of the miR-379/miR-410 gene cluster at the imprinted Dlk1-Dio3 locus enhances anxiety-related behaviour. *Hum Mol Genet.* **25**, 728-739.

McLoughlin, H.S., Fineberg, S.K., Ghosh, L.L., Tecedor, L., and Davidson, B.L. (2012). Dicer is required for proliferation, viability, migration and differentiation in corticoneurogenesis. *Neuroscience* **223**, 285–295.

McNeill, E., Van Vactor, D. (2012). MicroRNAs Shape the Neuronal Landscape. *Neuron* **75**, 363-379.

Mellios, N. & Sur, M. (2012). The Emerging Role of microRNAs in Schizophrenia and Autism Spectrum Disorders. *Front. Psychiatry* **3**, 39.

Mendrek, A., Stip, E. (2011). Sexual dimorphism in schizophrenia: is there a need for gender-based protocols? *Expert Rev Neurother.* **11**, 951-959.

Meyer-Lindenberg, A., Hariri, A.R., Munoz, K.E., Mervis, C.B., Mattay, V.S., Morris, C.A., Berman, K.F. (2005). Neural correlates of genetically abnormal social cognition in Williams syndrome. *Nat Neurosci.* **8**, 991-993.

Meyer, G., Kirsch, J., Betz, H., Langosch, D. (1995). Identification of a gephyrin binding motif on the glycine receptor beta subunit. *Neuron* **15**, 563-572.

Meziane, H., Ouagazzal, A.M., Aubert, L., Wietrzych, M., Krezel, W. (2007). Estrous cycle effects on behavior of C57BL/6J and BALB/cByJ female mice: implications for phenotyping strategies. *Genes Brain Behav.* **6**, 192-200.

Montagrin, A., Saiote, C., Schiller, D. (2017). The social hippocampus. *Hippocampus*, hipo.22797.

Moser, M.B., Moser, E.I. (1998). Functional differentiation in the hippocampus. *Hippocampus* **8**, 608-619.

Murugan, M., Jang, H.J., Park, M., Miller, E.M., Cox, J., Taliaferro, J.P., Parker, N.F., Bhave, V., Hur, H., Liang, Y., Nectow, A.R., Pillow, J.W., Witten, I.B. (2017). Combined Social and Spatial Coding in a Descending Projection from the Prefrontal Cortex. *Cell* **171**, 1663-1677.

Nadler, J.J., Moy, S.S., Dold, G., Trang, D., Simmons, N., Perez, A., Young, N.B., Barbaro, R.P., Piven, J., Magnuson, T.R., Crawley, J.N. (2004). Automated apparatus for quantitation of social approach behaviors in mice. *Genes Brain Behav.* **3**, 303-314.

Nageshappa, S., Carromeu, C., Trujillo, C.A., Mesci, P., Espuny-Camacho, I., Pasciuto, E., Vanderhaeghen, P., Verfaillie, C.M., Raitano, S., Kumar, A., Carvalho, C.M., Bagni, C., Ramocki, M.B., Araujo, B.H., Torres, L.B., Lupski, J.R., Van Esch, H., Muotri, A.R. (2016). Altered neuronal network and rescue in a human MECP2 duplication model. *Mol Psychiatry* **21**, 178-188.

Niu, Y., Shen, B., Cui, Y., Chen, Y., Wang, J., Wang, L., Kang, Y., Zhao, X., Si, W., Li, W., Xiang, A.P., Zhou, J., Guo, X., Bi, Y., Si, C., Hu, B., Dong, G., Wang, H., Zhou, Z., Li, T., Tan, T., Pu, X., Wang, F., Ji, S., Zhou, Q., Huang, X., Ji, W., Sha, J. (2014). Generation of gene-modified cynomolgus monkey via Cas9/RNA-mediated gene targeting in one-cell embryos. *Cell* **156**, 836-843.

Nudelman, A.S., DiRocco, D.P., Lambert, T.J., Garelick, M.G., Le, J., Nathanson, N.M., Storm, D.R. (2010). Neuronal activity rapidly induces transcription of the CREB-regulated microRNA-132, in vivo. *Hippocampus* **20**, 492-498.

Nueda, M.L., Baladrón, V., Sánchez-Solana, B., Ballesteros, M.A., Laborda, J. (2007). The EGF-like protein dlk1 inhibits notch signaling and potentiates adipogenesis of mesenchymal cells. *J Mol Biol.* **367**, 1281-1293.

O'Neill, L.A. (2009). Boosting the brain's ability to block inflammation via microRNA-132. *Immunity* **31**, 854-855.

Okabe, S. (2007). Molecular anatomy of the postsynaptic density. *Mol Cell Neurosci.* **34**, 503-518.

Okabe, S., Nagasawa, M., Kihara, T., Kato, M., Harada, T., Koshida, N., Mogi, K., Kikusui, T. (2013). Pup odor and ultrasonic vocalizations synergistically stimulate maternal attention in mice. *Behav Neurosci.* **127**, 432-438.

Pasquinelli, A.E., Ruvkun G. (2002). Control of developmental timing by micrornas and their targets. *Annu. Rev. Cell Dev. Biol.* **18**, 495-513.

Pathania, M., Torres-Reveron, J., Yan, L., Kimura, T., Lin, T.V., Gordon, V., Teng, Z.Q., Zhao, X., Fulga, T.A., Van Vactor, D., Bordey, A. (2012). miR-132 Enhances Dendritic Morphogenesis, Spine Density, Synaptic Integration, and Survival of Newborn Olfactory Bulb Neurons. *PLoS One* **7**, e38174.

Peça, J., Feliciano, C., Ting, J.T., Wang, W., Wells, M.F., Venkatraman, T.N., Lascola, C.D., Fu, Z., Feng, G. (2011). Shank3 mutant mice display autistic-like behaviours and striatal dysfunction. *Nature* **472**, 437-442.

Penzes, P., Cahill, M.E., Jones, K.A., VanLeeuwen, J.E., Woolfrey, K.M. (2011). Dendritic spine pathology in neuropsychiatric disorders. *Nat Neurosci.* **14**, 285-293.

Phillips, M., Pozzo-Miller, L. (2015). Dendritic spine dysgenesis in autism related disorders. *Neurosci Lett.* **601**, 30-40.

Pino, I., Rico, B., Marín, O. (2018). Neural circuit dysfunction in mouse models of neurodevelopmental disorders. *Curr Opin Neurobiol.* **48**, 174-182.

Rago, L., Beattie, R., Taylor, V., Winter, J. (2014). miR379-410 cluster miRNAs regulate neurogenesis and neuronal migration by fine-tuning N-cadherin. *EMBO J.* **33**, 906-920.

Rajman, M., Metge, F., Fiore, R., Khudayberdiev, S., Aksoy-Aksel, A., Bicker, S., Ruedell Reschke, C., Raoof, R., Brennan, G.P., Delanty, N., Farrell, M.A., O'Brien, D.F., Bauer, S., Norwood, B., Veno, M.T., Krüger, M., Braun, T., Kjems, J., Rosenow, F., Henshall, D.C., Dieterich, C., Schratt, G. (2017). A microRNA-129-5p/Rbfox crosstalk coordinates homeostatic downscaling of excitatory synapses. *EMBO J.* **36**, 1770-1787.

Rajman, M., Schratt, G. (2017). MicroRNAs in neural development: from master regulators to fine-tuners. *Development* **144**, 2310-2322.

Rasmussen, A.H., Rasmussen, H.B., Silahtaroglu, A. (2017). The DLGAP family: neuronal expression, function and role in brain disorders. *Mol Brain.* **10**, 43.

Rojas, D.C. (2014). The role of glutamate and its receptors in autism and the use of glutamate receptor antagonists in treatment. *J Neural Transm (Vienna)* **121**, 891-905.

Rong, H., Liu, T.B., Yang, K.J., Yang, H.C., Wu, D.H., Liao, C.P., Hong, F., Yang, H.Z., Wan, F., Ye, X.Y., Xu, D., Zhang, X., Chao, C.A., Shen, Q.J. (2011). MicroRNA-134 plasma levels before and after treatment for bipolar mania. *J. Psychiatr. Res.* **45**, 92-95.

Rubin, R.D., Watson, P.D., Duff, M.C., Cohen, N.J. (2014). The role of the hippocampus in flexible cognition and social behavior. *Front Hum Neurosci*., **8**: 742.

Saba, R., Störchel, P.H., Aksoy-Aksel, A., Kepura, F., Lippi, G., Plant, T.D., Schratt, G. (2012). Dopamine-regulated microRNA MiR-181a controls GluA2 surface expression in hippocampal neurons. *Mol Cell Biol.* **32**, 619-632.

Sala, C., Vicidomini, C., Bigi, I., Mossa, A., Verpelli, C. (2015). Shank synaptic scaffold proteins: keys to understanding the pathogenesis of autism and other synaptic disorders. *J Neurochem.* **135**, 849-858.

Santarelli, D.M., Beveridge, N.J., Tooney, P.A., Cairns, M.J. (2011). Upregulation of dicer and microRNA expression in the dorsolateral prefrontal cortex Brodmann area 46 in schizophrenia. *Biol Psychiatry.* **69**, 180-187.

Scattoni, M.L., Martire, A., Cartocci, G., Ferrante, A., Ricceri, L. (2013). Reduced social interaction, behavioural flexibility and BDNF signalling in the BTBR T+ tf/J strain, a mouse model of autism. *Behav Brain Res.* **251**, 35-40.

Schaefer, A., O'Carroll, D., Tan, C.L., Hillman, D., Sugimori, M., Llinas, R., Greengard, P. (2007). Cerebellar neurodegeneration in the absence of microRNAs. *J Exp Med.* **204**, 1553-1558.

Schneider, M., Debbane, M., Bassett, A.S., et al. (2014). Psychiatric disorders from childhood to adulthood in 22q11.2 deletion syndrome: results from the International Consortium on Brain and Behavior in 22q11.2 Deletion Syndrome. *Am J Psychiatry.* **171**, 627–639.

Schouten, M., Buijink, R., Lucassen, P.J., Fitzsimons, C.P. (2012). New Neurons in Aging Brains: Molecular Control by Small Non-Coding RNAs. *Front Neurosci*. **6**, 25.

Schurch, N.J., Schofield, P., Gierliński, M., Cole, C., Sherstnev, A., Singh, V., Wrobel, N., Gharbi, K., Simpson, G.G., Owen-Hughes, T., Blaxter, M., Barton, G.J. (2016). How many biological replicates are needed in an RNA-seq experiment and which differential expression tool should you use? *RNA* **22**, 839-851.

Schratt, G.M., Tuebing, F., Nigh, E.A., Kane, C.G., Sabatini, M.E., Kiebler, M., Greenberg, M.E. (2006). A brain-specific microRNA regulates dendritic spine development. *Nature* **439**, 283-289.

Schratt, G.M. (2009). microRNA at the synapse. *Nat. Rev. Neurosci*. **10**, 842-849.

Schwenk, F., Baron, U., Rajewsky, K. (1995). A cre-transgenic mouse strain for the ubiquitous deletion of loxP-flanked gene segments including deletion in germ cells. *Nucleic Acids Res.* **23**, 5080-5081.

Seitz, H., Youngson, N., Lin, S.P., Dalbert, S., Paulsen, M., Bachellerie, J.P., Ferguson-Smith, A.C., Cavaille, J. (2003). Imprinted microRNA genes transcribed antisense to a reciprocally imprinted retrotransposon-like gene. *Nat Genet* **34**, 261-262

Seitz, H., Royo, H., Bortolin, M.L., Lin, S.P., Ferguson-Smith, A.C., Cavaillé, J. (2004). A large imprinted microRNA gene cluster at the mouse Dlk1-Gtl2 domain. *Genome Res.* **14**, 1741-1748.

Sekita, Y., Wagatsuma, H., Nakamura, K., Ono, R., Kagami, M., Wakisaka, N., Hino, T., Suzuki-Migishima, R., Kohda, T., Ogura, A., Ogata, T., Yokoyama, M., Kaneko-Ishino, T., Ishino, F. (2008). Role of retrotransposon-derived imprinted gene, Rtl1, in the feto-maternal interface of mouse placenta. *Nat Genet.* **40**, 243-248.

Sheridan, S.D., Theriault, K.M., Reis, S.A., Zhou, F., Madison, J.M., Daheron, L., Loring, J.F., Haggarty, S.J. (2011). Epigenetic characterization of the FMR1 gene and aberrant neurodevelopment in human induced pluripotent stem cell models of fragile X syndrome. *PLoS One* **6**, e26203.

Siegel, G., Obernosterer, G., Fiore, R., Oehmen, M., Bicker, S., Christensen, M., Khudayberdiev, S., Leuschner, P.F., Busch, C.J., Kane, C., Hübel, K., Dekker, F., Hedberg, C., Rengarajan, B., Drepper, C., Waldmann, H., Kauppinen, S., Greenberg, M.E., Draguhn, A., Rehmsmeier, M., Martinez, J., Schratt, G.M. (2009). A functional screen implicates microRNA-138-dependent regulation of the depalmitoylation enzyme APT1 in dendritic spine morphogenesis. *Nat. cell Biol.* **11**, 705-716.

Siegert, S., Seo, J., Kwon, E.J., Rudenko, A., Cho, S., Wang, W., Flood, Z., Martorell, A.J., Ericsson, M., Mungenast, A.E., Tsai, L.H. (2015). The schizophrenia risk gene product miR-137 alters presynaptic plasticity. *Nat Neurosci.* **18**, 1008-1016.

Silverman, J.L., Yang, M., Lord, C., Crawley, J.N. (2010). Behavioural phenotyping assays for mouse models of autism. *Nat Rev Neurosci.* **11**, 490-502.

Silverman, J.L., Turner, S.M., Barkan, C.L., Tolu, S.S., Saxena, R., Hung, A.Y., Sheng, M., Crawley, J.N. (2011). Sociability and motor functions in Shank1 mutant mice. *Brain Res.* **22**, 120-137.

Silverman, J.L., Pride, M.C., Hayes, E.J., Puhger, K.R., Butler-Struben, H.M., Baker, S., Crawley, J.N. (2015). GABAB Receptor Agonist R-Baclofen Reverses Social Deficits and Reduces Repetitive Behavior in Two Mouse Models of Autism. *Neuropsychopharmacology* **40**, 2228–2239.

Smrt, R.D., Szulwach, K.E., Pfeiffer, R.L., Li, X., Guo, W., Pathania, M., Teng, Z.Q., Luo, Y., Peng, J., Bordey, A., Jin, P., Zhao, X. (2010). MicroRNA miR-137 regulates neuronal maturation by targeting ubiquitin ligase mind bomb-1. *Stem Cells.* **28**, 1060-1070.

Sukoff Rizzo, S.J., Crawley, J.N. (2017). Behavioral Phenotyping Assays for Genetic Mouse Models of Neurodevelopmental, Neurodegenerative, and Psychiatric Disorders. *Annu Rev Anim Biosci.* **5**, 371-389.

Sungur, A.Ö., Vörckel, K.J., Schwarting, R.K., Wöhr, M. (2014). Repetitive behaviors in the Shank1 knockout mouse model for autism spectrum disorder: developmental aspects and effects of social context. *J Neurosci Methods* **234**, 92-100.

Sungur, A.Ö., Schwarting, R.K.W., Wöhr, M. (2016). Early communication deficits in the Shank1 knockout mouse model for autism spectrum disorder: Developmental aspects and effects of social context. *Autism Res*. **9**, 696-709.

Sungur, A.Ö., Schwarting, R.K.W., Wöhr, M. (2017). Behavioral phenotypes and neurobiological mechanisms in the Shank1 mouse model for autism spectrum disorder: A translational perspective. *Behav Brain Res.* **17**, 30892-30896.

Stark, K.L., Xu, B., Bagchi, A., Lai, W.S., Liu, H., Hsu, R., Wan, X., Pavlidis, P., Mills, A.A., Karayiorgou, M., Gogos, J.A. (2008). Altered brain microRNA biogenesis contributes to phenotypic deficits in a 22q11-deletion mouse model. *Nat Genet.* **40**, 751-760.

Stoppel, D.C., Anderson, M.P. (2017). Hypersociability in the Angelman syndrome mouse model*. Exp Neurol.* **293**, 137-143.

Sztainberg, Y., Chen, H.M., Swann, J.W., Hao, S., Tang, B., Wu, Z., Tang, J., Wan, Y.W., Liu, Z., Rigo, F., Zoghbi, H.Y. (2015). Reversal of phenotypes in MECP2 duplication mice using genetic rescue or antisense oligonucleotides. *Nature* **528**, 123-126.

Tao, C., Zhang, G., Xiong, Y., Zhou. Y. (2015). Functional dissection of synaptic circuits: in vivo patch-clamp recording in neuroscience. *Front Neural Circuits* **9**: 23.

Tao, C.L., Liu, Y.T., Sun, R., Zhang, B., Qi, L., Shivakoti, S., Tian, C.L., Zhang, P., Lau, P.M., Zhou, Z.H., Bi, G.Q. (2018). Differentiation and Characterization of Excitatory and Inhibitory Synapses by Cryo-electron Tomography and Correlative Microscopy. *J Neurosci.* **38**, 1493-1510.

Tebbenkamp, A.T.N., Willsey, A.J., State, M.W., Šestana, N. (2014). The Developmental Transcriptome of the Human Brain: Implications for Neurodevelopmental Disorders. Curr Opin Neurol. 27, 149–156.

Tognini, P., Putignano, E., Coatti, A., Pizzorusso, T. (2011). Experience-dependent expression of miR-132 regulates ocular dominance plasticity. *Nat. Neurosci*. **14**, 1237-1239.

Tye, K.M., Deisseroth, K. (2012). Optogenetic investigation of neural circuits underlying brain disease in animal models. *Nat Rev Neurosci.* **13**, 251-266.

van den Buuse, M. (2010). Modeling the Positive Symptoms of Schizophrenia in Genetically Modified Mice: Pharmacology and Methodology Aspects. *Schizophr Bull.* **36**, 246–270.

Valluy, J., Bicker, S., Aksoy-Aksel, A., Lackinger, M., Sumer, S., Fiore, R., Wüst, T., Seffer, D., Metge, F., Dieterich, C., Wöhr, M., Schwarting, R., Schratt G. (2015). A coding-independent function of an alternative Ube3a transcript during neuronal development. *Nat Neurosci.* **18**, 666-673.

Vasudevan, S., Tong, Y., Steitz, J.A. (2007). Switching from repression to activation: microRNAs can up-regulate translation. *Science* **318**, 1931-1934.

Vessey, J.P., Vaccani, A., Xie, Y., Dahm, R., Karra, D., Kiebler, M.A., Macchi, P. (2006). Dendritic localization of the translational repressor Pumilio 2 and its contribution to dendritic stress granules. *J. Neurosci*. **26**, 6496-6508.

Vo, N., Klein, M.E., Varlamova, O., Keller, D.M., Yamamoto, T., Goodman, R.H., Impey, S. (2005). A cAMP-response element binding protein-induced microRNA regulates neuronal morphogenesis. *Proc. Natl. Acad. Sci. U.S.A* **102**, 16426-16431.

Wang, X., McCoy, P.A., Rodriguiz, R.M., Pan, Y., Je, H.S., Roberts, A.C., Kim, C.J., Berrios, J., Colvin, J.S., Bousquet-Moore, D., Lorenzo, I., Wu, G., Weinberg, R.J., Ehlers, M.D., Philpot, B.D., Beaudet, A.L., Wetsel, W.C., Jiang, Y.H. (2011). Synaptic dysfunction and abnormal behaviors in mice lacking major isoforms of Shank3. *Hum Mol Genet.* **20**, 3093-3108.

Wang, X., Bey, A.L., Katz, B.M., Badea, A., Kim, N., David, L.K., Duffney, L.J., Kumar, S., Mague, S.D., Hulbert, S.W., Dutta, N., Hayrapetyan, V., Yu, C., Gaidis, E., Zhao, S., Ding, J.D., Xu, Q., Chung, L., Rodriguiz, R.M., Wang, F., Weinberg, R.J., Wetsel, W.C., Dzirasa, K., Yin, H., Jiang, Y.H. (2016). Altered mGluR5-Homer scaffolds and corticostriatal connectivity in a Shank3 complete knockout model of autism. *Nat Commun.* **7**, 11459.

Welch, J.M., Lu, J., Rodriguiz, R.M., Trotta, N.C., Peca, J., Ding, J.D., Feliciano, C., Chen, M., Adams, J.P., Luo, J., Dudek, S.M., Weinberg, R.J., Calakos, N., Wetsel, W.C., Feng, G. (2007). Cortico-striatal synaptic defects and OCD-like behaviours in Sapap3-mutant mice. *Nature* **448**, 894-900.

Wheeler, G., Ntounia-Fousara, S., Granda, B., Rathjen, T., Dalmay, T. (2006). Identification of new central nervous system specific mouse microRNAs. *FEBS Lett* **580**, 2195-2200.

Winter, J. (2015). MicroRNAs of the miR379-410 cluster: New players in embryonic neurogenesis and regulators of neuronal function. *Neurogenesis* **2**, e1004970.

Werling, D.M., Geschwind, D.H. (2013). Sex differences in autism spectrum disorders. *Curr Opin Neurol.* **26**, 146-153.

Wöhr, M., Roullet, F.I., Hung, A.Y., Sheng, M., Crawley, J.N. (2011). Communication Impairments in Mice Lacking Shank1: Reduced Levels of Ultrasonic Vocalizations and Scent Marking Behavior. *PLoS One* **6**, e20631.

Wöhr, M., Silverman, J.L., Scattoni, M.L., Turner, S.M., Harris, M.J., Saxena, R., Crawley, J.N. (2013). Developmental delays and reduced pup ultrasonic vocalizations but normal sociability in mice lacking the postsynaptic cell adhesion protein neuroligin2. *Behav Brain Res.* **15**; 50-64.

Wöhr, M., Scattoni, M.L. (2013). Behavioural methods used in rodent models of autism spectrum disorders: current standards and new developments. *Behav Brain Res.* **251**, 5-17.

Wöhr, M., Orduz, D., Gregory, P., Moreno, H., Khan, U., Vörckel, K.J., Wolfer, D.P., Welzl, H., Gall, D., Schiffmann, S.N., Schwaller, B. (2015). Lack of parvalbumin in mice leads to behavioral deficits relevant to all human autism core symptoms and related neural morphofunctional abnormalities. *Transl Psychiatry* **5**: e525.

Won, H., Lee, H.R., Gee, H.Y., Mah, W., Kim, J.I., Lee, J., Ha, S., Chung, C., Jung, E.S., Cho, Y.S., Park, S.G., Lee, J.S., Lee, K., Kim, D., Bae, Y.C., Kaang, B.K., Lee, M.G., Kim, E. (2012). Autistic-like social behaviour in Shank2-mutant mice improved by restoring NMDA receptor function. *Nature* **486**, 261-265.

Wu, Y.E., Parikshak, N.N., Belgard, T.G., Geschwind, D.H. (2016). Genome-wide, integrative analysis implicates microRNA dysregulation in autism spectrum disorder. *Nat Neurosci.* **19**, 1463-1476.

Wu, H., Tao, J., Chen, P.J., Shahab, A., Ge, W., Hart, R.P., Ruan, X., Ruan, Y., Sun, Y.E. (2010). Genome-wide analysis reveals methyl-CpG-binding protein 2-dependent regulation of microRNAs in a mouse model of Rett syndrome. *Proc Natl Acad Sci USA* **107**, 18161-18166.

Xu, B., Hsu, B.K., Stark, K.L., Karayiorgou, M., Gogos, J.A. (2013). Derepression of a novel neuronal inhibitor is a major outcome of miRNA dysregulation due to 22q11.2 microdeletion. *Cell* **152**, 262–275.

Xu, X.L., Li, Y., Wang, F., Gao, F.B. (2008). The steady-state level of the nervous-system-specific microRNA-124a is regulated by dFMR1 in Drosophila. *J. Neurosci.* **28**, 11883-11889.

Xu, Y., Liu, H., Li, F., Sun, N., Ren, Y., Liu, Z., Cao, X., Wang, Y., Liu, P., Zhang, K. (2010). A polymorphism in the microRNA-30e precursor associated with major depressive disorder risk and P300 waveform. *J. Affect. Disord.* **127**, 332-336.

Yang, M., Abrams, D.N., Zhang, J.Y., Weber, M.D., Katz, A.M., Clarke, A.M., Silverman, J.L., Crawley, J.N. (2012). Low sociability in BTBR T+tf/J mice is independent of partner strain. *Physiol Behav.* **107**, 649-662.

Yang, Y., Wang, J.Z. (2017). From Structure to Behavior in Basolateral Amygdala-Hippocampus Circuits. *Front Neural Circuit*s, **11**:86.

Yizhar, O., Fenno, L.E., Prigge, M., Schneider, F., Davidson, T.J., O'Shea, D.J., Sohal, V.S., Goshen, I., Finkelstein, J., Paz, J.T., Stehfest, K., Fudim, R., Ramakrishnan, C., Huguenard, J.R., Hegemann, P., Deisseroth, K. (2011). Neocortical excitation/inhibition balance in information processing and social dysfunction. *Nature* **477**,171-178.

Zimmermann, A.M. (2012). Die Bedeutung der Aktin-bindenden Proteine Profilin1, ADF und n-Cofilin für die Morphologie hippocampaler Synapsen und das Verhalten der Maus. *Mensch & Buch*, ISBN: 3863872401.

Zimmermann, A.M., Jene, T., Wolf, M., Görlich, A., Gurniak, C.B., Sassoè-Pognetto, M., Witke, W., Friauf, E., Rust, M.B. (2015). Attention-Deficit/Hyperactivity Disorder-like Phenotype in a Mouse Model with Impaired Actin Dynamics. *Biol Psychiatry.* **78**, 95-106.

Zaboski, B.A., Storch, E.A. (2018). Comorbid autism spectrum disorder and anxiety disorders: a brief review. *Future Neurol.* **13**, 31-37.

Zhan, Y., Paolicelli, R.C., Sforazzini, F., Weinhard, L., Bolasco, G., Pagani, F., Vyssotski, A.L., Bifone, A., Gozzi, A., Ragozzino, D., Gross, C.T. (2014). Deficient neuron-microglia signaling results in impaired functional brain connectivity and social behavior. *Nat Neurosci.* **17**, 400-406.

Zhang, W., Peterson, M., Beyer, B., Frankel, W.N., Zhang, Z. (2014). Loss of MeCP2 From Forebrain Excitatory Neurons Leads to Cortical Hyperexcitation and Seizures. *J Neurosci.* **34**, 2754–2763.

Zhao, H., Tu, Z., Xu, H., Yan, S., Yan, H., Zheng, Y., Yang, W., Zheng, J., Li, Z., Tian, R., Lu, Y., Guo, X., Jiang, Y.H., Li, X.J., Zhang, Y.Q. (2017). Altered neurogenesis and disrupted expression of synaptic proteins in prefrontal cortex of SHANK3-deficient non-human primate. *Cell Res*. **27**, 1293-1297.

6. Appendix

6.1 List of figures

6.2 List of tables

6.3 List of online resources

miRBase: http://www.mirbase.org

Sfari: https://www.sfari.org

Targetscan: http://www.targetscan.org

6.4 List of abbreviations

3' UTR	3' untranslated region
AD	Alzheimer disease
AMPA	α-amino-3-hydroxy-5-methyl-4-isoxazolepropionic acid
AMPA-R	AMPA-receptor
Amph	Amphetamin
ANOVA	analysis of variance
Anti-miR	antago-microRNA; LNA
ADHD	Attention deficit hyperactivity disorder
Ago	Argonaut
AP5	2-amino-5-phosphopentanoic acid
APS	ammoniumperoxodisulfat
APT-1	acyl protein thioesterase
AS	Angelman syndrome
ASD	Autistic Spectrum Disorder
ASO	antisense oligonucleotides
BCA	bicinchoninic acid
BD	Bipolar Disorder
BDNF	brain derived neurotrophic factor
BLA	basolateral amygdala
bp	base pair
°C	Grad Celsius
CA	Cornu Ammonis region
Ca^{2+}	Calcium-Ionen
$CaCl_2$	Calcium chloride
ChR2	Chlamydomonas reinhardtii channelrhodopsin-2
CaMKII	Ca2+/calmodulin-dependent protein kinase II
Cnih2	Cornichon Family AMPA Receptor Auxiliary Protein 2
CNS	Central Nervous System
Creb	cAMP response element binding

cDNA	complementary DNA
C-terminus	carboxy-terminus
CTR	Control
CTX	Cortex
ddH2O	double destilled water
DEAH box	Asp-Glu-Ala-His box
DHX	DEAH box protein
DCGR8	DGCR8 DiGeorge syndrome critical region gene 8
DEG	Differentially Expressed Gene
DIV	Day In-Vitro
Dlgap3	Disks large-associated protein 3
DNA	deoxyribonucleic acid
DNase	desoxyribonuclease
DSM-5 edition	Diagnostic and Statistical Manual of Mental Disorders, fifth
DTT	dithiothreitol
E	Embryonic
ECL	enhanced chemiluminescence
EDTA	ethylenediaminetetraacetic acid
eGFP	enhanced Green Fluorescent Protein
EGTA	Ethylene glycol tetraacetic acid
EPM	Elevated Plus Maze
fEPSP	field Excitatory postsynaptic potential
FISH	fluorescent in situ hybridization
FMR(P)1	Fragile-X-Mental Retardation-(Protein) 1
FTD	Frontotemporal dementia
fw	forward
FXS	Fragile-X-Syndrome
g	gram
GABA	gamma-Aminobutyric acid
GluR	Glutamate receptor
GO	Gene Ontology

GTP	Guanosintriphosphat
h	hour
H_2O	Water
HC	Hippocampus
hiPSC	human induced pluripotent stem cell
HRP	horse radish peroxidase
kb	kilobase
KCl	Potassium chloride
kDa	kilo-Dalton
ko	knockout
l	liter
LDB	Light-Dark-Box
LNA	locked nucleic acid, antisense microRNA
LimK1	Lim-domain-containing protein kinase 1
LSM	Laser Scanning Micoscope
LTP	long-term potentiation
M	Molar
m	milli
m	meter
MAP	microtubule-associated protein
Mef2	myocyte enhancer factor-2
MEM	Modified eagles' medium
MgCl2	Magnesium chloride
mEPSC	miniature Excitory Postsynaptic Currents
µ	micro
miRISC	miRNA-containing RISC
min	minute
miRNA	microRNA
miR	microRNA
mut	mutant

mPFC	medial prefornatl cortex
mRNA	messenger RNA
MOV10	Moloney Leukemia Virus 10
MW	molecular weight
n	nano
NaDoc	Sodium desoxycholate
NaOH	Sodium hydroxide
NAc	Nucleus accumbens
NaCl	Sodium chloride
NB	Neuro Basal
NMDA	NMDA N-Methyl-D-aspartate
NMDA-R	NMDA-receptor
NpHR	Natronomonas pharaonis halorhodopsin
nt	nucleotide
N-terminus	amino-terminus
ns	not significant
OCD	Obsessive-compulsive disorder
OF	Open field
o.N.	over Night
PBS	phosphate buffered saline
PFC	Prefrontal cortex
Pfu	Pyrococcus furiosus
pH	lat.: „potentia hydrogenium"
Pnd	Postnatal day
Pol II	RNA polymerase II
Pum2	Pumilio 2
PPF	Paired pulse facilitation
PPI	Prepulse inhibition
pre-miRNA	precursor-microRNA
pri-miRNA	primary-microRNA

Prr7	Synaptic proline-rich membrane protein 7
PSD	Postsynaptic density
PSD-95	Postsynaptic densitiy protein 95
PTX	Picrotoxin
PVDF	Polyvinylidenfluorid
qPCR	quantitative Real-Time-Polymerase Chain Reaction
rev	reverse
Ribo-Seq	ribosome profiling by deep sequencing
RISC	microRNA-induced silencing complex
RLA	relative luciferase activity
RNA	ribonucleic acid
RNAseq	RNA Sequencing
rpm	revolutions per minute
RT	room temperature
RTT	Rett syndrome
s	second
SCZ	Schizophrenia
s.d.	standard deviation
SDS-PAGE	sodium dodecylsulfate polyacrylamide gel
s.e.m.	standard error of the mean
Shank	SH3 and multiple ankyrin repeat domains protein
siRNA	small interfering RNA
Sirt1	sirtuin 1
snRNA	small nuclear RNA
Src	Proto-oncogene tyrosine-protein kinase Src
stRNA	small temporal RNAs
TEMED	Tetramethylethylendiamin
Thy1	THYmocyte differentiation antigen 1
TST	Tail-suspension-test
U	Unit

Ube3A	Ubiquitin-protein ligase E3A
USV	Ultrasonic vocalization
UV	ultraviolet
V	Volt
vCA1	ventral hippocampal CA1
Veh	vehicle
vGAT	vesicular GABA transporter
vGlut	vesicular glutamate transporter
VTA	ventral tegmental area
% (v/v)	volumen percent
% (w/v)	weight percent
WBS	Williams-Beuren-Syndrome
wt	wildtype
ZT	Zeitgeber

6.5 List of academic teachers

My teachers at the University Osnabrück were:

Altendorf	Neuffer
Asaftei	Paululat
Brandt	Piehler
Deckers-Hebestreit	Reyer
Engelbrecht-Vandré	Scheibe
Güttner	Schrempf
Greie	Ungermann
Heinisch	Wahlbrink
Jeserich	Walder
Korb	Wieczorek
Krüppel	

My teachers at the Philipps-University Marburg were:

Buchholz	Pfefferle
del Rey	Schäfer
Dodel	Schratt
Höglinger	Schwarting
Jansen	Weihe
Oliver	Wöhr

6.6 Acknowledgements